2010

INTERFACIAL THERMAL CONDUCTIVITY USING MULTIWALL CARBON NANOTUBES

Carissa Don Russell
University of Kentucky, Carissa.d.russell@gmail.com

ABSTRACT OF THESIS

INTERFACIAL THERMAL CONDUCTIVITY USING MULTIWALL CARBON NANOTUBES

Shrinking volume, coupled with higher performance, microprocessors and integrated circuits have led to serious heat dissipation issues. In an effort to mitigate the excessive amounts of waste heat and ensure electronic survivability, heat sinks and spreaders are incorporated into heat generating device structures. This inevitability creates a thermal pathway through an interface. Thermal interfaces can possess serious thermal resistances for heat conduction. The introduction of a thermal interface material (TIM) can drastically increase the thermal performance of the component. Exceptional thermal properties of multiwall carbon nanotubes (MWCNTs) have spurred interest in their use as TIMs. MWCNTs inherently grow in vertically-oriented, high aspect ratio arrays, which is ideal in thermal interface applications because CNTs posses their superior thermal performance along their axis. In this paper, laser flash thermal characterization of sandwich-bonded and cap-screw-bonded aluminum discs for both adhesive-infiltrated and "dry", 100% MWCNT arrays, respectively. Thermal contact resistances as low as 18.1 mm^2K/W were observed for adhesive-infiltrated arrays and, even lower values, down to 10.583 mm^2K/W were measured for "dry" MWCNT arrays. The improved thermal performance of the arrays compared to thermal adhesives and greases currently used in the electronics and aerospace industries, characterize MWCNT arrays as a novel, lighter-weight, non-corrosive replacement.

KEYWORDS: Carbon Nanotubes, Thermal Interface Materials, Carbon Nanotube Arrays, Thermal Contact Resistance, Composite Thermal Interface Materials

Carissa Don Russell

December 17, 2010

INTERFACIAL THERMAL CONDUCTIVITY USING MULTIWALL CARBON NANOTUBES

By

Carissa Don Russell

Rodney J. Andrews, Ph.D.

Director of Thesis

James M. McDonough, Ph.D.

Director of Graduate Studies

December 17, 2010

RULES FOR THE USE OF THESES

Unpublished theses submitted for the Master's degree and deposited in the University of Kentucky Library are as a rule open for inspection, but are to be used only with due regard to the rights of the authors. Bibliographical references may be noted, but quotations or summaries of parts may be published only with the permission of the author, and with the usual scholarly acknowledgments.

Extensive copying or publication of the thesis in whole or in part also requires the consent of the Dean of the Graduate School of the University of Kentucky.

A library that borrows this thesis for use by its patrons is expected to secure the signature of each user.

Name	Date

THESIS

The Graduate School

University of Kentucky

2010

INTERFACIAL THERMAL CONDUCTIVITY USING MULTIWALL CARBON NANOTUES

THESIS

A thesis submitted in partial fulfillment of the requirements for the degree of
Master of Science in Mechanical Engineering
in the College of Engineering
at the University of Kentucky

By

Carissa Don Russell

Lexington, KY

Director: Dr. Rodney Andrews, Professor of Chemical and Materials Engineering

Lexington, KY

2010

For My Mom

ACKNOWLEDGEMENTS

I would first like to thank my advisor, Dr. Rodney Andrews, who I am grateful for the chance to work with. His consistent encouragement toward completing this thesis and furthering my education has made him an invaluable advisor in both my academic and professional career. I will be forever grateful for his guidance. I also want to thank Dr. Mark Meier and Dr. Kozo Saito for serving on my examining committee.

I would also like to thank Dr. Matthew Weisenberger for leading me into this exciting field. His technical support and consistent advice throughout many years has simply led me to the achievement of completing this thesis and furthering my research.

I want to extend thanks to the staff of the University of Kentucky Center for Applied Energy Research and especially the Carbon Materials group. I give special thanks to my fellow colleagues in the Carbon Materials Group, including John Craddock, David Jacques, Karen Petty, Ashley Morris, Mark Taylor, and Keith Etheredge.

I gratefully acknowledge funding and technical support from the US Army Aviation and Missile Research, Development and Engineering Center (AMRDEC). I want to especially thank Bob Evans, Keith Roberts, and Taylor Owens for seeing the importance of this research within the Smaller Lighter Cheaper project and for allowing me to further my research as a fellow colleague.

I would also like to thank Rich Foedinger and Simon Chung and the entire Materials Science Corporation (MSC) for their consistent technical support.

Finally, my thanks go to my family and friends. My husband, Cooper, for encouraging me and, most importantly, believing in me. For my mom for instilling in me the importance of hard work and achievement. My family and friend's support have led me to the person I am today and words cannot express how they mean to me.

TABLE OF CONTENTS

LIST OF TABLES

LIST OF FIGURES

Chapter 1 General Introduction and Outline

1.1 Motivation

Advances in technology and further miniaturization of microelectronics have led to serious thermal management issues. High power outputs within smaller electronics packaging continues to be a problem in the creation of higher performing integrated circuits [1]. For future generation microprocessors, integrated networks, and other highly integrated circuits and systems, power dissipation levels will reach 1 W/mm^2 by 2020 [2]. This is a drastic increase compared to an average power dissipation of 0.68 W/mm^2 in 2008. The thermal budget, i.e. the difference in the operating temperature to the temperature of the heat sink, remains unchanged. This problem can be addressed only if there is efficient thermal transport between the heat source and heat sink surfaces [3]. The thermal contact resistance must be decreased between the interfacial surfaces to create a higher temperature difference between convective surfaces and heat dissipating devices, such as a heat spreader.

High power electronics housed inside missile airframes is another issue requiring a thermal pathway for heat dissipation. The goal of electronics survivability is challenged by the guidance electronics producing power outputs up to 50 W for an indefinite amount of time. The power generating electronics are not 100 % effective, and therefore, generate excessive amounts of waste heat. Traditionally, the guidance electronics housings are composed of conductive aluminum, which conducts heat rapidly so that it can be dissipated to the outside air. However, carbon fiber reinforced epoxy composites provide a stronger, light weight, non-corrosive alternative to aluminum. The replacement of highly thermally conductive aluminum with carbon fiber reinforced composites possessing in-plane thermal conductivities less than less than 1 W/mK creates a thermal management issue [4-5]. In an attempt to dissipate more heat through composites, heat spreaders are often incorporated into the structure. However, conducting heat to the contacting heat spreader, involves a path through an interface. To reduce the resistance to heat through the interfaces, high conductivity thermal interface materials are placed between plies and also between the composite shell and heat spreader.

1.2 Introduction

Any surfaces, either within integrated circuits, composite layers, or any engineering application are not perfectly smooth on a microscopic level. When placing two solid substrates in contact with one another, disparities and voids limit the area of contact between the surfaces [3, 6]. For heat to transport from one surface to the other, it is limited to micro-contact points. The actual surface area in contact is close to 1-2 % of the area if no pressure is added [7]. Air is a poor conductor of heat, therefore replacing the air between surfaces with a thermal interface material (TIM) that conforms to the disparities and fills the volume of an interface between the micro-contact points can drastically increase heat transfer. Thermal interface materials (TIMs) minimize the contact resistance to heat conduction between contacting surfaces in a thermal gradient [3, 8-9]. Minimizing the interfacial thermal contact resistance between substrates is one of the most important properties for increasing the thermal performance of the entire component [10-13]. This principle can be described by simply modeling the two substrates (aluminum) and the TIM (CNT array) by resistors in series [9, 14-15]. The thermal resistance of the two solid substrates (R_1 and R_2) can be found by Equation 1.1, where L is the thickness, k is the thermal conductivity and A is the surface area. The thermal resistance across the interface is Equation 1.2, which is the contact resistance over the contact surface area, because contact resistance is, by definition, the thermal resistance per unit area. Because the resistances are in series, they can be added to equal the total resistance of the assembly, as Equation 1.3 demonstrates.

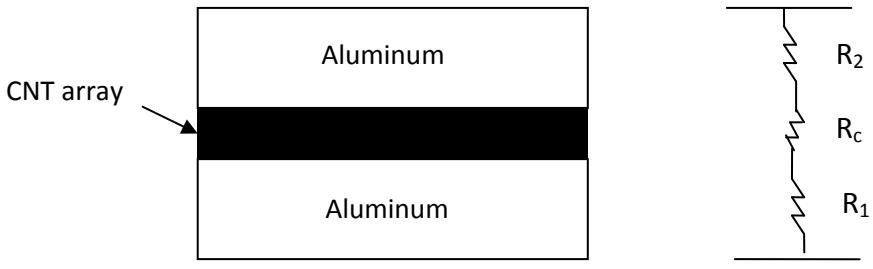

Figure 1.1 Thermal contact resistance simplified to resistors in series

$$R_1 = \frac{L_1}{k_1 A_1}, R_2 = \frac{L_2}{k_2 A_2} \tag{1.1}$$

$$R_i = \frac{R_c}{A_c} \tag{1.2}$$

$$R_{total} = R_1 + R_2 + R_i \tag{1.3}$$

The CNT array, TIM layer, has an exaggerated thickness in Figure 1.1. In reality, the thickness of the CNT array is negligible, compared to the substrates. Therefore, the array is not a third layer; it is represented as a contact with unknown thermal resistance. The 2-layer model used to calculate the contact resistance can be further described as Equation 1.4. All thermal characteristics are known for the two solid substrates and the entire sandwich assembly, allowing the Netzsch LFA 427 software to determine the unknown contact resistance between the two layers by Equation 1.5.

$$\frac{L_{tot}}{k_{tot}A_{tot}} = \frac{L_1}{k_1A_1} + \frac{L_2}{k_2A_2} + \frac{R_c}{A_c} \tag{1.4}$$

Assuming, all surface areas are equal, $A_{tot} = A_1 = A_2 = A_c$, and the thermal conductivity of the two aluminum substrates are equal, $k_1 = k_2$, and replacing the thermal conductivity, k, with its definition gives Equation 1.5 used to calculate thermal contact resistance.

$$R_c = \frac{L_{tot}}{\alpha_{tot}C_{ptot}\rho_{tot}} - \frac{2L_1}{\alpha_1C_{p1}\rho_1} \tag{1.5}$$

Interfacial thermal resistance is a measure of a materials resistance to heat flow, specifically at an interface between two solid substrates. Heat transfer by conduction is carried either by free electrons of lattice vibrational waves consisting of phonons. Conductive materials, such as metals, primarily conduct heat by free electrons. Nonconductors, such as resins or epoxies, or semiconductors, such as epoxy-infiltrated multiwall carbon nanotubes (MWCNTs), transmit thermal energy through phonons [16]. When joining metals with semiconductors or nonconductors, the relationship between surfaces and phonons is very complex. Phonons, which travel by lattice vibrational energy, are dominated by thermal conductivity expressed as Equation 1.1 [17], where C_v is specific heat, v is sound speed, and λ is the phonon mean free path (mfp).

$$k = \frac{C_v v \lambda}{3} \tag{1.1}$$

Heat transfer by phonons poses a problem at an interface, due to the inherent differences in vibrational properties of materials [18]. When two dissimilar materials meet, an acoustic impedance ($Z = \frac{p}{vS}$ where p is sound pressure and S is surface area) mismatch occurs based on the differences in a material's intrinsic properties of density and sound speed [19]. This is a very

important consideration in choosing a TIM, especially as composite TIMs consisting of metallic particles dispersed into epoxy are becoming increasingly more common.

TIMs can be found in many different mediums and material compositions. Desired characteristics of a TIM are high conductivity, conformability to surface roughness, and similar crystalline structure to the adherent substrate to prevent impedance mismatch and phonon scattering [19]. The most common are thermal greases, phase change materials, solders, and gels, as described in Table 1. High conductivity and conformability are achieved by dispersion of metallic particles, some on the nanometer scale, within polymers or adhesives [3, 7, 19]. Another candidate for a highly conductive filler within epoxy is MWCNTs, as reported values of conductivity are shown to be as high as 3000 W/mK for a single MWCNT [13]. A theoretical study by Berber *et al.* reported significantly higher values at 6600 W/mK [20] for SWNTs.

Table 1.1 Overview of common thermal interface materials

Thermal Interface Material	**Chemical Composition** [7]	**Thermal Contact Resistance R_c in an Ideal Interface (mm^2K/W)** [21]	**Advantages**	**Disadvantages**
Thermal Greases	Typically silicone matrix material with dispersed metallic particles	10	No curing process, high thermal conductivity, low viscosity to fill crevices of surface	Possible pump-out
Phase Change Materials	Typically alumina (Al_2O_3)or boron nitride (BN) fillers in epoxy, polyolefin, or low molecular weight polyesters	10	High viscosity, less pump-out, stable, no cure required	Lower thermal conductivity than greases, pressure needed with application, which increases mechanical issues
Solders	Examples are AuSn solders, InPb solders, Pure Indium	5	When heated has low viscosity allowing material to flow across entire surface, high thermal conductivity	Reacts with copper to form intermetallic compounds that reduce thermal conductivity
Gels	Typically Al, alumina (Al_2O_3), Ag in silicone, olefin matrices	8	Mechanically resilient, pure, electrical resistance	Degrade at high temperatures, curing process needed

This project, supported by the Carbon Group at the University of Kentucky Center for Applied Energy Research (UK CAER), investigated the potential use of multiwall carbon nanotubes (MWCNTs) to fill voids within heat producing components for more conductive heat flow, a common thermal management issue.

1.3 Outline

The project objective was to produce and characterize MWCNT arrays for interface application. The arrays (“dry”, un-infiltrated and infiltrated) were grown by chemical vapor deposition (CVD),

as described in Andrews *et al*. [22-23]. One area of focus was to produce single-piece (3" x 36") polymer infiltrated multiwall carbon nanotube arrays, tailored for application as thermally conductive film adhesive thermal interface material (TIM). The other area of focus was to harvest intact, un-infiltrated, or dry, MWCNT arrays. This route offered more flexibility toward the final TIM, enabling downstream processing, including surface modification, metal sputter coating, and infiltration with conductive materials. Both infiltrated and un-infiltrated arrays were successfully harvested in 3" x 36" intact sections by a novel approach, and sections of the free-standing arrays were directly sandwiched between two aluminum 6061 discs to simulate a typical interface. The application of our MWCNT arrays as TIMs is for the installation of the array between carbon fiber/epoxy composites and heat spreaders and also between integrated circuit components. All thermal tests were conducted between the aluminum because the properties of Al 6061 are widely known and homogenous; thermal diffusivity and thermal contact resistance are calculated based on parameters of the substrate assuming homogeneity [24-25].

The MWCNT arrays infiltrated with thin-film epoxy and subsequently harvested as a conductive film adhesive and tested for thermal performance in TIM applications by LFA are described in Chapter 2. The "dry", un-infiltrated MWCNT arrays also possess adhesive properties, albeit with lesser adhesive forces compared to adhesive-infiltrated arrays. Other works characterize dry MWCNT arrays as dry adhesives [26] that essentially adhere to contact points for heat transport through interfaces. "Dry" MWCNT arrays with applied pressures are also widely investigated in interface applications as TIM materials [6, 14, 27-28] and characterized here in Chapter 3. The development of MWCNT arrays is a complex process with numerous parameters that can be controlled during the synthesis process. One of the challenges for this project was balancing the synthesis parameters and implementing refining techniques to achieve the optimal MWCNT array suitable for TIM applications.

1.4 Review of Literature

Unique properties of carbon nanotubes (CNTs) have increased interest in them as a multi-functional material in many different industries and mediums. They possess exceptional mechanical [29], electrical [30], and thermal [20] properties. This work investigates CNTs for their remarkable thermal properties for the installation within a thermal interface application where small, light-weight, and extremely conductive materials are preferred.

1.4.1 Carbon Nanotubes

The unique properties of CNTs are related to their helical structure and high aspect ratio. The ideal nanotube is a single walled carbon nanotube (SWNT), shown in Figure 1.1. It is a sheet of carbon atoms arranged hexagonally (known as graphene) rolled into a cylinder [20, 31-33]. Multiwall carbon nanotubes (MWCNTs) are composed of SWNTs nested within each other, as illustrated in Figure 1.2. MWCNTs were synthesized for use in this work, due to the simpler, more easily reproducible process.

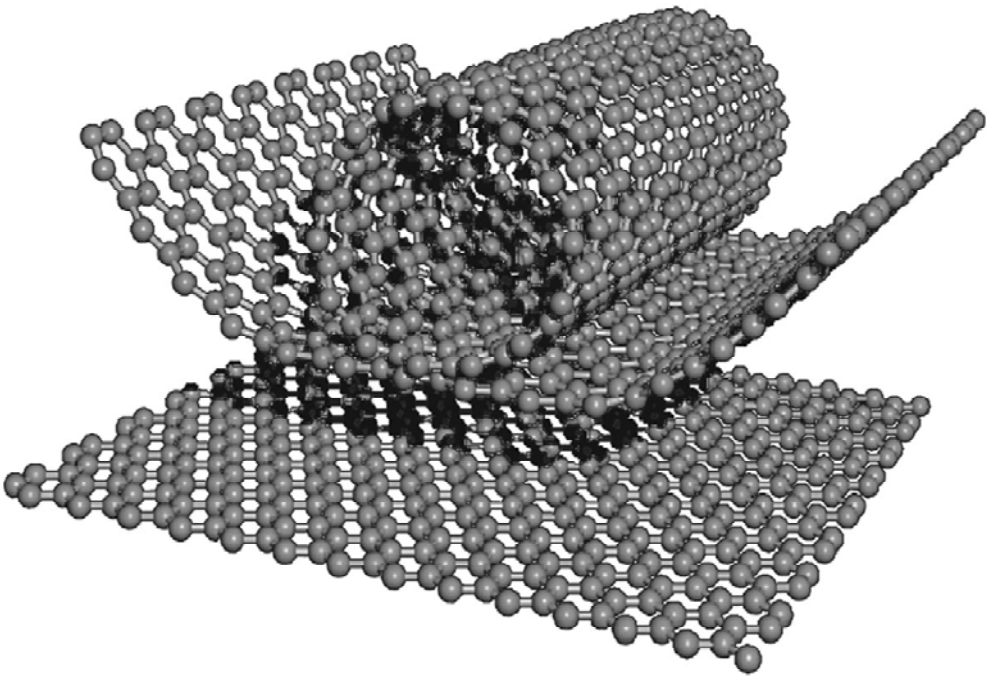

Figure 1.2 Structure of NT on the atomic level [33]

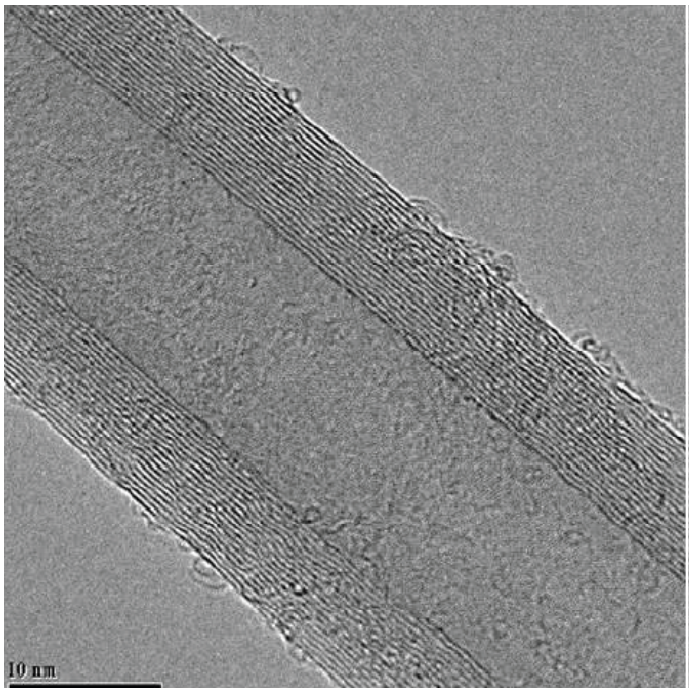

Figure 1.3 Image of (~30 nm diameter) MWCNT structure by transmission electron microscopy (TEM)

The hexagonal arrangement of very strong sp^2 bonded carbon atoms (graphene) are what give CNTs their amazing strength and thermal conductivity [34]. NTs possess a Young's modulus of 1 TPa, stronger than steel at 100 GPa modulus [29]. The stiff arrangement also results in a high speed of sound and, subsequently, a high thermal conductivity. Interestingly, one of the best thermal conductors, diamond, is held together by sp^3 bonds, which are weaker than graphite sp^2 bonds [20]. As referenced previously, the thermal conductivity dominated by phonon transport is expressed as Equation 1.1, proportionally relating thermal conductivity to sound speed. Phonon velocity along the axis of a SWCNT can be as high as $2x10^5$ m/s [35] due to the strong sp^2 bonds.

CNTs higher thermal conductivity (3000-6600 W/mK [13, 20, 31]), compared to graphite and diamond, can be attributed to the larger phonon mean free path (mfp) through the length of the nanotube. High aspect ratio, single walled carbon nanotubes have the highest phonon mean free path and, in turn, the highest thermal conductivity at 6600 W/mK [20]. The values of thermal conductivity found for a single NT, are significantly higher than the experimentally observed conductivity found for bulk NTs in the form of MWCNT arrays recorded at 20 W/mK [31] - 75 W/mK [36]. The interlayer coupling between graphene sheets and between other

CNTs encourages phonon scattering at the interaction points where the mean free path is interrupted.

The extraordinary mechanical properties of multiwall carbon nanotubes (MWCNT) has spurred much interest in their use as reinforcing agents in various matrices [32, 37]. The high surface area to volume allows for a greater adhesion to the surrounding polymer matrix for a more robust and stiff composite. Essentially CNTs are an alternative to carbon fiber, with low transverse thermal conductivity at 8 W/mK [32] and inferior mechanical properties (Young's Modulus of 220-580 GPa [32]), in typical composite applications.

1.4.2 Free Standing MWCNT arrays

Mixing NTs with adhesives to utilize their unique properties on a practical, large-scale is a complex issue. When MWCNTs with thermal conductivities of 3000 W/mK [13] are coupled with adhesives of low conductivity (0.3 W/mK [18] or 0.2 W/mK [7]), an acoustic impedance mismatch is created due to the difference in density and sound speed between the two materials [38]. Therefore, simply mixing NTs with adhesive (eg. dispersion techniques such as high-shear melt mixing [39]), results in very low improvements in thermal conductivity of about 0.7 W/mK [13, 40-41]. Translating the phonon transport capabilities of NTs into a functional composite form is under investigation in this work. Vertically aligned nanotubes seem to be a very probable solution to harnessing the conductivity of the NT in a useful, composite form.

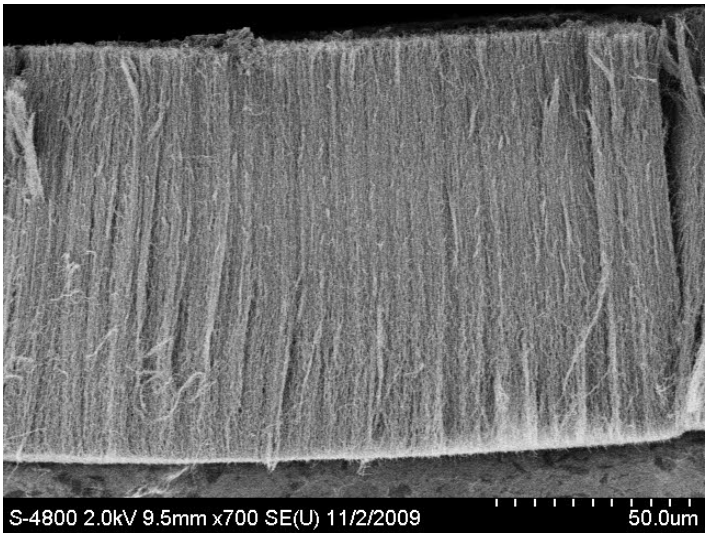

Figure 1.4 Cross sectional view of MWCNT array

Vertically oriented CNT arrays (Figure 1.3) are ideal in thermal interface applications because CNTs posses this superior thermal performance along their axis. The MWCNTs highly aligned geometries create a lengthy mean free path (mfp), which is the distance a phonon travels between scatterings, for exceptional phonon transport capabilities [42]. Most phonons have various wavelengths and frequencies; however the phonons that are carrying most of the heat are large waves with a mfp between 1-100nm [19]. The high frequency phonons travel better though materials with high Young's modulus, E. Within a dispersion of NTs in epoxy, the high frequency phonons that are travelling through nanotubes attempt to propagate to the epoxy, with significantly smaller Young's moduli and the path is interrupted, resulting in scattering at an interface [19]. When MWCNTs are oriented into highly aligned arrays perpendicular to adherent surfaces, they are inherently positioned to transport heat via high frequency phonons along their axis. However the values of conductivity found for MWCNT arrays are around 74-83 W/mK [36], far from the thermal conductivity found for one single NT (3000-6600 W/mK [13, 20]). The array in actuality has many defects within the NTs, a possibility of CNT ends capped by epoxy, and many nanotube interactions, thus increasing phonon scattering. There is much area for improvement in optimizing the arrays to take advantage of the exceptional thermal conductivity of CNTs.

Most of the current research on MWCNT arrays for thermal management, involves a small scale growth via the CVD method on the substrates—carbon fiber composites [43-44], copper substrate [45], silicon wafers [14, 46], metal foil [6], glass [15], and silicon substrate [47]. However, some adherent surfaces, such as integrated circuit boards, cannot be exposed to the operating temperatures in the CVD chamber required for NT synthesis. Also, in the case of carbon fiber composite adherents, the parameters of CVD synthesis affect the mechanical and morphological properties of the fiber [44]. For such applications, the arrays must be free from the growth substrate in a single, unbroken piece for direct installation. Thus, crude harvesting techniques are also employed to rid the array of the growth substrate for redistribution. These techniques, commonly on a small scale, either involve razor blade extraction of the NT array from the substrate [12] or etching techniques to release the adhesive from the adherent [10, 18]. Our group at the University of Kentucky successfully developed a novel method to harvest 3" x 36" sections (Figure 1.4) that can be directly applied to any commercial applications.

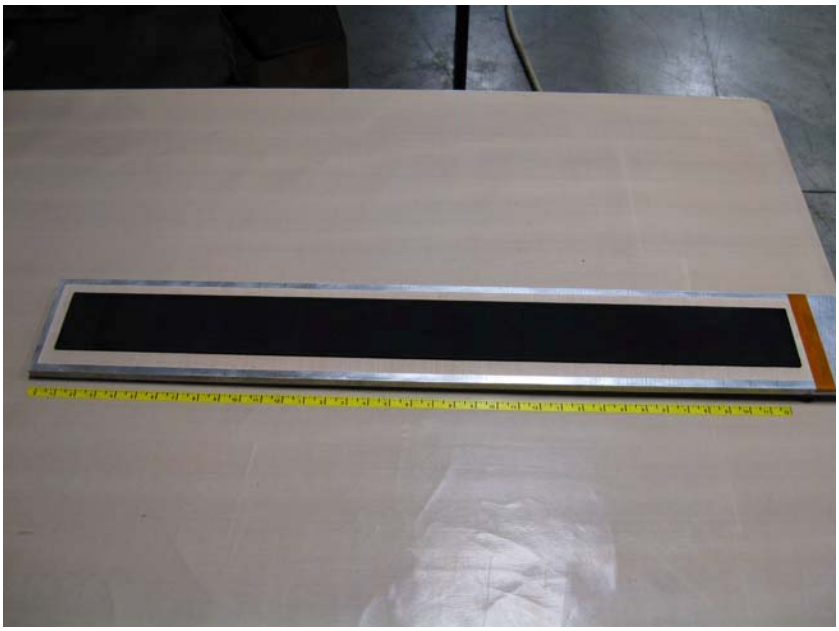

Figure 1.5 3”x36” section of MWCNT array

1.4.3 Transition Zone

There are many optimization techniques that are widely used for decreasing phonon scattering, and ultimately decrease resistance to heat through the interface. One very common approach is to remove any amorphous material on the top of the array to expose nanotube tips. This can be accomplished via reactive ion etching [48] or plasma etching [18, 46]. Ensuring the nanotubes make good contact with the substrate will ensure a thermal pathway for high frequency phonons to carry heat between the nanotubes to the adherent.

Another technique utilized to increase the adhesion to the interface surfaces is known as establishing a conductive transition zone (TZ). The difference in vibrational energy between nanotubes and adherents causes an acoustic impedance mismatch and potential phonon scattering can occur at this interface. Introducing a conductive transition zone here, with similar crystalline structure to the CNTs and the substrates, ensures a reduction in impedance mismatch. A transition zone is commonly created by evaporating gold onto the nanotube tips [18, 48], oxidizing the NTs to metalize the tips, or other chemical modifications that enhance adhesion [49]. Ganguli *et al* [48] infused MWNTs in epoxy and, in order to reduce phonon scattering between the nanotube tips and substrate, gold was thermally evaporated on the surface of the array. They measured thermal conductivity values of 262 W/mK across the interface, which is a drastic improvement over the interface with no MWCNTs (1 W/mK). In all

cases improving adhesion to the substrate, reducing phonon scattering by ensuring the mating of the nanotubes to the substrate, and the addition of a conductive transition zone resulted in an improvement in thermal transport properties.

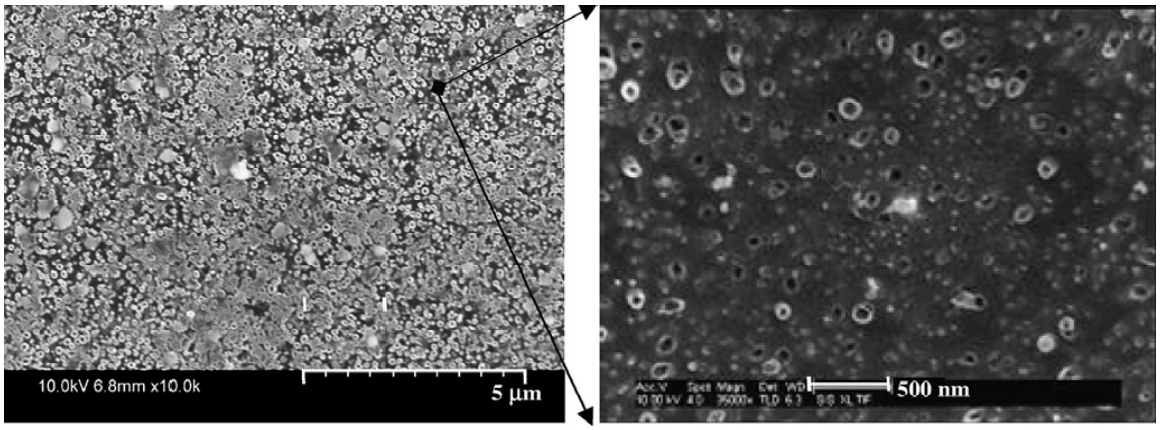

Figure 1.6 SEM images of the top view of an array after 32 watt RF oxygen plasma etching for 30 minutes taken from S. Sihn *et al* [18]

1.4.4 Thermal Performance of MWCNT arrays

Xu and Fisher [14] reported dry arrays reduced thermal interface resistances down to 19.8 mm^2K/W with a pressure of 445 kPa (65 psi). The addition of phase change material (PCM) to the dry MWCNT array generated resistance values down to 5.2 mm^2K/W. CNT interfaces were thermally characterized by Xu *et al.* [50] using a photothermal method. The interfaces possessed thermal contact resistances of around 12-16 mm^2K/W. Cola *et al.* [27-28] measured, by a photoacoustic technique, thermal resistance values down to 8 mm^2K/W with an applied pressure of 350 kPa (50 psi) for a silicon-CNT-gold interface. Cola *et al.* [51] also measured, using the same photoacoustic technique, contact resistances of interfaces of two CNT arrays at moderate pressures down to 4 mm^2K/W. The contact resistances values are competitive with gels and thermal greases currently used within integrated circuits at 8 mm^2K/W and 10 mm^2K/W, respectively [21].

The other scope of research for MWCNTs in TIMs application involves infiltrating with polymers possessing adhesive properties to sandwich between two surfaces and achieve a bonded joint. When MWCNT arrays are coupled with low thermal conductivity epoxy (~0.3 W/mK [18]) the arrays are sacrificing a loss in thermal properties for the sake of adhesive properties. This is due to the impendence mismatch between CNTs and epoxy [5]. Reported in the previous section, Ganguli *et. al* [48] infiltrated epoxy in MWNTs and, in order to reduce phonon scattering both

between the nanotubes and the surrounding matrix and the CNT tips and substrate, gold was thermally evaporated on the surface of the array. The metalized nanotube tips produced thermal conductivities of up to 262 W/mK. Sihn *et al.* [18] measured thermal conductivities of the adhesive joint composed of conductive graphite sheets sandwiching MWCNTs infiltrated with polymer adhesive. The CNT tips were plasma-etched to reveal any tips capped by the polymer and a layer of Au was evaporated onto the surface of the array. They achieved thermal conductivities up to 250 W/mK. Both show improvements on orders of magnitude over a joint bonded by just epoxy possessing through-thickness thermal conductivity of < 1 W/mK [18, 48].

1.5 Conclusion

Multiwall carbon nanotubes, discovered by Iijima in 1991 [52] are one of the most unique and multi-functional materials. They possess extremely high thermal conductivities, are light-weight, are mechanically resilient, operate at high heat loads, and survive in torturous environments [53]. These properties, along with thermal interface material research, suggest that MWCNTs are a very promising candidate for a TIM that meets increasing demands in heat conduction.

When MWCNTs are grown in highly aligned, anisotropic arrays, they are inherently at the ideal orientation to conduct heat through the axis of the nanotubes. When sandwiched between a heat generator and heat sink (i.e., perpendicular to the surfaces), heat conduction, dominated by phonon transport through ideally defect-free and vertically aligned CNTs, is orders of magnitude more effective compared to polymer adhesives or purely air.

There are also many advantages to MWCNT arrays compared to phase change materials, greases, and even solder. CNTs are less dense and receptive to modifications and improvements [50]. Surface modification and metallic coatings dramatically reduce thermal insulation. Synthesis parameters can control the quality of NTs within the array governed by the magnitude of defects and amorphous carbon. Our modifications are outlined in Chapter 4 titled Refined Techniques to Purify and Improve the Use of MWCNTs as TIMs. This work shows that MWCNT arrays have the ability to create interface materials with required thermal performance of an exceptional TIM.

Chapter 2 Adhesive Infiltrated Multiwall Carbon Nanotube Arrays as Thermal Interface Materials

2.1 Introduction

Carbon nanotubes inherently possess exceptional mechanical, electrical, and thermal properties. These unique properties make them a great candidate for incorporating CNTs into composite materials. Combining CNTs with polymer matrices create applications for adhesives that were previously unattainable by unmodified or common composite polymer matrices. Commercial TIMs and adhesives mentioned in Chapter 1 used in the electronics and aerospace industry are not meeting increasing thermal budget requirements [2]. Replacing current metallic fillers with vertically aligned CNT arrays with significantly higher conductivity is under investigation in this work.

The MWCNTs were grown on a quartz substrate using chemical vapor deposition (CVD) [23] and a proprietary, novel method of harvesting the arrays from the quartz substrate forming free-standing arrays was employed. Most research involving MWCNT arrays as TIMs, as discussed in Chapter 1, are limited by the attachment of the array to the growth substrate; the array only has one side available for bonding [6, 14-15, 43-47]. Our CNT free-standing arrays, with both upper and lower CNTs exposed, can be directly useful to industry and engineering applications.

2.2 Experimental

Laser flash apparatus (LFA Netzsch 427) thermal tests of CNT arrays were performed to demonstrate the thermal performance of the material under conditions in an actual interface. Aluminum 6061 was chosen as the material to sandwich-bond arrays under constant heat and pressure. Discs of 12.7 mm (0.5 inch) diameter and 3.12 mm (0.125 inch) thick were machined from aluminum sheets with a mirror polished and a mill finish side (r_A = 0.643 μm). To replicate an actual interface, mill finish surfaces were bonded together using epoxy-infiltrated MWNT array TIM. The best suited TIM is a material that conforms to the interface surface voids in the substrate for a more continuous heat flow [54].

2.2.1 Carbon Nanotube Synthesis

The MWNTs were grown on a quartz substrate using a chemical vapor deposition (CVD) process in order to achieve a controlled diameter and quality for uniform coverage [11]. The nanotubes

were grown normal to the substrate surface in 3" x 36" sections. The catalytic decomposition of a ferrocene–xylene mixture was fed through a capillary tube at 175 °C, which is a temperature above the boiling point for xylene (140 °C) and below the decomposition temperature of ferrocene (190 °C). Ferrocene was chosen as an effective precursor for iron (Fe), which is a catalyst for carbon nanotube growth. The vapor was then swept across a quartz substrate in a furnace at a temperature of approximately 800 °C. Various parameters were optimized such as feed rate and temperature to aid in the growth of high quality carbon nanotubes [55]. The resulting lengths of the grown nanotubes were between 50-100 µm. Combined with the average outer diameter of 30 nm, the aspect ratio of a single MWCNT within the array was approximately between 1,600 and 3000. This high aspect ratio, allows the MWCNT to fit into the crevices of surface imperfections, ideal for a TIM [35]. However, longer MWCNT lengths have more opportunity for defects that create phonon scattering and reduce the thermal transport capabilities. A study by Garcia *et al.* [56] at MIT found the optimal length of a carbon nanotube aligned perpendicular to prepreg-based carbon fiber composites, is approximately 20 µm. The paper also addresses the difficulty in attaining this length, and used 60–150 µm long CNTs in the study.

There are many parameters to consider when synthesizing MWCNT arrays and the difficulty is controlling the delicate balance between these parameters, while obtaining continuous arrays for large, commercial applications. The packing of MWCNTs within an array is an important parameter to consider for heat transfer applications [57]. The average MWCNT areal packing factor was approximately 16 %. This is consistent with other research by Baratunda A. Cola *et al.* [9] who observed a 15 % packing factor and by Jun Xu [58] who observed 1 % to 22 % volume ratios of MWCNTs to air. The substrates were weighed before and after the runs to gravimetrically determine the approximate number of nanotubes on the slide. From this, areal densities were calculated between 2.0-3.5 mg/cm^2 (0.3-0.35 g/cc bulk densities). Assuming a hexagonal orientation of the MWCNTs, as shown in Figure 2.1, the packing factors are calculated. The maximum amount of NTs per area is calculated based on Equation 2.1, where h is found from Figure 2.1 and NT characteristics. From the mass on the slide, the areal density and packing factor is calculated. The 16 % packing factor can be observed in the SEM image of a MWCNT array produced by our CVD method in Figure 2.2. Most of the volume is air, not particularly good for thermal conduction, but allows volume for epoxy or polymers to infiltrate within the array and create adhesive arrays.

$$A_{hex} = \frac{3h^2\sqrt{3}}{2} \tag{2.1}$$

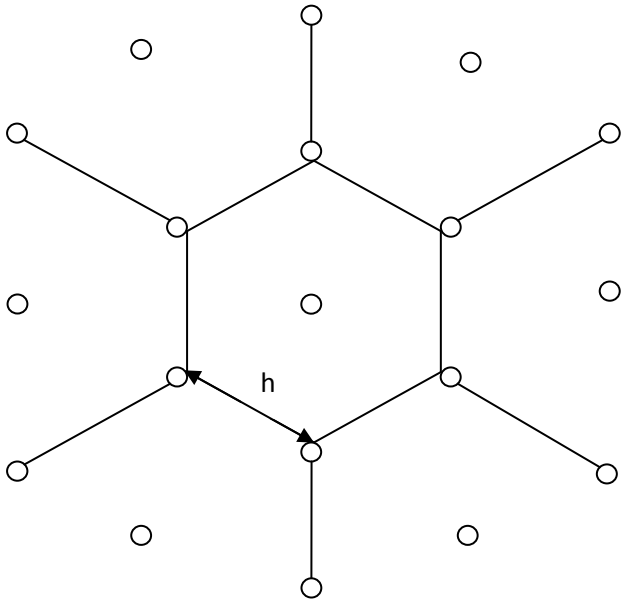

Figure 2.1 Theoretical hexagonal orientation of MWCNTs from an aerial view

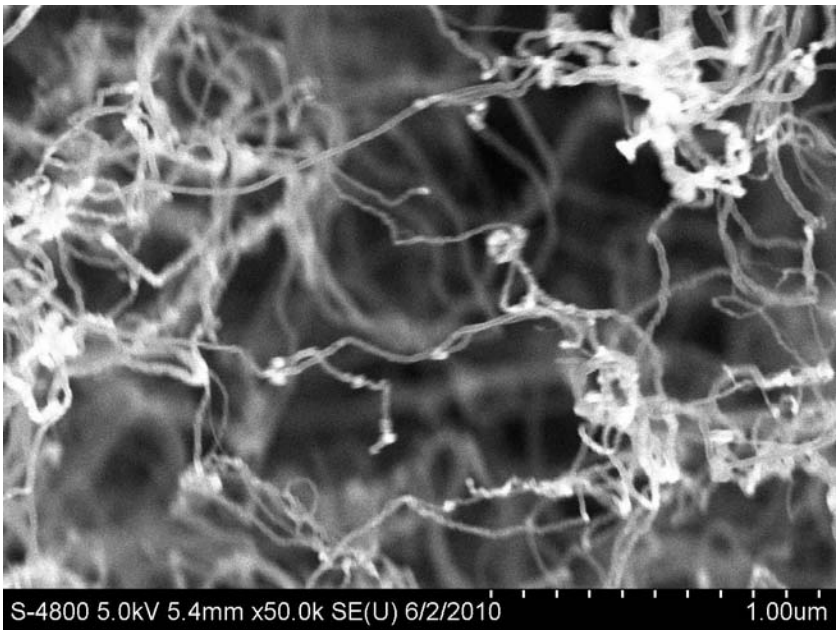

Figure 2.2 SEM image of MWCNT array; notice the array is mostly composed of air (~85 vol. %)

2.2.2 Polymer Infiltration

Three different polymers were infiltrated into the MWCNT arrays designated SR-4-3 thin-film epoxy (Epoxy 1), RMC 0138 (Epoxy 2), and a Cyanate Ester thin adhesive film. A homogenous infiltration was achieved by capillary-driven wetting using typical vacuum-bag curing processes [59]. The arrays were then harvested from the quartz substrate as free-standing arrays, allowing the array to be bonded on both sides by the aluminum discs. The free-standing array was sandwiched between two Al 6061 discs bonded at 75psi at 150C for 2 hours. Figure 2.3 shows the side view of a bonded Al sandwich, taken after the sample was coated with spray graphite.

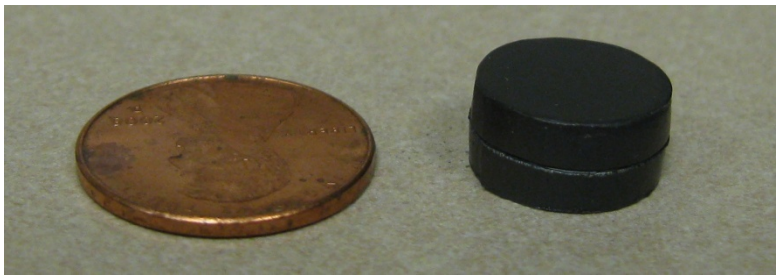

Figure 2.3 Side view of MWCNT array bonded Al 6061 (0.5" diameter) sandwich

The overall goal was to achieve an even, homogenous infiltration of the polymer through the MWCNT array without capping over the upper and lower MWCNT tips with any polymeric layers. Work by T. Borca-Tasciuc [60] found that MWCNT arrays less than 150 µm in thickness are more likely to be evenly infiltrated completely through the thickness. Our arrays 50-100 µm were, by this standard, ideal candidates for infiltration. However, if the array is over-infiltrated, the CNT tips will not achieve contact with the aluminum substrate for adequate phonon transport through the system. We successfully infiltrated the arrays with epoxy, demonstrated by the nanotube tips appearance in Figure 2.4. The tips are not capped by polymeric material; therefore they will adequately reach and adhere to the substrate for heat transfer through the tips.

The SEM image in Figure 2.4 does not reveal a noticeable layer of epoxy sitting on the top of the array. To accurately determine the thickness of the resin layer, a transition electron microscopy (TEM) could be employed. However, the resin thickness is not visible in the SEM images; therefore they theoretically have thicknesses in the nm range. To explore the effect that epoxy could have upon the thermal resistance between the nanotube tips and the aluminum

substrate, calculations of thermal resistance for a 10 nm, 100 nm, and a 10 µm layer of resin (L) are shown in Table 2.1. A thermal conductivity of 0.3 W/mK represented each resin layer and they possessed thermal contact resistance (R_c=L/k) at values of 0.03, 0.33, and 33.3 mm^2K/W for the 10 nm, 100 nm, and 10 µm, respectively. The contact resistance of the resin on the nm scale and are on orders of magnitude lower than the contact resistance of MWCNT arrays (~10 mm^2K/W). A resin layer in the µm range would, however, have a significant effect on the thermal resistance of the NT array TIM. This thickness of the infiltrant would be visible via SEM imaging, however. Therefore, the thicknesses of resin in the nm-range on the tips of the arrays do not significantly affect the thermal performance of the infiltrated array.

Table 2.1 Thermal resistance of epoxy layers on NT array

k (W/mK)	L (nm)	Rc (mm^2K/W)	R (K/W)
0.3	10	0.03	0.00026
0.3	100	0.33	0.0026
0.3	10000	33.3	0.26

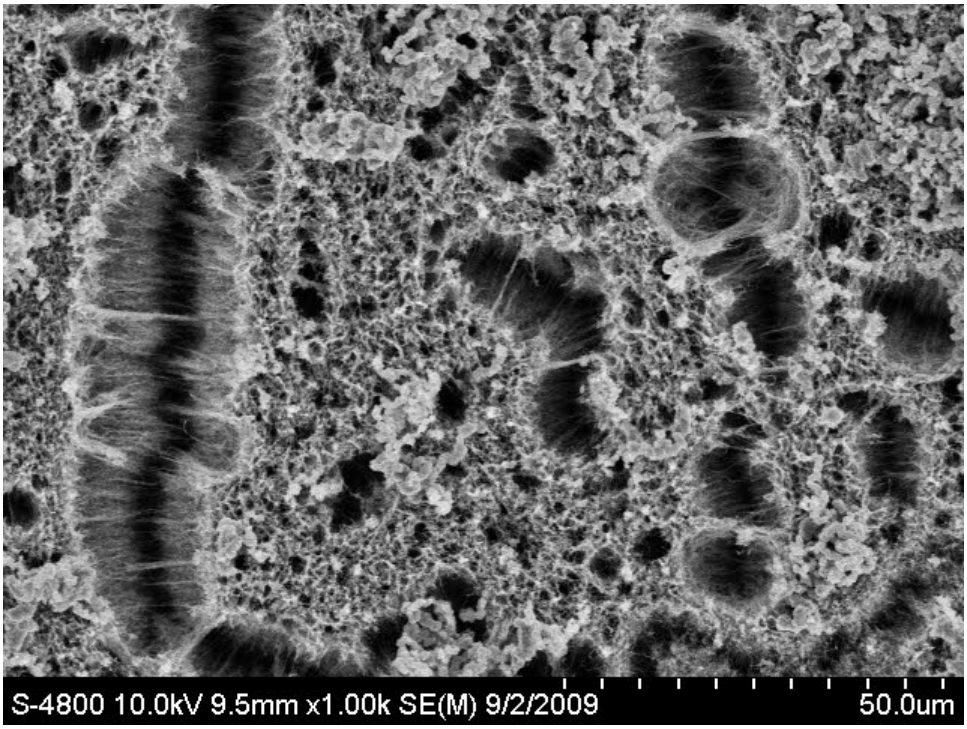

Figure 2.4 View looking normal to growth substrate of a MWCNT array infiltrated with epoxy

The arrays, designated MWCNT followed by the infiltrant and the fabrication number, and the corresponding NT areal density, packing factor, weight percent (wt. %) epoxy, exothermic curing

heat, and normalized exothermic heat of curing, which is the array's heat of curing normalized to the epoxy infiltrant's heat of curing and the wt. % epoxy, are described in Table 2.3. The weight percent of polymer infiltrated into the MWCNT arrays was determined gravimetrically by a Thermogravimetric Analyzer (TGA, TA Instruments Q500). The exothermic curing heat was determined using a Differential Scanning Calorimeter (DSC, TA Instruments Q100).

Table 2.2 Array properties of epoxy-infiltrated MWCNT arrays

Sample	NT Areal Density (mg/cm^2)	NT bulk density (assuming 100 micron length) (g/cc)	Packing Factor (% of Max NT/ cm^2)	TGA wt. % Epoxy (Ave.)	DSC Exothermic Curing Heat (J/g) (Ave.)	Normalized Exothermic Heat of Curing (Ave)
MWCNT - Epoxy1 - 43	3.40	0.34	18	44.04	83.95	75.73 %
MWCNT - Epoxy1 - 44	3.16	0.32	16	30.31	64.20	84.15 %
MWCNT - Epoxy1 - 45	3.28	0.33	17	35.06	58.15	65.90 %
MWCNT - Epoxy2 - 69	2.43	0.24	13	38.02	106.23	79.94 %
MWCNT - Cyanate Ester - 71	2.79	0.28	14	43.83	85.04	63.59 %

The multilayer systems that were compared to the array sandwiches include two stacked aluminum discs with no adhesive, baseline polymers of Epoxy 1, Epoxy 2, Cyanate Ester, Hysol EA 9396, commercial adhesives of Aavid Ther-O-Bond 1500 (TOB 1500), TOB 1600, TOB 4949, Arctic Silver (2 part thermal adhesive), Arctic Alumina (2 part thermal adhesive), Chomerics T412DST (double-sided thermally conductive tape), and silver-filled epoxy resin (~22 vol. % silver).

2.2.3 Bonding Adhesive MWCNT arrays to aluminum substrate

The development of epoxy-infiltrated MWCNT, in view of the importance of adhesion, ensures better contact to the mating surfaces. Wei Lin *et al*. [49] improved conductivity by 2 orders of magnitude and improved adhesion with the addition of a molecular phonon coupler, which is a formulation of chemicals used to bond the NT array to its opposing substrate for enhanced phonon transport. A van der Waals force dominated adhesion has interfacial strengths at < 0.05 MPa. Lin found, through die shear tests, the interfacial strengths of the assembly were 0.23-0.36 MPa. The large improvement in conductivity was related to this improved adhesion.

The epoxy-infiltrated MWCNT array bonded to the aluminum substrate is shown in Figure 2.5. The top two pictures were the designated "cut side", which is the side of the array cut from the

quartz slide. The “top side” is the top of the array where carbon is continuously deposited onto the quartz substrate. The cut side displayed much better contact with the substrate. The best phonon transport is through the tips of the NTs, which were clearly reaching, and appear to be adhered to, the aluminum. The pictured top side on the bottom of the figure reveals a layer of amorphous carbon present preventing the MWCNT tips from reaching the aluminum substrate. The amorphous carbon served as an insulating layer. The difference in the crystalline structure of the nanotube, amorphous carbon, and aluminum was, most likely, a source for phonon scattering [19]. Further characterization, possible sources for amorphous carbon and subsequent “cleaning” of the array are explained in detail in Chapter 4.

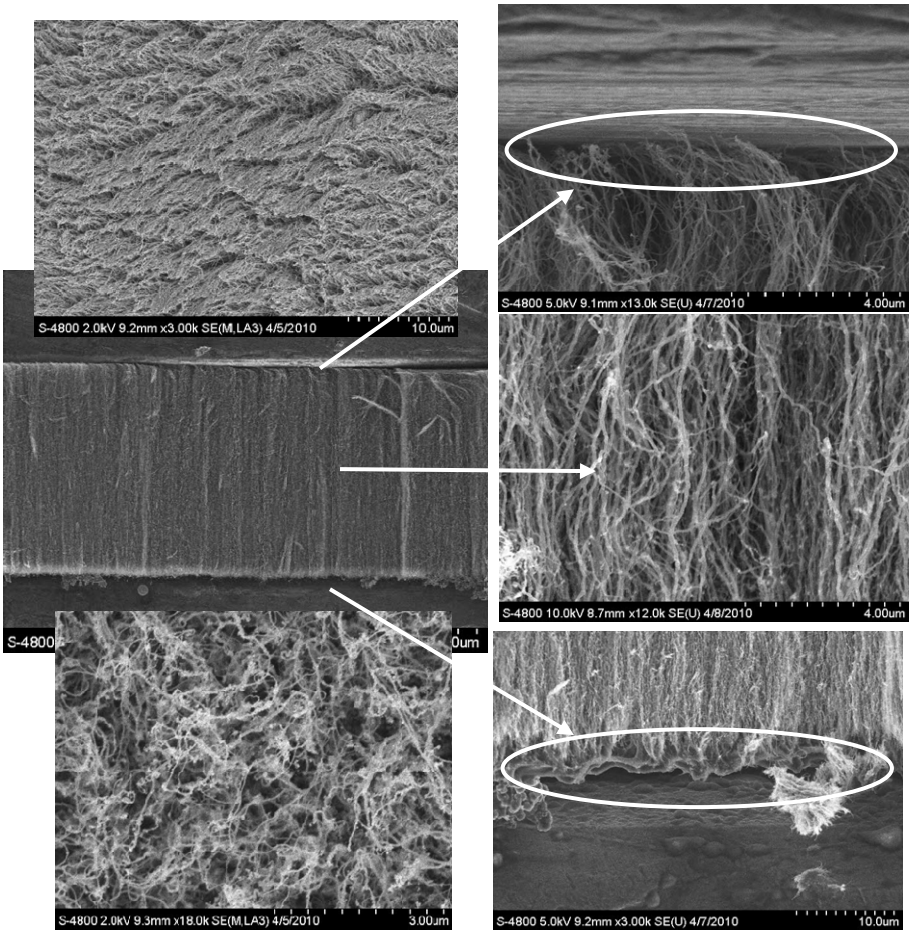

Figure 2.5 SEM image of the side view of MWCNT demonstrating contact mechanics of the array to the aluminum substrate; notice the cut side (pictured at the top) had good contact and the top side (pictured at the bottom) had poor contact.

2.2.4 Thermal Testing

The thermal diffusivity was found for the aluminum sandwich samples with and without thermal interface material using a modern laser flash apparatus Netzsch LFA 427. A model of the set-up is shown in Figure 2.6.

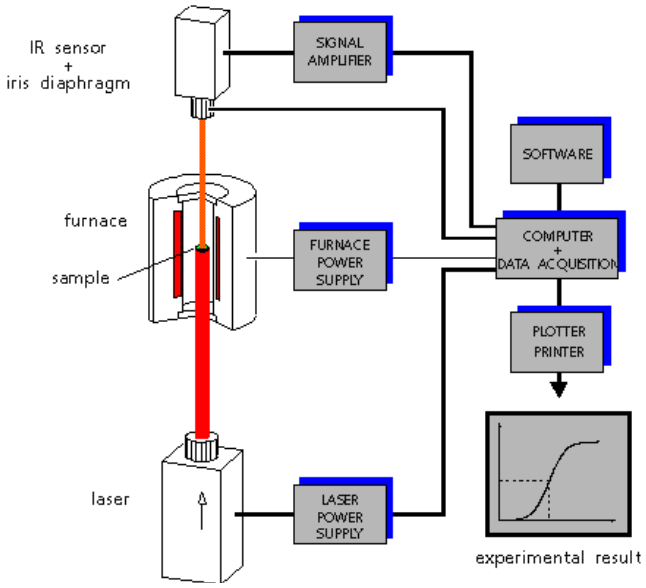

Figure 2.6 LFA 427 simplified model

Samples were mounted in the LFA furnace chamber. A laser pulse of 0.5 ms and 450 V was used to irradiate the bottom surface of the sample. The samples were coated with spray graphite to optimize energy absorption from the laser beam and to minimize reflection of the aluminum surface. The heat diffused through the sandwich system and the infra red detector measured the temperature at the top surface, as seen in Figure 2.7, as a function of time. The temperature rise reached equilibrium in a very short time as seen in Figure 2.8. The thermal diffusivity is determined using

$$\alpha = \frac{0.138L^2}{t_{1/2}} \tag{2.1}$$

Where $t_{1/2}$is the time where the temperature rise reaches half of the maximum value and L is the sample thickness.

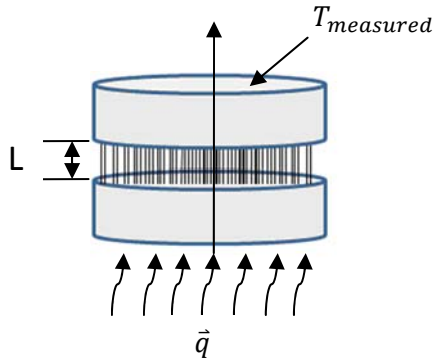

Figure 2.7 Heat transfer through sandwich assembly

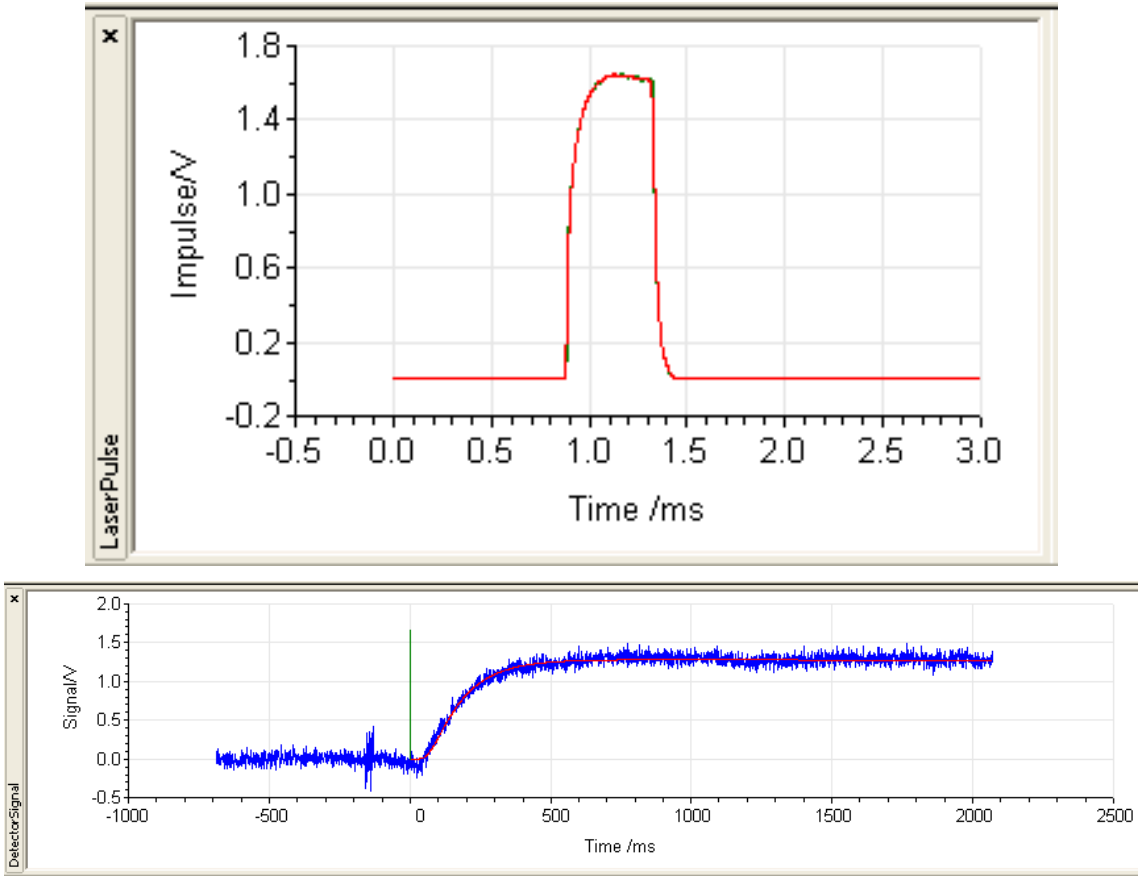

Figure 2.8 Laser pulse upper and detector signal lower from the Netzsch LFA 427 analysis software

The LFA calculated diffusivity and thermal contact resistance with derived equations for conduction in transient heat transfer. Radiation was neglected because the temperature differences and maximum temperatures (< 300 °C) are not high enough and convection is also inapplicable [61]. To determine why convection can be neglected, scaling analysis of air trapped

in a cavity created by contacting two aluminum surfaces is used to calculate a Rayleigh (Ra) number. The Ra number is a dimensionless number that determines whether heat transfer is dominated by conduction or convection. There is a critical Ra number (Ra_c = 300 in this case), above which there is convection and below which no convection. The Ra number can be a combination of two different numbers—Sa number and Fourier (Fo) number.

$$Fo = \frac{heat\ conduction}{heat\ accumulation} = \frac{\alpha t}{l^2} \tag{2.2}$$

$$Sa = \frac{bouyancy\ force}{viscous\ force} = \frac{\rho l^3 g}{\mu l v} \tag{2.3}$$

Where α is diffusivity, t is characteristic time, l is the interface length, ρ is density, g is acceleration due to gravity, μ is viscosity, and v is velocity. Each of these characteristics for the air trapped between two aluminum surfaces is described in Table 2.3. The Ra number is 100, which is well below the critical number of 300, therefore convection can be neglected.

Table 2.3 Rayleigh number calculation to determine the influence of convection

chracteristic length (cm)	characteristic time (s)	diffusivity (cm^2/s)	g (cm/s^2)	Sa	Fo	$Ra = \frac{Sa}{Fo}$
0.1	1	0.1	1000	1000	10	100

The LFA measures the diffusivity based on "pulsed" heat conduction, where the initial temperature distribution within a thermally insulated solid of uniform thickness L is T(x, 0). The temperature distribution at any later time, t, is given by [62]

$$T(x,t) = \frac{1}{L}\int_0^L T(x,0)dx + \frac{2}{L}\sum_{n+1}^{\infty} exp\left(\frac{-n^2\pi^2\alpha t}{L^2}\right) * cos\left(\frac{n\pi x}{L}\right)\int_0^L T(x,0)cos\left(\frac{n\pi x}{L}\right)dx \tag{2.4}$$

If a radiant pulse, q (J/cm^2) is instantaneously and uniformly absorbed at the small g at the front surface (x = 0) of a thermally insulated solid of uniform thickness L (cm), the temperature distribution at that instant is

$$T(x,0) = \frac{q}{\rho C_p g}\ for\ 0 < x < g\ and\ T(x,0) = 0\ for\ g < x < L \tag{2.5}$$

So the temperature at time t is defined as

$$T(x,t) = \left[\frac{1}{L}\int_0^g \frac{q}{\rho C_p g}dx + \frac{1}{L}\int_g^L 0dx\right] + \frac{2}{L}\sum_{n+1}^{\infty} exp\left(\frac{-n^2\pi^2}{L^2}\alpha t\right) * cos\left(\frac{n\pi x}{L}\right)\left[\int_0^g \frac{q}{\rho C_p g} cos\left(\frac{n\pi x}{L}\right)dx + \int_g^L 0 \cdot cos\left(\frac{n\pi x}{L}\right)dx\right] \quad (2.6)$$

$$T(x,t) = \frac{1}{L}\frac{q}{\rho C_p}\left[1 + 2\sum_{n+1}^{\infty} exp\left(\frac{-n^2\pi^2}{L^2}\alpha t\right) cos\left(\frac{n\pi x}{L}\right) sin\left(\frac{n\pi g}{L}\right)\frac{L}{n\pi g}\right] \quad (2.7)$$

Since g is very small, $sin\left(\frac{n\pi g}{L}\right) \approx \frac{n\pi g}{L}$ and at x=L $\sum_{n+1}^{\infty} cos(n\pi) = \sum_{n+1}^{\infty}(-1)^n$, then

$$T(L,t) = \frac{q}{\rho C_p L}\left[1 + 2\sum_{n+1}^{\infty}(-1)^n exp\left(\frac{-n^2\pi^2}{L^2}\alpha t\right)\right] \quad (2.8)$$

Introducing two dimensionless parameters V(L, t) and ω, where T_{max} is the maximum temperature at the rear surface, as defined as

$$V(L,t) = \frac{T(L,t)}{T_{max}} \quad (2.9)$$

$$\omega = \frac{\pi^2 \alpha t}{L^2} \quad (2.10)$$

So (2.11)

$$V = 1 + 2\sum_{n+1}^{\infty}(-1)^n exp(-n^2\omega)$$

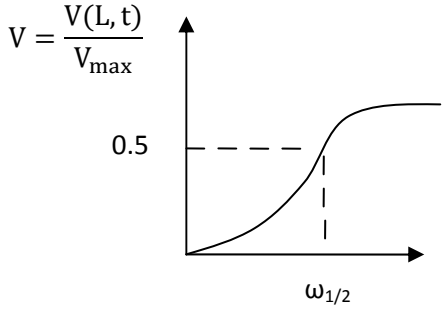

Figure 2.9 Detector signal vs. time represented as dimensionless parameters V and ω

For $V = \frac{1}{2}$, $\sum_{n+1}^{\infty}(-1)^n exp(-n^2\omega) = -\frac{1}{4} \rightarrow \omega = 1.38 = \frac{\pi^2 \alpha t}{L^2}$

Giving Equation 2.1 for diffusivity

$$\alpha = \frac{0.138L^2}{t_{1/2}} \tag{2.1}$$

All measurements were taken at 25 °C in an atmosphere of high-purity argon at 150 ml/min. The furnace environment must be controlled since heat transport is sensitive to gas composition. Diffusivity errors are reduced when the gas in the chamber is controlled. The Cape-Lehman model was used to calculate the thermal diffusivity across the entire sample thickness, and the thermal contact resistance was calculated using a two layer (2L + heat loss + contact resistance) heat loss model. When analyzed by the two layer method, the interface layer, of negligible thickness (< 100 μm), with respect to the overall sandwich thickness (~2 mm), was represented by contact resistance, thus avoiding the need for input programming of detailed information concerning the thermal properties of the NT arrays. However, the Al 6061 material properties were input in the program. The thermal diffusivity was found for the solid aluminum discs with the LFA and the diffusivity curve was input for the "top layer" and "bottom layer" in the 2L method. The input for specific heat (C_p) was 1, and a coefficient of thermal expansion was input as 0, because all measurements were taken at room temperature disregarding the possibility of expansion at higher temperatures.

To define thermal contact resistance, a simplified steady state heat transfer model is first considered. Contact resistance is a resistance to heat transfer caused by an interface. The interface poses resistance to heat transfer because of imperfections in the mating of two surfaces [3, 6, 9]. Contact resistance is manifested by a virtual temperature jump, but typically there is no actual discontinuity in the temperature field. It's the difference between the extrapolated linear portions of the temperature fields in the bodies of the solid surfaces, shown in Figure2.10a. The actual temperature gradient looks similar to the red curve. The curvature in the temperature field near the interface is caused by local contact spots; heat is channeling through finite size contact spots. The best possible heat transfer exists within a solid material, as seen in Figure 2.10b. The goal of a TIM is to decrease the resistance to heat across the interface.

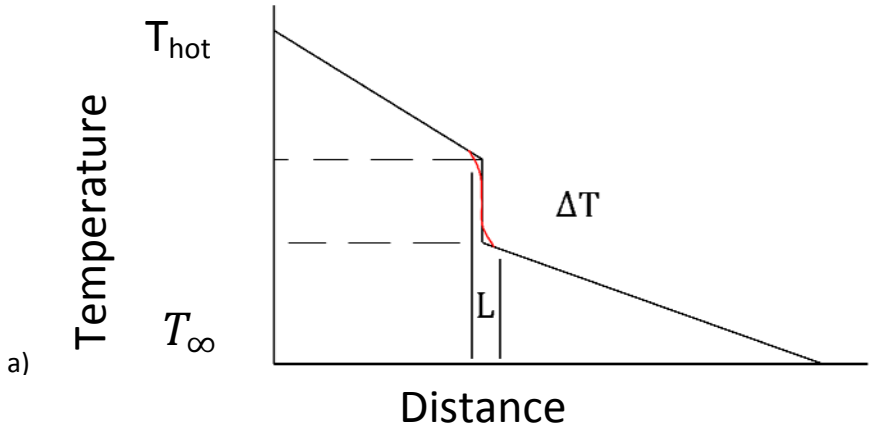

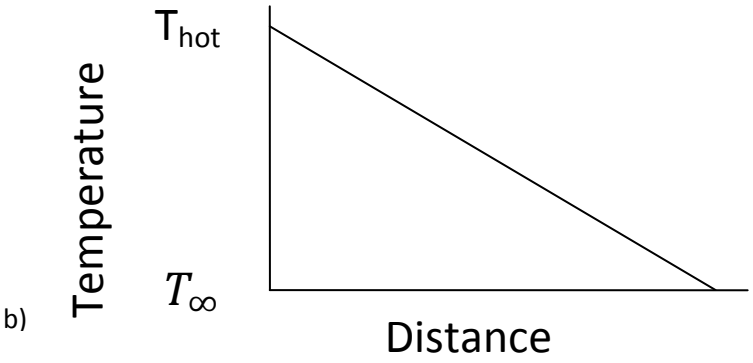

Figure 2.10 a) Schematic depicting temperature drop across an interface of two materials; b) Schematic depicting temperature drop across a solid material

As previously discussed, the flow of heat through a solid is primarily due to conduction, neglecting contributions of convention and radiation. The rate of heat conduction, at steady state, defined by Fourier's first law is

$$\dot{Q} = -kA\frac{\Delta T}{L};\ \vec{q} = -k\frac{\Delta T}{L} \tag{2.12}$$

where k is the thermal conductivity, A is the interface cross-section area, ΔT is the temperature gradient, and L is the thickness.

As shown in Figure 2.10a, thermal contact resistance, which is thermal resistance per unit area, is the ratio of the virtual temperature jump, to the heat flux, due to the presence of the interface, given by [12]

$$R_c = \frac{|\Delta T|}{\vec{q}} \tag{2.13}$$

Using Fourier's first law for $\vec{q}$, the contact resistance equation can be rearranged into

$$R_c = \frac{L}{k} \tag{2.14}$$

This proves that the interfacial contact resistance can be reduced by increasing the conductivity of the interface material, successfully mating the contacting surfaces for a larger heat transfer area and ensuring the interface is as thin as possible.

Thermal diffusivity is also an important consideration for thermal management. It is a measure of how quickly a material can reach the temperature of its surroundings. To define thermal diffusivity, a time-rate-of-change thermal conduction energy balance is shown in Equation 2.15.

$$\begin{bmatrix} rate\ of\ heat \\ conducted\ in \end{bmatrix} + \begin{bmatrix} rate\ of\ heat \\ generated\ within \end{bmatrix} = \begin{bmatrix} rate\ of\ heat \\ conducted\ out \end{bmatrix} + \begin{bmatrix} rate\ of\ energy \\ stored\ within \end{bmatrix} \tag{2.15}$$

$$\left[\dot{Q}_{out} - \dot{Q}_{in}\right] = \dot{Q}_{gen} - \frac{dE}{dt} \tag{2.16}$$

Where $E = mC_v dT = A\delta_x \rho C_v dT$ and it can be assumed that there is no heat generated within the TIM.

$$\left(-kA\left.\frac{dT}{dx}\right|_{x+\delta_x}\right) - \left(-kA\left.\frac{dT}{dx}\right|_{x}\right) = -A\delta_x \rho C_p \frac{dT}{dt} \tag{2.17}$$

Taking the differential thickness to zero gives

$$\lim_{\delta_x \to 0} -kA\left[\frac{\left(\left.\frac{dT}{dx}\right|_{x-\delta_x}\right) - \left(\left.\frac{dT}{dx}\right|_{x}\right)}{\delta_x}\right]\delta_x = -A\delta_x \rho C_p \frac{dT}{dt} \tag{2.18}$$

$$-k\frac{d^2T}{dx^2} = \rho C_p \frac{dT}{dt} \tag{2.19}$$

Creating a constant, $\alpha = \frac{k}{\rho C_p}$

$$\frac{dT}{dt} = \alpha \frac{d^2T}{dx^2} \tag{2.20}$$

Where α is thermal diffusivity, which can be directly measured by LFA [63]. Thus, the value of thermal diffusivity increases with a materials ability to adjust heat (k) and decreases with the amount of heat needed to change the temperature of the material (C_p). The thermal diffusivity as well as contact resistance, as defined in Equation 2.14 is important properties of the TIMs. Another property of the array which is independent of the interface properties, such as thickness, is the effective thermal conductivity, k_{eff} defined by

$$k_{eff} = \frac{t_i}{R_c} \tag{2.21}$$

where t_i is the interface thickness[25]. Effective thermal conductivity essentially normalizes the contact resistance to the thickness of the interface. After thermal testing, the samples were mounted in epoxy resin plane perpendicular to the interface, and polished, then measured for interface thickness. The interface thicknesses were measured by optical microscopy at twenty locations.

2.3 Results

Each of the sandwich-bonded specimens containing various interface materials were tested for overall through-thickness thermal diffusivity (α), thermal interface contact resistance (R_c), and effective interfacial thermal conductivity (k_{eff}). A plot of the thermal diffusivity across the entire sandwich and the commensurate contact resistance through the interface, both on a log scale is seen in Figure 2.11. The list of samples was recorded in order of decreasing thermal performance.

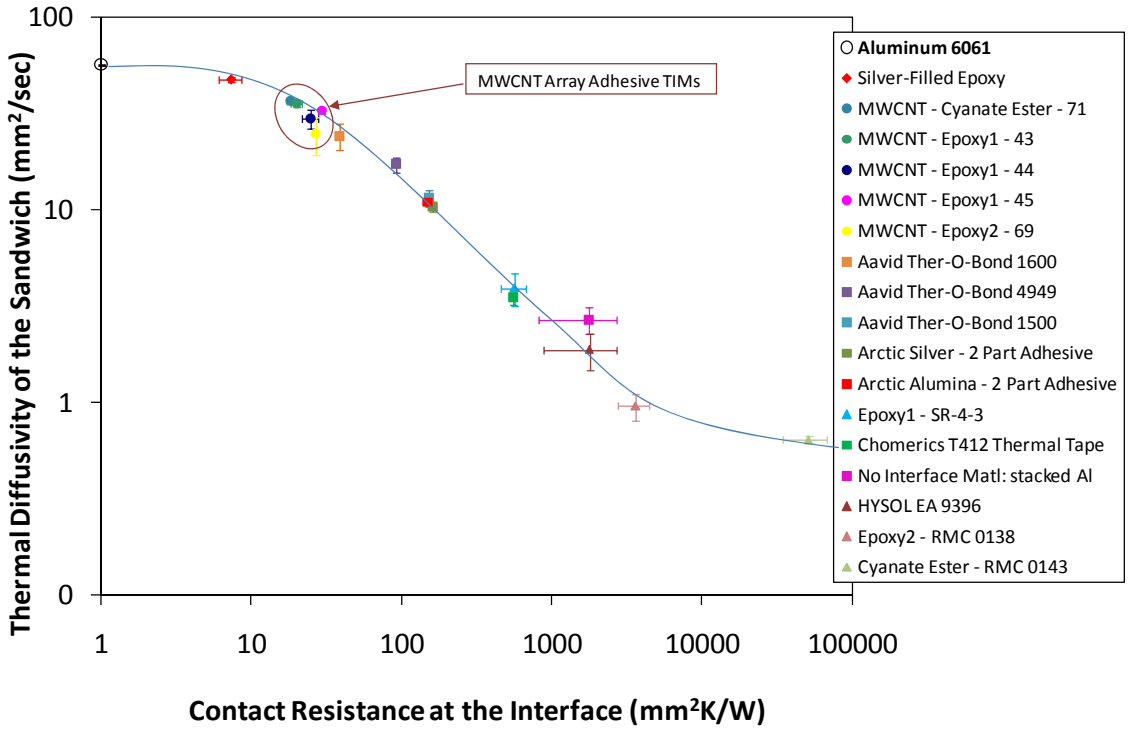

Figure 2.11 Thermal diffusivity of the sandwich plotted against contact resistance at the interface of interface materials bonding mill-finish Al substrates

As expected, the solid aluminum has the highest diffusivity and no contact resistance; it is intuitively the perfect interface. The silver-filled epoxy is followed by the epoxy-infiltrated arrays. The silver-filled epoxy had ~ 22 vol. % conductive silver dispersed within resin, whereas the infiltrated MWCNT arrays had ~15 vol. % conductive NTs infiltrated within resin. To accurately compare the two, the concentration of NTs within the array would need to reach about 22 vol. %, which would ultimately improve the thermal performance, possibly reaching the high diffusivity of the silver-filled epoxy. The MWCNT arrays outperformed the commercial thermal adhesives, TOB 1600, TOB 4949, TOB 1500, Arctic Silver, and Arctic Alumina, listed in order of decreasing thermal performance. Specimens bonded with the SR-4-3, double-sided thermally conductive tape, HYSOL EA 9396 epoxy resin, RMC 0138 epoxy resin, and Cyanate Ester epoxy resin produced the lowest thermal diffusivity across the assembly. The two aluminum substrates on top of each other without a TIM showed a very low thermal diffusivity value (2.682 mm^2/s). The rough surfaces of the aluminum (r_A=0.643 µm) create voids in the contacting surfaces, causing poor contact. The reduction in contact area results in a reduced rate of heat conduction through the thickness of the sample. Bonding the Al substrates with the

commercial epoxy adhesives Hysol EA9396, RMC 0138, and Cyanate Ester resulted in even poorer thermal performance than the stacked aluminum sample. Here the polymer adhesives essentially functioned as a thermal insulating barrier. The introduction of conductive thermal interface materials resulted in significantly higher diffusivity values.

The overall diffusivity of the assemblies versus effective thermal contact resistance in Figure 2.11 formed a clear S-curve, on the log-log scale, within the results. This suggests that, for moderate contact resistances, there exists a linear relationship between log contact resistance and log diffusivity (i.e. half-rise time measured by the LFA). It's intuitive that the maximum diffusivity value is the solid aluminum sample and the arrays are approaching this value following the outline of the curve. Also, on the low end, the epoxy resins exhibit lower diffusivity values and higher contact resistance values and the curve clearly approaches this minimum value.

Thermal diffusivity values as obtained for Figure 2.11 are across the entire assembly of aluminum discs bonded by MWCNT arrays. One layer diffusivity values for MWCNT - 66 (just the MWCNT array by itself – no aluminum substrates), an array with thickness of 69 µm, was also found using the Netzsch LFA 427 Cape-Lehman 1 layer method. The value of diffusivity for MWCNT - 66, displayed in Figure 2.12, was 84 mm^2/s compared to a solid graphite standard with thermal diffusivity of 66 mm^2/s. The MWCNT - 66 array material had a thermal diffusivity 27 % higher than graphite, at only 10 % the density of graphite (0.2 g/cc). Materials with very high thermal diffusivities do not maintain a thermal gradient well. They simply tend to quickly conduct thermal energy, minimizing the gradient, while also minimizing the degree of internal temperature rise.

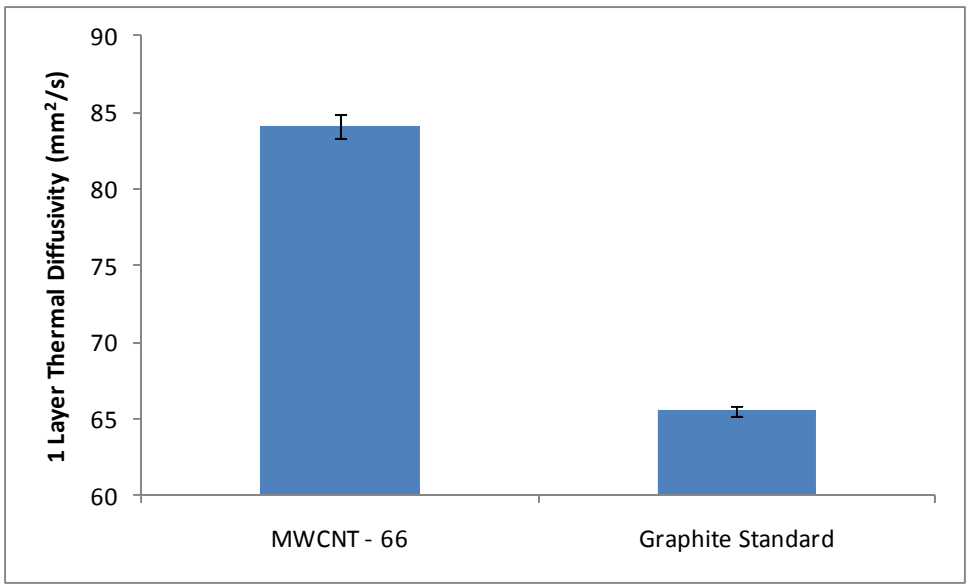

Figure 2.12 Thermal diffusivity of array MWCNT 66 and graphite

Diffusivity is a useful thermal property to describe the multilayer systems; however the most important property to define the ability of a material to serve as a thermal interface material is interfacial thermal contact resistance, R_c. Equation 2.13 defines R_c as the ratio of the virtual temperature jump to the heat flux across the interface. The goal is to reduce this temperature gradient by decreasing the interfacial contact resistance across the interface. Replacing the heat flux with Equation 2.12 simplifies our contact resistance to Equation 2.14; the ratio of interface thickness to conductivity of the interface material. If the conductivity is infinitely high, contact resistance will be approaching zero. This proves that the interfacial contact resistance can be reduced by increasing the conductivity of the interface material and ensuring the interface is as thin as possible. The relatively large thickness of the arrays (~100 µm) was a factor that limited the thermal performance of the diffusivity and contact resistance. To optimize the NT arrays for more effective thermal transport, the arrays should be reduced in length for a shorter bond-line thickness.

The lowest contact resistance was found through the interface composed of silver-filled epoxy and the epoxy-infiltrated MWCNT arrays. The lowest interfacial thermal contact resistance observed for the epoxy-infiltrated CNT arrays was down to 18.1 mm^2K/W for the MWCNT – Cyanate Ester-71 array. This characterizes the epoxy-infiltrated MWCNT arrays as a replacement for metallic interface materials, where light weight adhesives that can withstand high temperatures and torturous environments are preferred over thermal greases or polymers

with metallic fillers [5]. This is discussed further in Chapter 3, with the thermal testing of the dry arrays under high vacuum (~1x10^{-5} mbar) and at higher temperatures (up to 150 °C).

An intrinsic property of the TIM, less dependent of interface parameters, is the effective thermal conductivity (k_{eff}) [25]. It essentially normalizes the thermal performance of the interface per bond-line thickness as t_i/R_c. The thermal diffusivity and the interfacial contact resistance are both functions of the thickness of the interface, which makes the properties dependent on the fabrication of the assembly. While each sample was given a constant curing pressure (75 psi, 150 °C, for 2hrs) and measures were taken to harvest the CNT arrays with similar contact area and thickness, human error affects the nature of the assembly. To compare the CNT arrays to each other as well as to other TIMs, effective thermal conductivity is a crucial thermal property, which is seen in Figure 2.13.

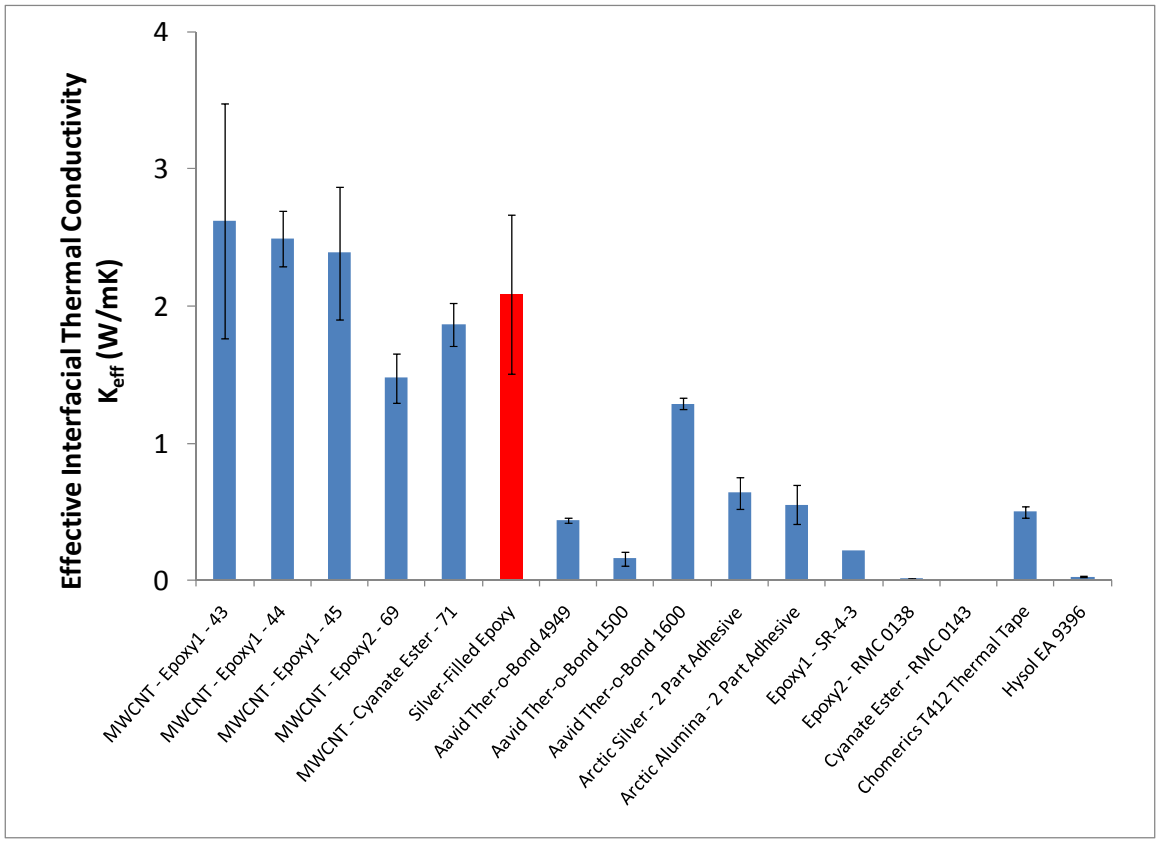

Figure 2.13 Effective interfacial conductivity of sandwich assemblies

The values of effective thermal conductivity of the MWCNT arrays are higher than the commercial materials, and some samples, such as MWCNT-Epoxy1-43, with a k_{eff} of 2.62 W/mK,

were as good as the effective conductivity value of the benchmark material, silver-filled epoxy (~22 vol. % silver) with 2 W/mK. This further emphasized the importance of the interface thickness. The K_{eff} is a property essentially independent of the thickness, and the drastic improvement of MWCNT over the commercial materials, when thickness is normalized, revealed that the MWCNT arrays would have possessed great improvements over commercial materials in diffusivity and contact resistance with shorter bond-lines.

2.4 Concluding Remarks

The present chapter contains a characterization of epoxy-filled multiwall carbon nanotube arrays. The LFA thermal results suggest improvements of epoxy-infiltrated MWCNT arrays over commercial thermal adhesives currently used in many different interface applications. Air is a poor conductor of heat, therefore for electronics or other heat producing sources, interfaces of air must be filled with TIMs for effective heat transport to a heat sink or the surrounding environment. A TIM must possess high conductivity and conformability to surface imperfections and voids. MWCNTs with these inherent characteristics, when infiltrated with the thin-film epoxy resins, possess adhesive characterizations and make great contact with surfaces for efficient heat conduction.

The arrays presented here out-perform most commercial adhesives used in thermal interface material applications, such as polymers with metallic fillers. When the MWCNT arrays bond two aluminum discs, simulating actual interface conditions, the thermal interface contact resistance values were as low as 18.1 mm^2K/W, where commonly used commercial adhesives only reached 38.68 mm^2K/W. Decreasing contact resistance will drastically increase the thermal performance of a component.

The aligned MWCNT array, with diffusivity values higher than isotropic graphite, exhibit excellent thermal transport performance in many applications. However, there is much area for improvement in the development of epoxy-filled MWCNT arrays. The thermal performance can be drastically increased by reducing the thickness of the interface layer while increasing the concentration of carbon nanotubes within the contact area, which greatly influences the effective thermal conductivity. Further research will focus on the delicate balance of these parameters, while obtaining continuous arrays for large, commercial applications.

Chapter 3 Dry Multiwall Carbon Nanotube Arrays as Thermal Interface Materials

3.1 Introduction

The discussion of adhesive-infiltrated multiwall carbon nanotube arrays in Chapter 2 revealed improvements over thermal adhesives currently used in TIMs applications. This chapter describes un-infiltrated, or "dry", multiwall carbon nanotube arrays and the comparison of thermal properties between the arrays and commercial thermal greases—both non-permanent bonds.

The only difference between the adhesive-infiltrated arrays in Chapter 2 and the "dry" 100 % MWCNT arrays presented here is the absence of polymer. The dry arrays were grown identical to the arrays described in Chapter 2 by CVD synthesis techniques on 3" x 36" quartz substrate. Novel harvesting techniques were used to obtain a free-standing array that can be directly applied to an interface. With no binder or adhesives, the dry arrays were characterized for interfacial contact resistance by 2-layer, cap-screw bonded discs with pressure provided by four cap screws forcing the Al discs closed.

3.2 Experimental

The dry arrays were thoroughly analyzed through various techniques including determination of diffusivity and contact resistance by laser flash (LFA Netzsch 427) and analysis by scanning electron microscopy (SEM). The thermal tests of the CNT arrays were performed under pressure loads provided by 4 cap-screws in the cap-screw bonded sandwich assembly. Each cap-screw was given equal torques of 2 in-oz, 3 in-oz, or 4 in-oz. The increasing torque allowed for an increase in pressure of 578 kPa, 866 kPa, and 1155 kPa, respectively. Higher contact pressures increase the contact surface area and result in more successful void filling by the highly conductive MWCNTs. Thermal properties as a function of torque are described in this chapter.

3.2.1 Carbon Nanotube Synthesis

The MWCNTs synthesis for this chapter is identical to the process described in Section 2.2.1. The substrates were weighed before and after the runs to determine the approximate number of nanotubes on the slide. From this, areal densities were calculated between 0.97-2.67 mg/cm^2 (0.1-0.27 g/cc bulk densities). Assuming a hexagonal orientation of the MWCNTs, as shown in

Figure 2.2, a packing factor was calculated of about 13 %. The low conductivity of air at 25 °C is 0.0262 W/mK [64]. The large volume of air allowed for infiltration of more conductive materials such as Arctic Silver thermal grease and various nano metallic materials; details will be discussed in Chapter 4.

3.2.2 Cap-Screw Bonded Sandwich Assembly

Aluminum 6061 was chosen as the material to cap-screw-bond the dry array sandwich assembly. Discs of 12.7 mm (0.5 inch) diameter and 3.12 mm (0.125 inch) thick were machined from aluminum sheets with a mirror polished and a mill finish side (r_A=0.643 µm). The Al sandwiches were held together with four cap-screws M1 Size, 4 mm Length, and 0.025 mm pitch. Because the dry arrays are not infiltrated with adhesive materials, the thermal tests were conducted under various pressure loads to increase the contacting surface area. Each of the cap-screws were given a torque of 2, 3, or 4 in-oz by a torque-limiting screwdriver pictured in Figure 3.1, to test each sandwich assembly at the various applied pressures of 578, 866, and 1155 kPa, respectively. A schematic of the top view of the cap-screw-bonded sandwich is shown in Figure 3.2 and Figure 3.3 shows the top view of the actual aluminum sandwich.

Figure 3.1 Utica TT-1 Torque Limiting Screwdriver used to apply small 2-4 in-oz torques to cap-screw assembly

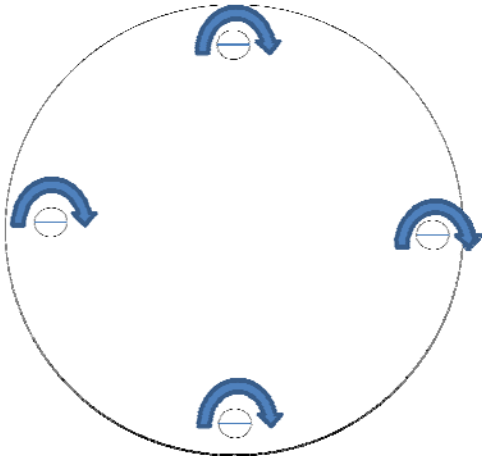

Figure 3.2 A torque-limiting screw driver applies a torque to each cap-screw to apply pressure to the interface

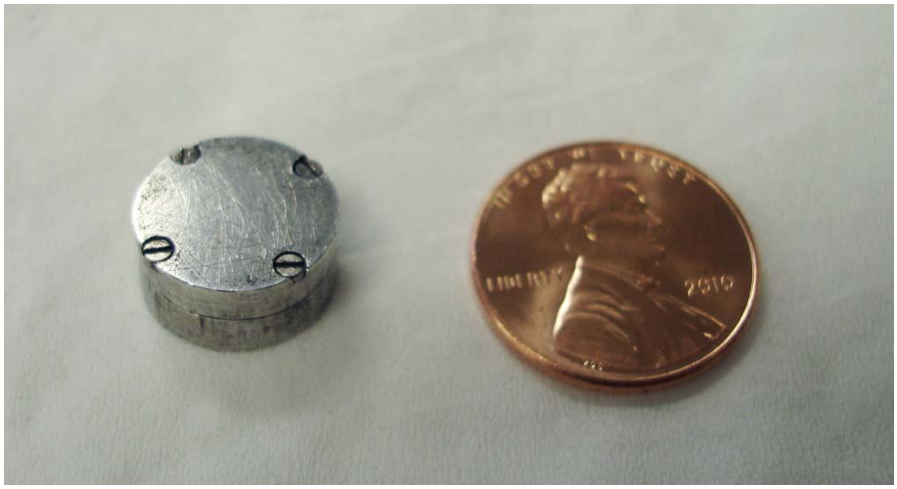

Figure 3.3 Un-infiltrated “Dry”, cap-screw-bonded MWCNT TIM LFA specimen

All thermal greases were tested in “hand pressed” together Al sandwiches. To replicate an actual interface, with uneven mating surfaces, the mill finish surfaces were cap-screw bonded or, in the case of the greases, pressed together. Arguably, the most important property for a TIM is the ability of the material to wet and conform to the mating surfaces, allowing more continuous heat flow [65].

The arrays, designated MWCNT followed by the fabrication number, and corresponding NT areal density, bulk density, and packing factor, are described in Table 3.1, assuming a hexagonal orientation as pictured in Figure 2.1.

Table 3.1 Array properties of un-infiltrated “dry” MWCNT arrays

	NT Areal Density (mg/cm^2)	**NT bulk density (assuming 100 micron length) (g/cc)**	**Packing Factor (% of Max NT/ cm^2)**
MWCNT - "Dry" As-Produced - 72	2.67	0.27	14
MWCNT- "Dry" As-Produced - 37	0.97	0.1	11

The multilayer systems that were compared to the array sandwiches include a cap-screw bonded assembly with no TIM, commercial greases of Zerotherm ZT100 Thermal Compound, Prolima Nano Aluminum Thermal Compound, Rosewill Thermal Compound, Antec Formula 5 Thermal Compound, Ceramique Arctic Silver Thermal Compound, and Arctic Silver 5 Thermal Compound. These thermal compounds are primarily used in the electronics industry at a TIM between high power components and their heat sinks.

3.2.3 Dry MWCNT Adhesion

As mentioned in Chapter 2, dry MWCNTs demonstrated adhesion between individual MWCNTs exceeding a typical interaction dominated by van der Waals forces (< 0.05 MPa) [49]. Work by Yang Zhao *et al.* [26] describe this interaction as mimicking hairs on a gecko’s foot. They measured adhesion forces between MWCNTs and an opposing surface at about 11.7 N/cm^2 (0.117 MPa), exceeding the adhesion forces associated with a gecko’s foot at 10 N/cm^2 (0.1 MPa) [66]. These strong adhesion forces characterized the MWCNTs as dry adhesives. This is ideal in TIMs applications, not only because the nanotube tips make adhesive contact with the substrate surface, as seen in Figure 3.4a, but also because the MWCNTs are adhered to one another, seen in Figure 3.4b. Another important finding from Yang Zhoa *et al.* [26] was that MWCNT arrays with heights of around 100 µm, a characteristic of MWCNT – “dry” As-produced - 72, had adhesion strengths of only about 2 mN/cm^2 (0.2 Pa). In their work, the optimal height of MWCNT arrays with respect to adhesion properties was 5-10 µm. The MWNCT- “dry” As-produced – 37 is composed of nantotubes with lengths of about 50 µm, closer to the optimal height. The thermal properties greatly improved with this shorter length, as will be described in Section 3.3. As discussed previously, tall characteristics of NT arrays (MWCNT – 72) is a limiting factor for thermal transport capabilities based on the definition of thermal contact resistance

($R_c = \frac{L}{k}$), theory of phonon transport, and, as described by Zhoa, also based on adhesion properties.

a) 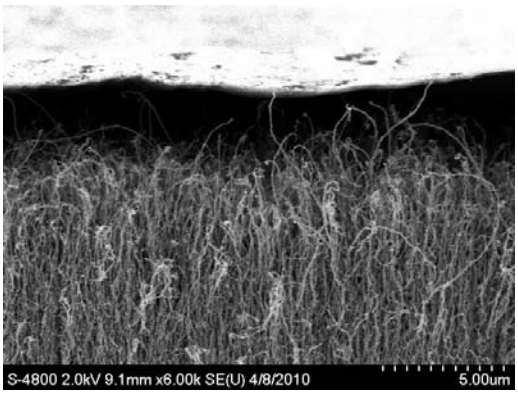

b) 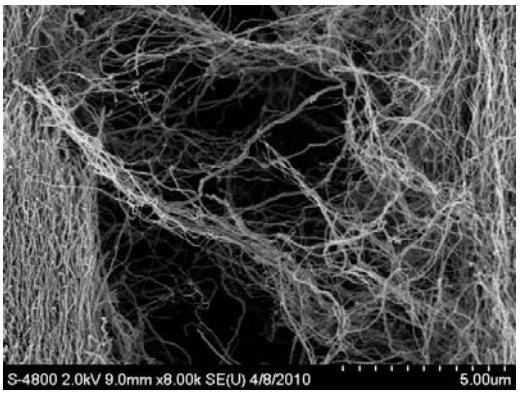

Figure 3.4 Dry MWCNT-37 demonstrating a) dry adhesion forces with substrate and b) dry adhesion forces between MWCNTs

Because of the adhesion between MWCNTs, shown in Figure 3.4b, the arrays essentially functioned as a solid, aiding in handleability. The ease of installation of dry MWCNT arrays is pictured in Figure 3.5a. The greases, which are liquid in nature and must be ejected from a tube, seen in Figure 3.5b, and spread evenly across the substrate are considerably messier than dry arrays.

a) 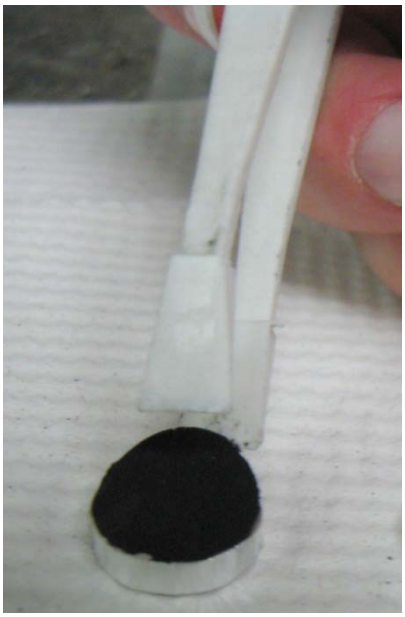
b) 

Figure 3.5 Installation of a) Dry MWCNT array and b) Zerotherm ZT100 Thermal Grease

Further, the arrays contain no binder or adhesives, leaving them both re-workable and suitable for application in high vacuum and high temperature environments. The re-workability of the arrays has not been tested within the scope of this thesis, however it is theoretically understood. A Thermogravimetric Analysis (TGA), in a N_2 atmosphere (100 ml/min), of Epoxy-1 (SR-4-3) is shown in Figure 3.6. The epoxy is essentially all pyrolized by 550 °C with a residual of 41.98 wt. % at 550 °C ± 1.53 wt. %. An un-infiltrated array MWCNT -37 was also analyzed by TGA in N_2 up to 1000 °C in Figure 3.7. The nanotubes survived up to about 700 °C, due to residual O_2 in the furnace. For high temperature applications, dry arrays will survive up to around 700 °C, where infiltrated arrays will start to pyrolize at around 400 °C.

Carbon nanotubes survive in high vacuum, the use-environment of satellite applications, where epoxy and other infiltrants will out-gas into into the environment. A turbo- pump vacuum pulled a vacuum down to 1×10^{-5} mbar in the sample furnace of the Netzsch LFA 427 in order to thermally test materials in an environment similar to the vacuum of space. MWCNT – "Dry" As-Produced – 37 was tested in high vacuum (HV) conditions and the thermal results are shown in Figure 3.8. The list of samples was recorded in order of decreasing thermal performance. The MWCNT array not only survived in the torturous environment, it served as a thermally conductive material through the interface of the cap-screw bonded assembly and showed improvements over tests in atmospheric conditions.

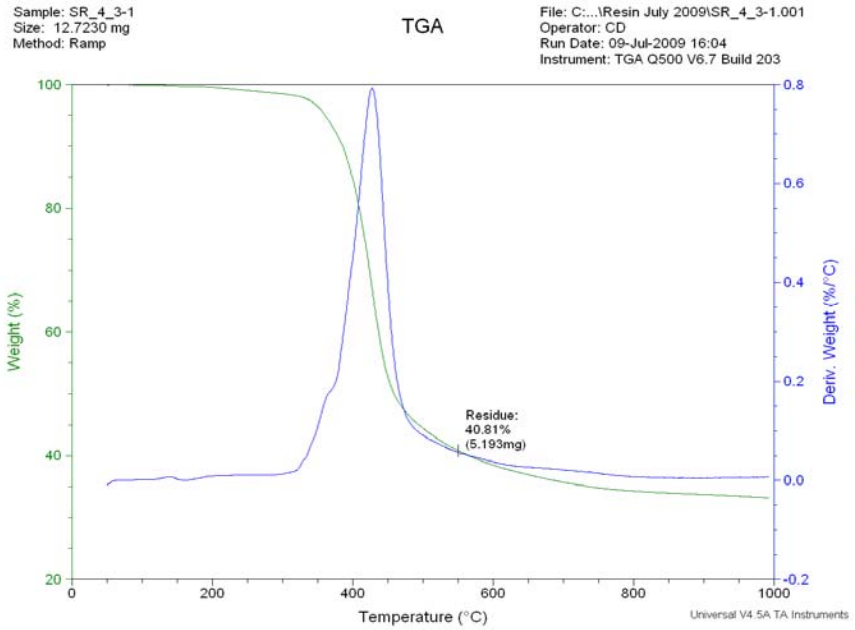

Figure 3.6 Thermogravimetric Analysis (TGA), in N_2, of epoxy; notice the carbonization of epoxy at around 400 °C

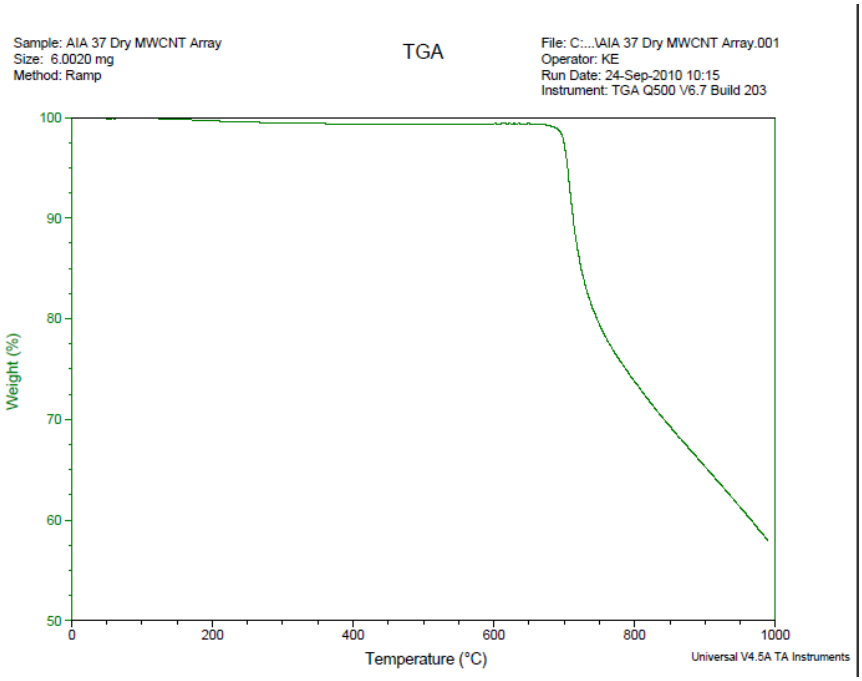

Figure 3.7 Thermogravimetric Analysis (TGA), in N_2, of a “dry” MWCNT array

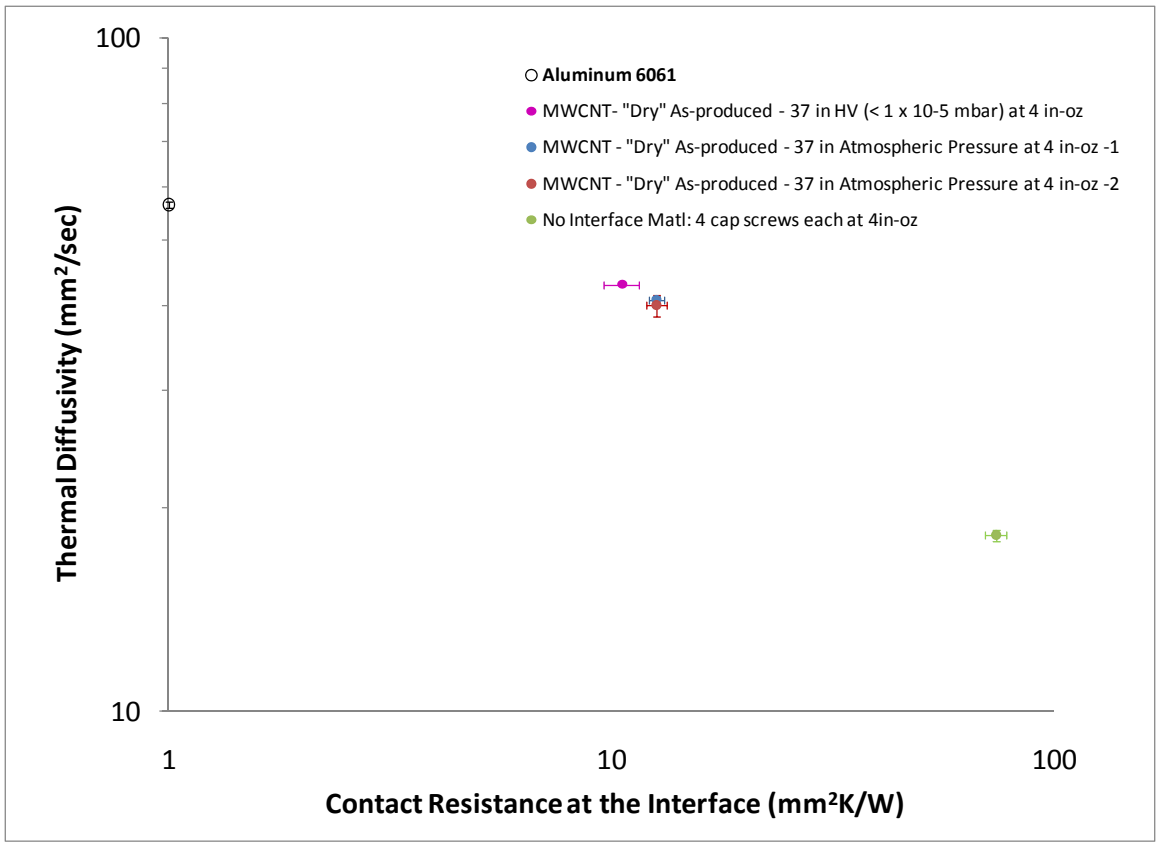

Figure 3.8 MWCNT – 37 thermal diffusivity and contact resistance in high vacuum application (<1 x 10^{-5} mbar) and at atmospheric pressure (1013.25 mbar)

3.2.4 Thermal Testing

The thermal diffusivity and interfacial thermal contact resistance was found for the cap-screw-bonded aluminum sandwich samples with and without thermal interface material using a modern laser flash apparatus Netzsch LFA 427. The theory of interfacial heat transport is described in Section 2.2.4.

Samples were mounted in the LFA furnace chamber. A laser pulse of 1 ms and 650 V was used to irradiate the bottom surface of the sample. The samples were coated with spray graphite to enhance energy absorption from the laser beam and to minimize reflection of the aluminum surface. Diffusivity and thermal contact resistance was calculated by the LFA Analysis software for samples given a torque of 2, 3, and 4 in-oz on each cap-screw for applied pressures of 578, 866, and 1155 kPa, respectively.

3.3 Results

Each of the interface materials were tested for thermal diffusivity (α), thermal interface contact resistance (R_c), and effective thermal conductivity (k_{eff}). A plot of the thermal diffusivity across the entire sandwich and the commensurate contact resistance through the interface, both on a log scale is seen in Figure 3.9. The list of samples was recorded in order of decreasing thermal performance.

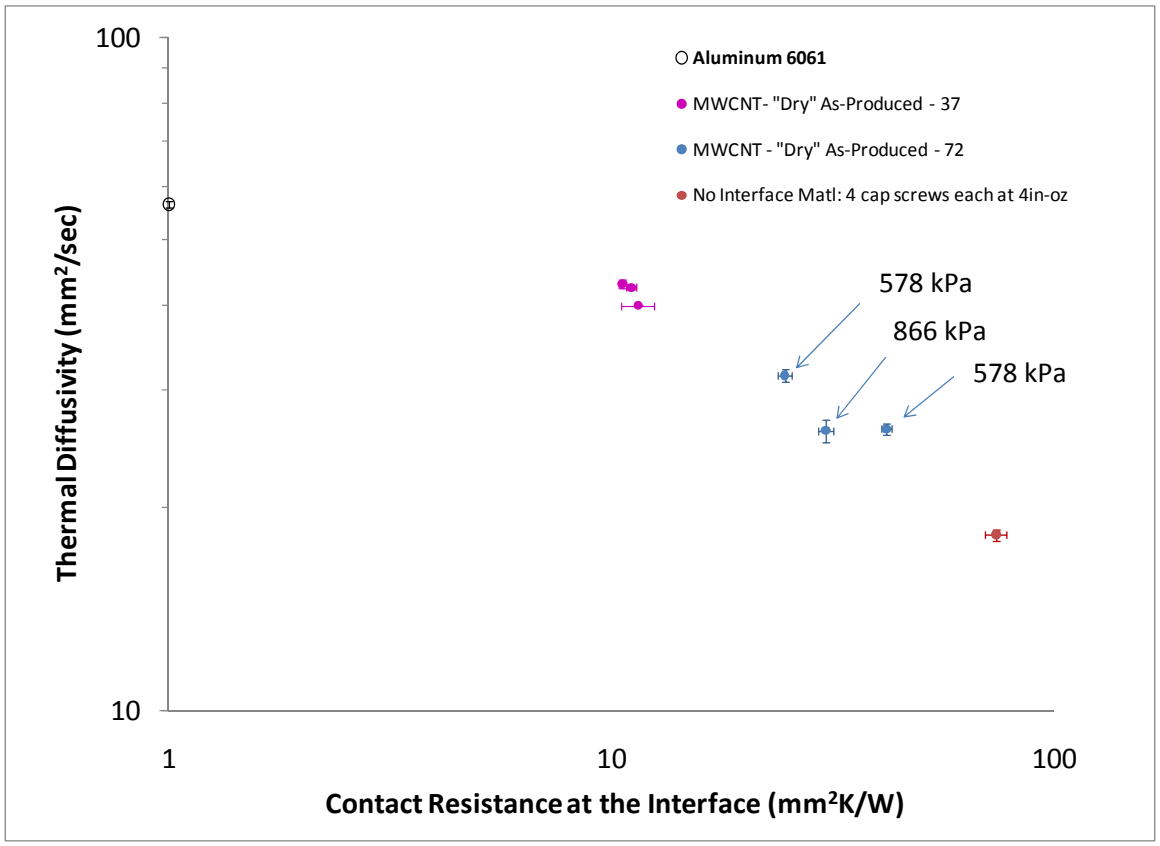

Figure 3.9 Thermal diffusivity of the sandwich plotted against contact resistance at the interface of MWCNT arrays cap-screw-bonding mill-finish Al substrates

As expected, the solid aluminum has the highest diffusivity and no contact resistance; it is intuitively the perfect interface and the sandwich containing no interface material has poor thermal properties. The MWCNT arrays posses contact resistances down to 10.583 mm^2K/W, which is considerably lower than the 18.1 mm^2K/W observed for the adhesive-infiltrated MWCNT array. Also, the MWCNT-37 array significantly out-performed the MWCNT-72 array, with half the contact resistance and about 37 % higher diffusivity values compared to the 72 array. There exhibited different thermal characteristics possibly inherent to the arrays

themselves. SEM imaging was used to take a look at these two very different dry arrays in order to explain the excellent thermal properties of the 37 array, addressed in this section.

As the applied pressure from the cap screws increases, thermal properties improve; diffusivity increases and contact resistance decreases. More pressure resulted in smaller bond-line thickness of the interface which created a shorter length for phonons to travel. Less phonon scattering occurs if forced along a shorter pathway [42]. Higher contact pressure also increased the contacting surface area. The mill-finish surface of the aluminum, with all of its imperfections and cavities, is full of air gaps and voids, as illustrated in Figure 3.10. When the interface is filled with a compressible material, i.e. a MWCNT array [67], applying pressure on the substrates fills the valleys in the surfaces more effectively, increasing thermal transport [12].

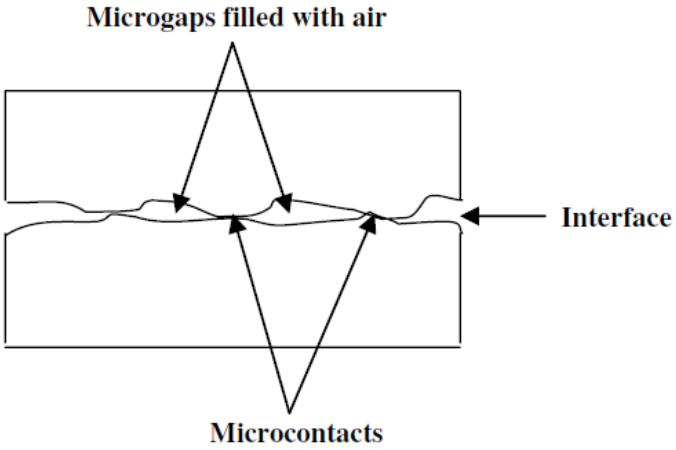

Figure 3.10 An enlarged illustration of an interface [12]

Work by Cola *et al*. [6] increased the conformability of the array by growing MWCNT arrays on metal foils. The CNT-foil material conformed to the surface voids, thus increasing contact points between the CNT and the substrate. They achieved thermal contact resistances down to 10 mm^2K/W at pressures of about 300 kPa. The void-filling, highly conformable material was a great TIM that decreased thermal resistance through the interface.

In an effort to further characterize MWCNT "dry" array 37, SEM images were taken of the "cut side", "top side", and the side of the array. The images reveal an exceptionally superior array compared to all other "dry" arrays considered. As defined in Chapter 2, the "cut side" of the array is the side of the array cut from the quartz slide. The "top side" is the top of the array where carbon is continuously deposited onto the quartz substrate.

An excess of carbon deposited on the slide in the amorphous form is a recurring problem typical in the CVD synthesis of CNTs [68]. The result is the "top side" layer can possess a build-up of amorphous carbon, which acts as a thermally insulating barrier preventing the MWCNT tips to reach the aluminum substrate. Further characterization, possible sources for amorphous carbon and subsequent "cleaning" of the array are explained in detail in Chapter 4.

The lack of amorphous carbon build-up on the "top side" of the array, shown in Figure 3.11, is one reason why the MWCNT-37 array was exceptional to other "dry" arrays produced with our CVD synthesis techniques. An addition reason the 37 array had excellent thermal properties is due to the shorter length of nanotubes. Notice in Figure 3.12, the 100 % increase in thickness of the MWCNT array from the 37 array to the 56 array. The average length of our "dry" as-produced nanotubes was around 100 µm. The MWCNT – 37 array has an average thickness of 50 µm. According to equation 2.14 for interfacial contact resistance, $R_c = \frac{L}{k}$, the resistance can be reduced by increasing the conductivity of the interface material and ensuring the interface is as thin as possible. The thinner array creates a shorter bond-line thickness, L, and it is intuitive that the resistance to heat flow will decrease, as seen in the thermal results in Figure 3.9.

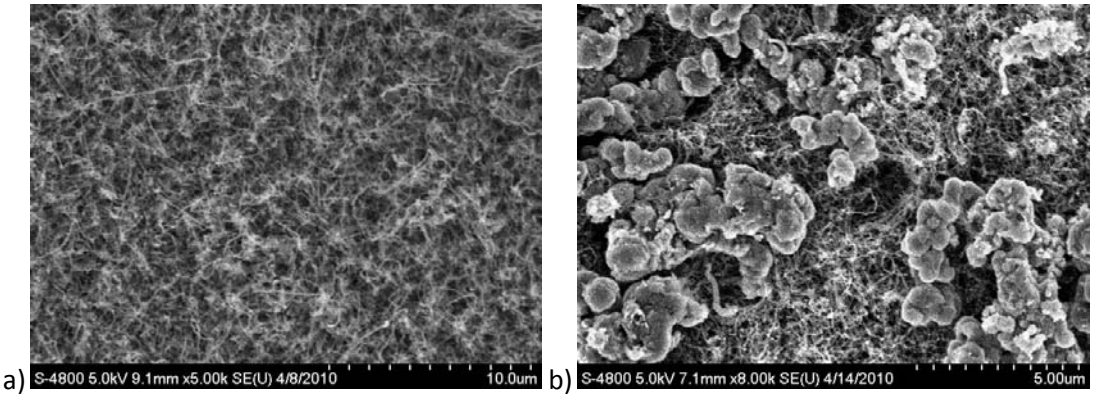

Figure 3.11 Top side" view of a)MWCNT – "dry" As-produced – 37 array and b)MWCNT – "dry" As-produced – 56 array; notice the lack of amorphous carbon on the 37 array

a) 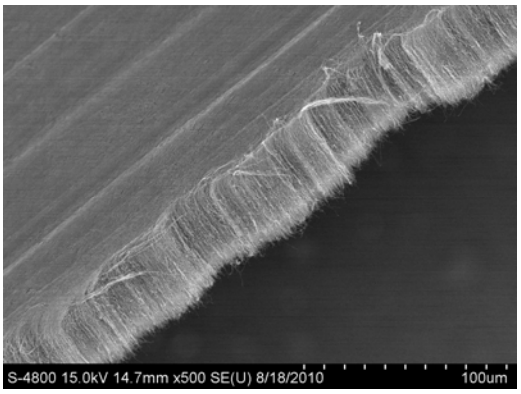

b) 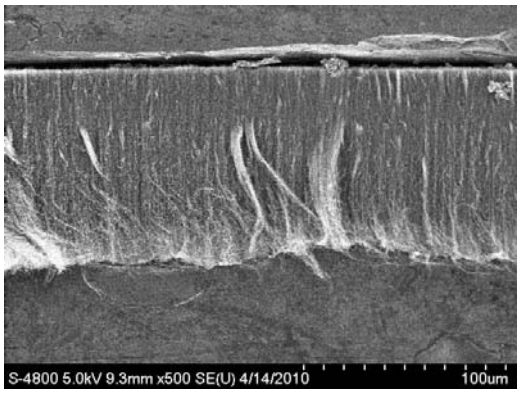

Figure 3.12 Side view of a)MWCNT – "dry" As-produced – 37 array and b)MWCNT – "dry" As-produced – 56 array; notice the different thicknesses

a) 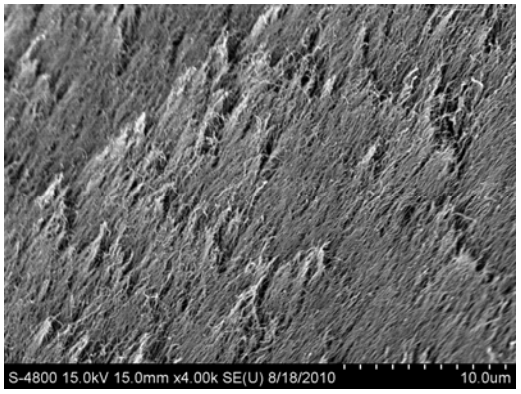

b) 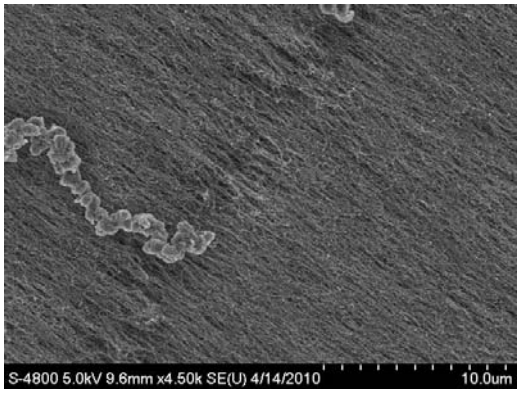

Figure 3.13 "Cut side" view of a) MWCNT – "dry" As-produced – 37 array and b) MWCNT – "dry" As-produced – 62 array

Another qualitative observation of MWCNT – 37 array is the large amount of exposed CNT tips viewed on the "cut side", shown in Figure 3.13. Comparing the top side of MWCNT -37 (Figure 3.13a) to the top side of the MWCNT- "dry" As-produced-62 array (Figure 3.13b) further reinforces the large magnitude of CNTs aligned and available to adhere to and contact the surfaces of the substrate for greater heat transport efficacy. The synthesis parameters for producing the 37 array were documented and care will be taken to duplicate the synthesis process to create other thinner, purer MWCNT array for TIM applications.

The dry MWCNT 37 and 72 arrays were tested by LFA Netzsch 427 in the cap-screw-bonded sandwiches. The commercial greases hand pressed together between two aluminum discs were compared to the cap-screw assemblies, at an applied pressure of 1155 kPa, in Figure 3.14. The list of samples was recorded in order of decreasing thermal performance. The MWCNT arrays thermal properties in a thermal interface application are comparable to thermal greases used in the electronics industry today. This verified that the CNT arrays could be a replacement for

thermal greases in industry. Thermal greases, as discussed previously, are messier than a solid CNT array. Also, in torturous environments, such as high temperature or high vacuum, MWCNTs will outlast greases, which are subject to vaporization and thermal degradation; this will be discussed later in this chapter.

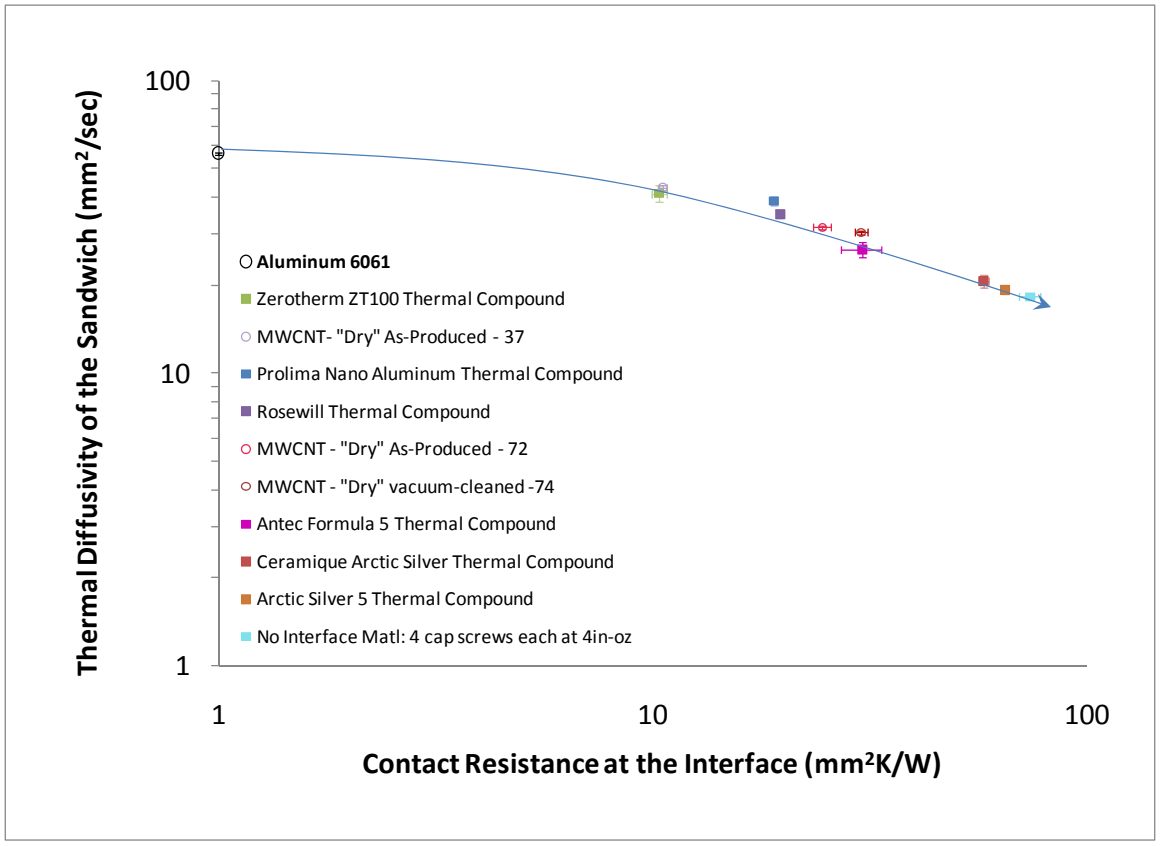

Figure 3.14 Thermal diffusivity of the sandwich plotted against contact resistance at the interface of MWCNT arrays cap-screw-bonded mill-finish Al substrates compared against commercial greases

It's intuitive that the maximum diffusivity value is the solid aluminum sample and the arrays are approaching this value following the outline of the curve. However, the interesting result is that the overall diffusivity of the assemblies versus thermal contact resistance at the interface in Figure 3.14 formed a linear relationship, on the log-log scale, within the range of measured results. The linear relationship between log contact resistance and log diffusivity (i.e. half-rise time measured by the LFA), is similar to the results in Figure 2.14 for moderate contact resistances of the adhesive-infiltrated MWCNT arrays. The 2-layer model used to calculate the contact resistance is based on work by Hung Joo Lee [24] who, independently, presented a model to calculate contact resistance in 2 layer and 3 layer composites. Lee extended the

transient laser-flash method that calculates thermal diffusivity through a solid, thoroughly explained in Chapter 2, to calculate contact resistance for multilayered models. In this way, interfacial thermal contact resistance was calculated out from the half-rise time from the flash method. Further research by Milosevic [25] explained the calculation of thermal contact resistance between two contacting bodies of known resistance by the transient laser-flash method. Milosevic explained that the contact resistance is not simply just the difference in the thermal resistance of the two solids in contact. The adhesive layer, in our case commercial adhesives or greases or MWCNT arrays, can either act as a contact (2-layer model) or as another layer (3-layer model). For a 2-layer model, the interface thickness is considered negligible with respect to the substrates, therefore contact resistance is relevant. A 3-layer model would then, by default, have two contact resistances, upper and lower, and is characterized by an effective thermal diffusivity, α_{eff}, of the measureable, non-negligible, interface material and the transient thermal interface resistance is written as Equation 3.1.

$$R_c = \frac{L_i}{\alpha_{eff}\rho_i c_i} \tag{3.1}$$

In our case, the 2-layer method considers R_c as simply the difference in thermal resistances, represented in Equation 1.2. To explain the relationship between the total diffusivity and the contact resistance of the interface layer, it is appropriate to recall Equation 1.4 for the 2-layer model introduced in Chapter 1.

$$\frac{L_{tot}}{k_{tot}A_{tot}} = \frac{L_1}{k_1 A_1} + \frac{L_2}{k_2 A_2} + \frac{R_c}{A_c} \tag{1.4}$$

With this mathematical expression, and the simplified expression in Equation 3.2, the mathematical relation between total diffusivity, α_{tot}, and contact resistance, R_c, can be proven. The properties L_{tot}, L_1, α_1, C_1, ρ_1 are input into the LFA, C_{ptot}, ρ_{tot} are deduced based on the inputs, and the LFA measures the total thermal diffusivity, α_{tot} . Therefore, the LFA analysis calculates R_c as the difference in the thermal resistances.

$$\frac{L_{tot}}{\alpha_{tot}C_{ptot}\rho_{tot}} = \frac{2L_1}{\alpha_1 C_{p1}\rho_1} + R_c \tag{3.2}$$

Another thermal property of the interface layer presented in Milosevic's work [25] is the effective thermal conductivity, K_{eff}, defined in Equation 2.21. The plot of log diffusivity versus log contact resistance is the heart of thermally characterizing the interface materials, however

both of these parameters are bond-line thickness, L_i, dependent. The goal was to keep the bond-line constant for every interface material; however experimental error affects the fabrication of the assemblies. The K_{eff} essentially normalized the thermal performance of the interface per bond-line thickness as t_i/R_c. The comparison of effective thermal conductivity for the CNT arrays to one another and to other TIMs is seen in Figure 3.15. The bond-line thickness was documented above the appropriate bar. In order to measure bond-line thickness, the samples were mounted in epoxy resin plane perpendicular to the interface and polished. The interface thicknesses were measured by optical microscopy at twenty locations. The purpose of the K_{eff} characterization is to compare the interface materials themselves, independent of the slight variations associated with sandwich assembly. However, the calculation of t_i/R_c is not completely independent of the bond-line thickness, t_i, therefore it is appropriate to note the thickness of the interface.

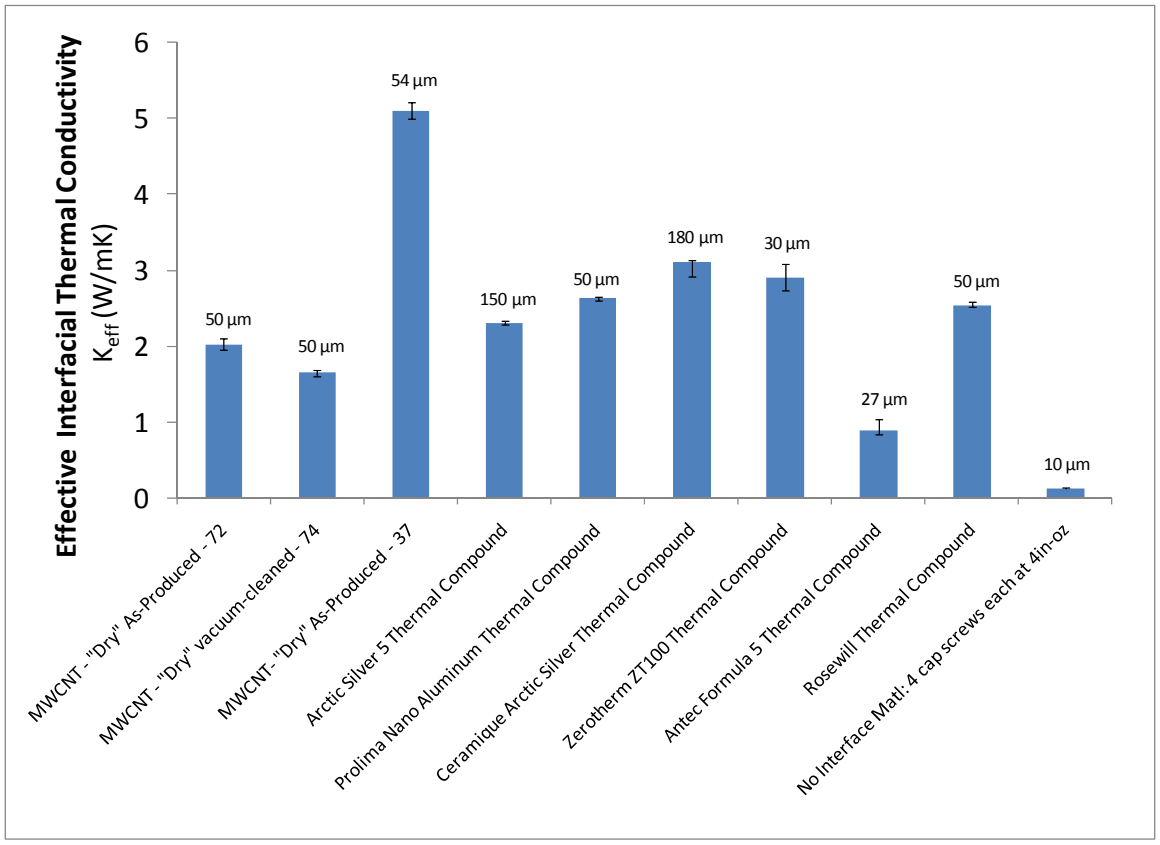

Figure 3.15 Effective interfacial thermal conductivity of "dry" MWCNT arrays and thermal greases. Dry arrays were cap-screw bonded and secured with 4 M1 cap-screws torque to 4 in-oz (1155 kPa), and thermal grease bonded hand-pressed assemblies

It was interesting to note the cap-screw assembly with no interface material had the shortest bond-line and, therefore, the shortest distance for heat to transfer. However, the poor thermal conductivity of air 0.0262 W/mK [64] created a serious "bottleneck" for conductive heat flow. With the addition of a TIM, effective conductivity dramatically increased.

The values of effective thermal conductivity of the MWCNT arrays are comparable to the thermal greases. The MWCNT- "Dry" As-produced - 37 has the highest effective conductivity at 5.10 W/mK. This is the highest value observed for the NT arrays and over 60 % higher than the 3.11 W/mK value found for Ceramique Arctic Silver. The MWCNT-37 is almost twice the value found for the highest adhesive-infiltrated MWCNT array, MWCNT-Epoxy1-43, with a k_{eff} of 2.62 W/mK. With the exception of MWCNT – 37, the NT arrays performed very similarly to the thermal greases. This characterizes "dry", un-infiltrated vertically aligned MWCNT arrays as a TIM that could provide a replacement for thermal greases. Aside from having excellent thermal properties, MWCNT arrays, theoretically, are easier to handle, can withstand high temperatures and high vacuum environments, making them superior to thermal greases. MWCNTs can withstand in environments of up to 700 °C (in N_2), shown in Figure 3.7, when thermal greases will vaporize at around 150 °C. Typical integrated circuits made of silicon components operate at temperatures up to 105 °C. A replacement for silicon, however, are components composed of gallium arsenide (GaAs), which is a compound used in higher power applications, allow operation temperatures to reach 125 °C [5]. GaAs components often make-up satellites and other spacecraft because of higher power output requirements over a long period of flight time. The interfaces on satellites must withstand higher temperatures and high vacuum environments in space, while still conducting heat. MWCNTs can withstand higher temperatures and higher vacuum. The later was addressed by thermal tests in the LFA under high vacuum ($< 1 \times 10^{-5}$ mbar) previously shown in Figure 3.8. The MWCNT still conducts heat even in high vacuum environments, where thermal greases would out-gas to the high-vacuum environment.

3.4 Concluding Remarks

The present chapter contains a characterization of "dry", un-infiltrated carbon nanotube arrays. The results suggest improvements of "dry" MWCNT arrays over commercial thermal greases currently used in many different interface applications. A TIM must possess high conductivity, conformability, and adhesion to, and filling of, surface imperfections and voids. In some high power applications, TIMs must also possess the ability to conduct heat even in torturous

environments. MWCNT arrays will survive in high temperature, up to 700 °C, and high vacuum, reported here at < 1 x 10^{-5} mbar, where thermal greases will be subject to thermal degradation and possibly out-gas from the interface.

For future generation microprocessors and microelectronics, the polymers, solders, and phase change materials must be replaced with TIMs of higher conductivities, better adhesion, and higher elastic modulus [2]. Our MWCNT arrays that naturally grow vertically packed into array mats via the CVD synthesis method have these inherent characteristics. The conductivity through the axis of the MWCNTs is up to 3000 W/mK [13], and, when tested by LFA in an interface applications, they possess thermal contact resistances down to 10.6 mm^2K/W under moderate pressures. MWCNTs are mechanically resilient with a Young's Modulus of ~1 TPa [29], allowing them to conform to the surface voids commonly found in machined surfaces. Dry MWCNTs possess adhesive characterizations as well, with adhesive forces greater than van der Waals dominated adhesion. The dry arrays made great contact with surfaces for efficient heat conduction.

The arrays presented here perform as well as most commercial greases used in thermal interface material applications. When the MWCNT arrays cap-screw-bonded two aluminum discs, simulating actual interface conditions, the thermal interface contact resistance values were as low as 10.583 mm^2K/W, where commonly used commercial greases reached 10.36 mm^2K/W. Decreasing contact resistance will drastically increase the thermal performance of a component. The dry arrays thermally outperformed adhesive-infiltrated arrays presented in Chapter 2. The smallest resistance value found for adhesive-infiltrated arrays was 18.1 mm^2K/W, over 60 % higher than 10.583 mm^2K/W (MWCNT-37). Adhesive-infiltrated MWCNT arrays TIMs, both permanently bond and provide for reduced thermal contact resistance. When infiltrating highly conductive MWCNTs with low conductivity epoxy, the vastly different thermal properties result in phonon scattering. Huang *et al*. [13] was one of the first to develop MWCNTs embedded in polymer for the use in TIMs applications. In an effort to explain the low conductivity of epoxy-infiltrated arrays (1.21 W/mK) compared to experimental values of conductivity for nanotubes (3000 W/mK), phonon scattering was the phenomenon.

Phonons, which are lattice vibrational waves that transport heat in nonconductive and semiconductive materials, possess different frequencies and wavelengths [19]. The propagation of phonons within aligned, stiff MWCNTs are at a much higher frequency compared to polymer

material with a lower elastic modulus. Within composite MWCNT/epoxy systems, the high frequency phonon path through CNTs is interrupted when they reach polymeric material of dissimilar crystalline structure and acoustic impedance. With inherent defects within NTs, nanotube ends capped by epoxy, and nanotube interactions, an acoustic impedance mismatch occurs [48], decreasing thermal transport efficacy.

There are special applications for permanently bonded TIMs, specifically in the case of composite components for missile airframes. The TIMs in these components are asked to be multifunctional—they are placed between plies for heat conduction through the thickness of the component and also to form a permanent bond between the composite layers. Most applications for TIMs within integrated circuits are not meant to form a permanent bond, as this would preclude re-workability of the component. The re-workable, dry adhesive properties of un-infiltrated arrays are preferred and, in this application, there are excellent thermal properties as seen throughout this chapter.

Chapter 4 Refined Techniques to Purify and Improve the Use of MWCNTs as TIMs

4.1 Introduction

The CVD technique for MWCNT synthesis involved continuous depositing of carbon and catalyst onto the quartz slide. The result is an array of highly aligned carbon nanotubes; however, the result can also involve a build-up of amorphous carbon impurities on the top of the array, seen in the previous chapter, and a large volume of free volume "air" (up to 85 % observed in "dry" arrays). Because the synthesis of nanotubes is a highly complicated process, this could be due to many different factors. One possible reason for the amorphous build-up could be from an excess of deposited catalyst [69]. The parameters of nanotube growth can be varied independently. A catalyst feed rate reduction could aide in the reduction of amorphous carbon. However, a reduced feed rate would ultimately result in a lower nanotube packing factor. A parametric study varying all growth parameters must be done to find the configuration that best reduces the growth of amorphous carbon; however, this is outside the scope of this thesis. Whatever the source for the amorphous carbon, the resulting thermal insulation must be reduced [68]. Different techniques for minimizing amorphous carbon on the arrays are presented in this chapter including water cleaning, vacuuming, and tape cleaning. Also

presented here are techniques for improving the thermal conductivity of the MWCNT arrays by replacing the volume of air within the array with conductive greases and polymers.

4.2 Experimental

4.2.1 "Cleaning" the MWCNT Arrays

The resulting amorphous carbon deposited on the "top side" of the array is shown in Figure 4.1. The "top side" of the array was the side where the carbon was continuously deposited. The "cut side" was the side of the array that has been harvested from the quartz slide. The "cut side", as pictured in Figure 4.2, was much more aligned and does not contain any amorphous carbon insulating layers. The "cut side" is the benchmark for a purified "top side".

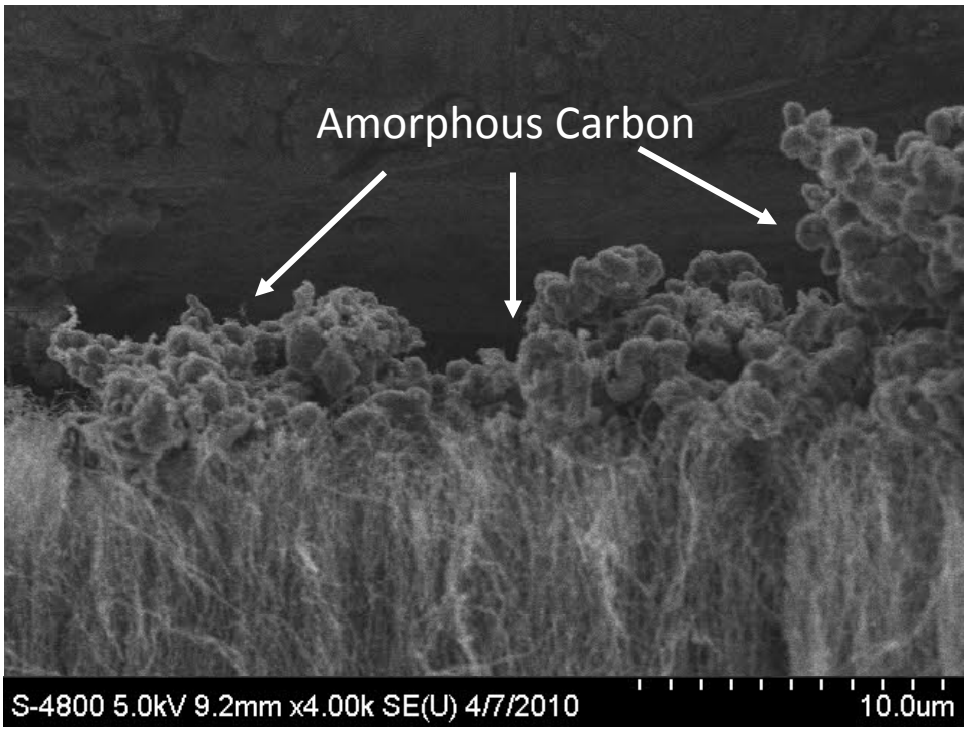

Figure 4.1 "Top Side" of MWCNT-71 Array revealing amorphous carbon impurities

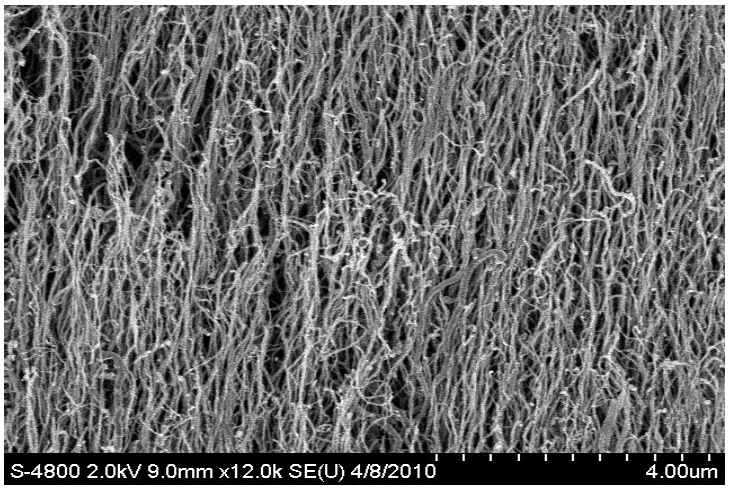

Figure 4.2 MWCNT- 37 “cut” side; notice the highly aligned MWCNT tips

Water cleaning, vacuuming, and tape cleaning techniques were explored in an attempt to rid the arrays of the amorphous carbon. The water cleaning technique is pictured in Figure 4.3-4.5. The array was simply dipped in deionized (DI) water for one minute and given two slow passes under the water, as pictured in Figure 4.4a. The loosely packed amorphous carbon was left floating in the water, whose appearance is seen in Picture 4.4b, leaving the MWCNT array in Figure 4.5. The “cleaned” array was left to dry for approximately 1 day. The harvesting of the “cleaned” array was not successful, however. Instead of harvesting the array as a continuous solid material, it began cracking and there were no pieces salvaged for testing. It seems that water cleaning not only removed amorphous carbon, but also sections of the array. The array was submersed into the water, which damaged the adhesive bonds between the NTs [49]. The water created pools on top of the array and the evaporation process from the pools caused cracking and ultimately an unmanageable material. The poor results from the water cleaning discouraged any further research involving this cleaning technique.

a)  b) 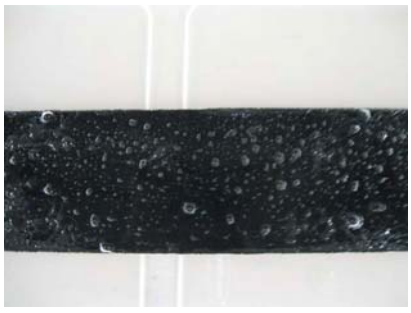

Figure 4.3 MWCNT arrays submersed in DI water to allow the lighter amorphous carbon to float to the top in an effort to purify the array of excess amorphous carbon

a)  b) 

Figure 4.4 a)The array was given two slow passes under the water to loosen the amorphous carbon from the top b) The remaining amorphous carbon and also sections of the NT array left behind

Figure 4.5 The MWCNT array drying after water cleaning

After discovering the effect the water had on the entire volume of the array, other methods were employed in an attempt to only affect the top where the excess carbon was located. The arrays were cleaned by a vacuum technique and a pressure sensitive adhesive (from a 3M sticky note). The vacuum technique involved simply running a bagless canister vacuum nozzle close to the top of the array for two passes along the entire array. SEM images (all at 10k magnification) were taken before (a) and after (b) implementing the vacuum cleaning technique as seen in Figure 4.6. It appears that vacuuming the array did work to remove much of the amorphous carbon. Figure 4.6b is now similar to the image of the non-vacuumed array “cut side” in Figure 4.7, which as mentioned previously, is the benchmark for vacuuming the arrays.

a) 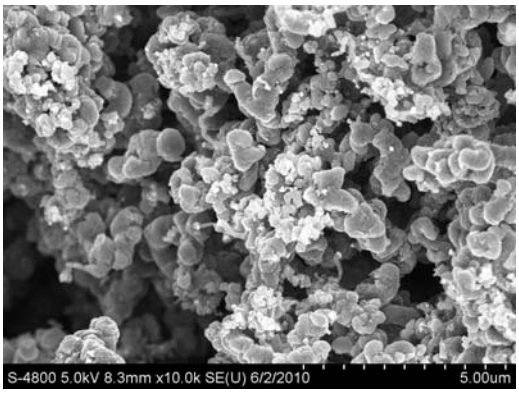

b) 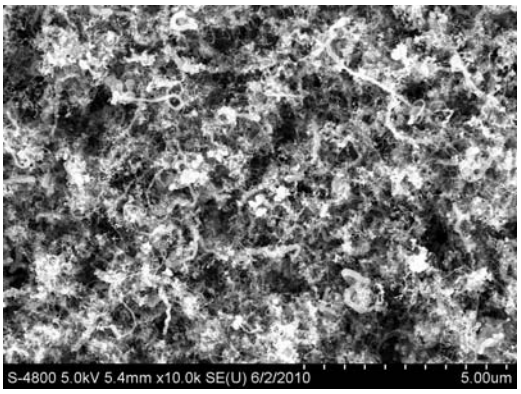

Figure 4.6 SEM images at 10k magnification showing results of vacuum cleaning the array; a) notice the visible amorphous carbon on the non-vacuum array and b) the very little visible amorphous carbon on the vacuum array

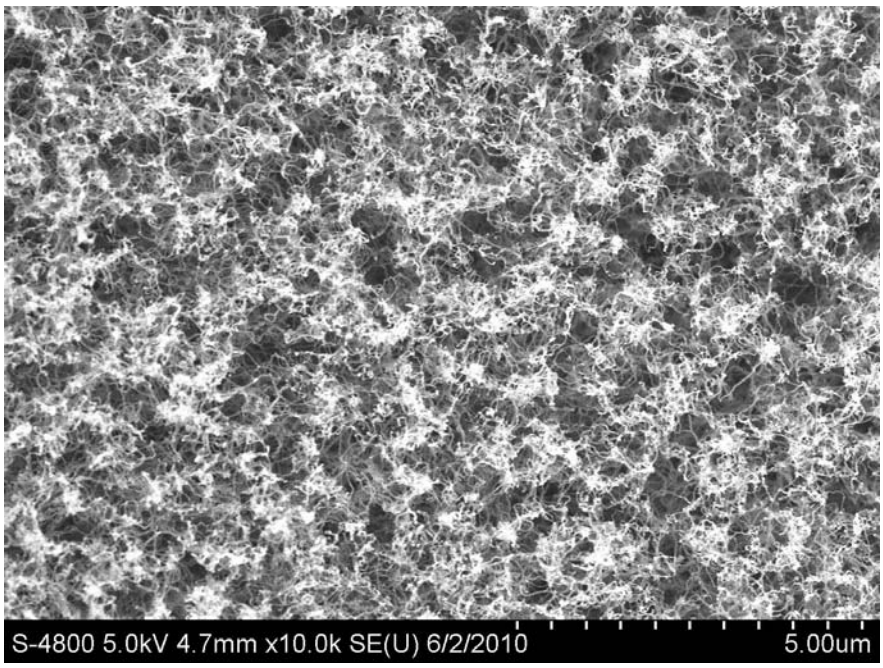

Figure 4.7 The "cut side" of the MWCNT – "dry" vacuum cleaned – 74; notice how similar it looks to Figure 4.6b

For further validation for the success of vacuuming the arrays, less magnified images were taken on the SEM. Figure 4.8 of the as-produced array and vacuum-cleaned array visually revealed the improvements in the purification of the arrays. Unaffected is the un-aligned geometry of the top of the NT arrays. Vacuum cleaning does rid the top of most of the insulating amorphous carbon; but there is much area for improvement in purifying the array to reveal aligned NT tips.

a) 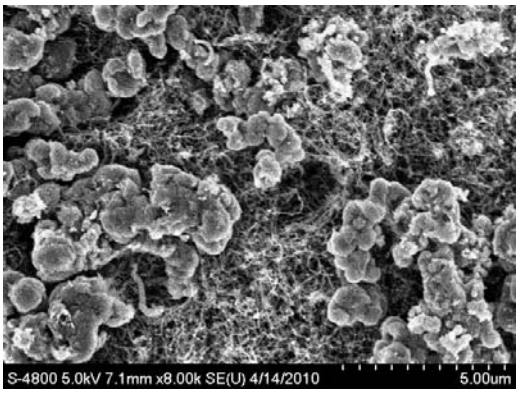

b) 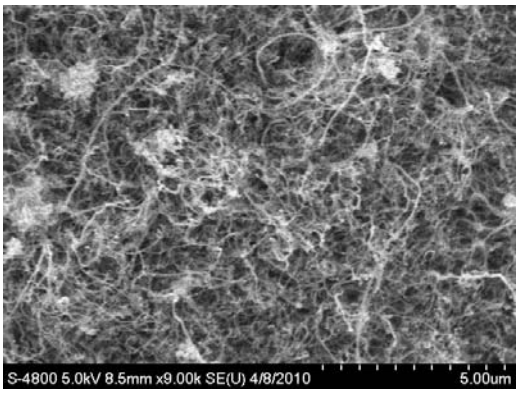

Figure 4.8 Low magnification images of "top sides" of as-produced and vacuum-cleaned arrays; a) MWCNT- "dry" As-produced - 56 revealing amorphous carbon b) MWCNT-"dry" vacuum-cleaned – 73 with very little amorphous carbon

Another purification technique explored was cleaning the NT array with the pressure sensitive adhesive shown in Figures 4.9 and 4.10. This is just a preliminary test lightly based on work by Liangti Qu *et al* [70] that altered NT array surfaces using adhesive tape. The adhesive was lightly placed on the "top side" of the array and successfully removed excess amorphous carbon and sections of the aligned MWCNT array as well. This adhesive tape method test on the small scale is just an initial test that demonstrated the application that this method can have to alter the surface of arrays. It will be implemented on a larger scale and further explored through SEM and LFA analysis.

a) 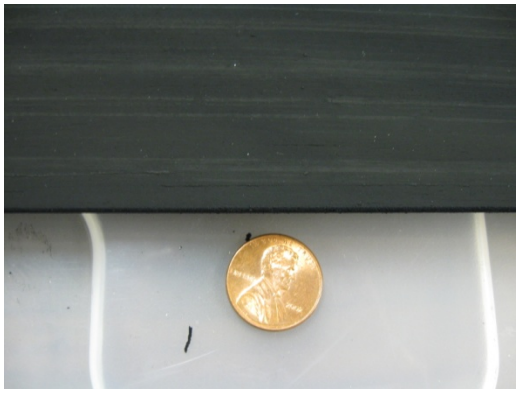
b) 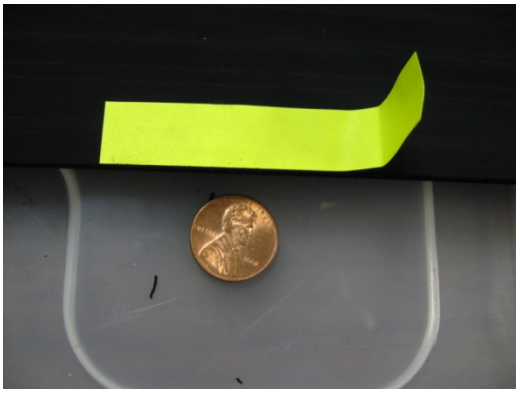

Figure 4.9 Sticky note cleaning of array a) typical section of array on quartz slide to be cleaned with a small amount of visible amorphous carbon b) pressure sensitive adhesive lightly pressed onto the NT array

a) 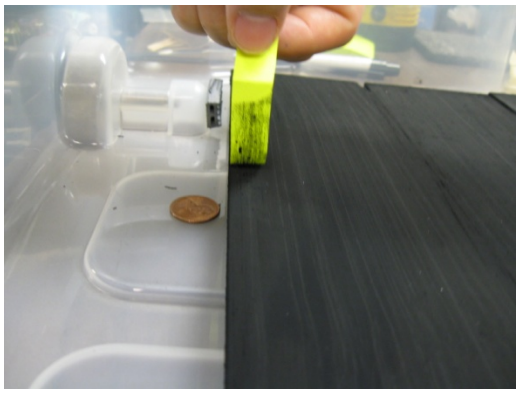 b) 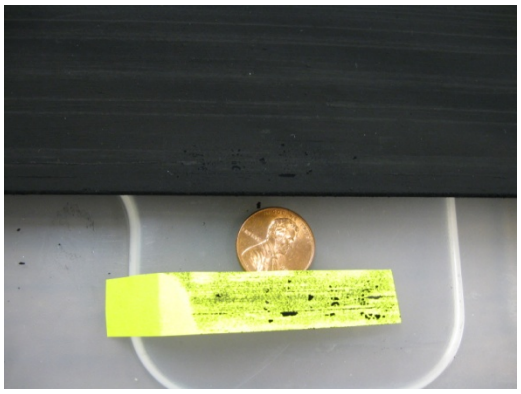

Figure 4.10 a)Pulling off sticky note with attached excess amorphous carbon b) image of amorphous carbon attached to the sticky note

The most successful cleaning technique employed in this chapter was the vacuum cleaning method. The array designated MWCNT- 74 was successfully vacuumed from MWCNT -72 "dry" as-produced array, harvested, and thermally tested. The slide was weighed after vacuuming and the NT areal density of 2.43 mg/cm^2 was calculated, based on the method presented in Chapter 2. An approximate weight of 0.1 g of the original MWCNT – 72 array was removed by the vacuuming technique. We assumed that most of what was removed was amorphous.

Table 4.1 Array properties of un-infiltrated "dry" MWCNT arrays with the addition of the vacuum-cleaned array

	NT Areal Density (mg/cm^2)	**NT bulk density (assuming 100 micron length) (g/cc)**	**Packing Factor (% of Max NT/ cm^2)**
MWCNT - "Dry" As-Produced - 72	2.67	0.27	14
MWCNT - "Dry" vacuum-cleaned - 74	2.43	0.24	13
MWCNT - "Dry" As-Produced - 37	0.97	0.10	11

4.2.2 Conductive Material Infiltration

Five different conductive materials were infiltrated into the MWCNT arrays designated Arctic Silver 5 Thermal Compound, 2.5 % nano copper, 2.5 % nano silver, Transient Liquid Phase Sinter (TLPS) CELV310, TLPS CELF108. An SEM image of the Arctic Silver 5 thermal compound is shown in Figure 4.11; notice the nano-sized metallic particles in epoxy binder. In theory, infiltrating a "dry" array with conductive nano particles to replace the free volume "air", with a low conductivity of 0.0262 W/mK [64], will increase the through-thickness conductivity through the

interface. A depiction of a conventional thermal interface material of metallic particles within epoxy is shown in Figure 4.12. The resin binder allows conformability and adhesion of the TIM and the metallic particles provide conductivity. In theory, infiltrating conductive resin into the MWCNT arrays will achieve conformability, adhesion, and additional conductivity from the binder combined with the inherently high conductivity from the NT arrays for a superior TIM.

The average nanotube in our arrays had a diameter of 30 nm. With the hexagonal orientation, shown in Figure 2.1, and an 11-15 % packing factor, there is about 80 nm length of air between each nanotube. The materials chosen had metallic particles smaller than 80 nm in diameter in an effort to permeate through the space between the nanotubes and create a more conductive volume. The MWCNT – 74 vacuum-cleaned array was gold (Au) sputter coated prior to infiltration with conductive adhesives. This, in theory, will improve infiltration because the conductive particles are more attracted to the metallic walls of the NTs of similar chemical composition [18, 48]. The Au-coated MWCNT tips will also reduce impedance mismatch and phonon scattering due to the creation of a transition zone between CNTs and the adherent substrate [49].

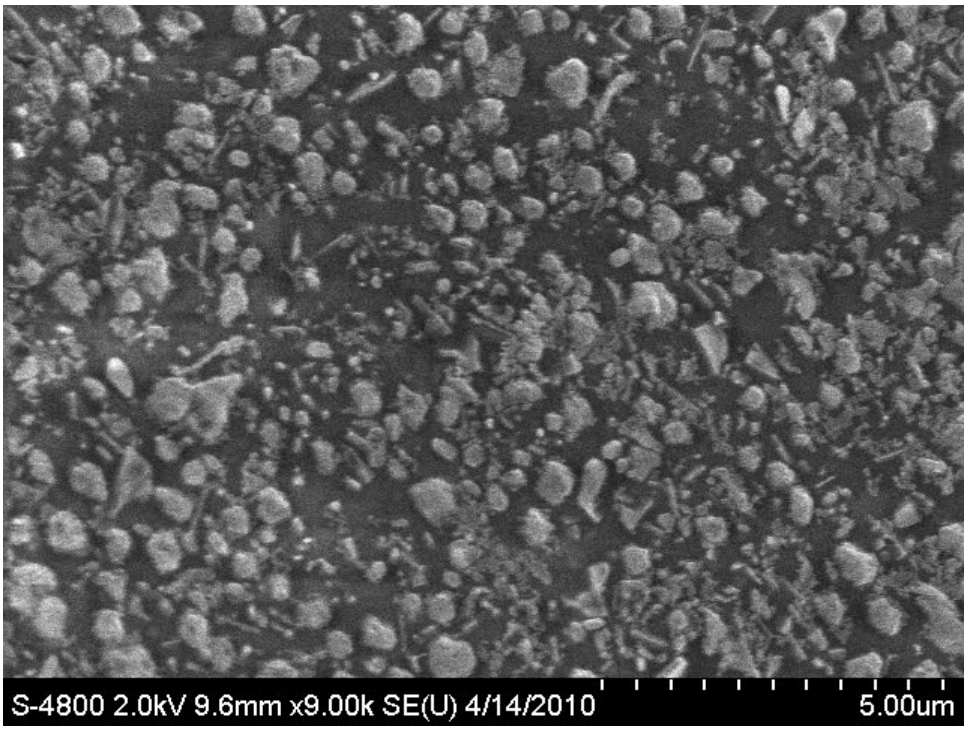

Figure 4.11 Arctic Silver thermal grease

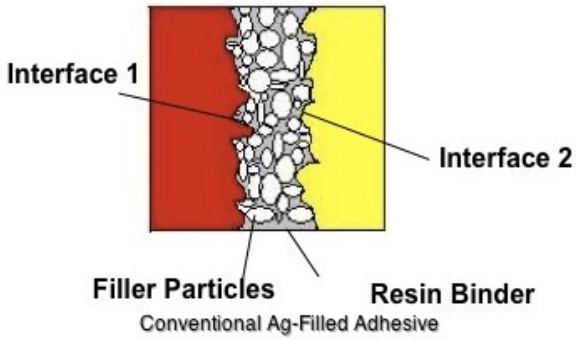

Figure 4.12 Schematic of an interface bonded by a conventional thermal interface material of conductive fillers in epoxy

The arrays were harvested from the quartz substrate as free-standing arrays, allowing the array to be sputter coated with gold and infiltrated on both sides. This was not on the large scale as described in Chapter 2. The infiltration of the conductive material was performed post harvesting from the quartz substrate on a sample-by-sample basis. In the case of the resin infiltrated with nano-sized particles of copper and silver and TLPS material, the free-standing arrays were sandwiched between two Al 6061 discs bonded at 75 psi at 200 °C for 45 minutes using a ramp of 10 °C/minute.

4.2.3 Nano Resins and TLPS Infiltration

The infiltration technique for the 2.5 % nano silver and 2.5 % nano copper and the two TLPS materials is illustrated in Figures 4.13-4.15.

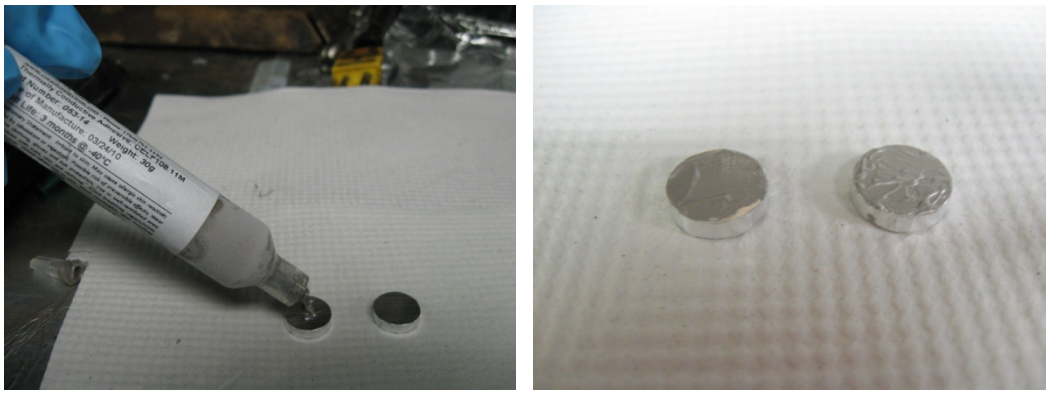

Figure 4.13 Even, homogenous coverage of 2.5% nano silver onto both sides of the Al 6061 substrates

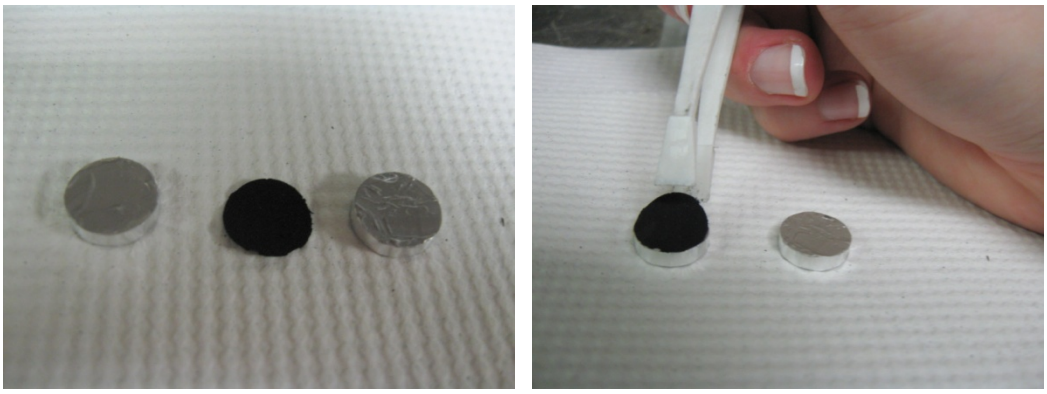

Figure 4.14 Placement of MWCNT array onto the 2.5 % nano silver-covered Al discs

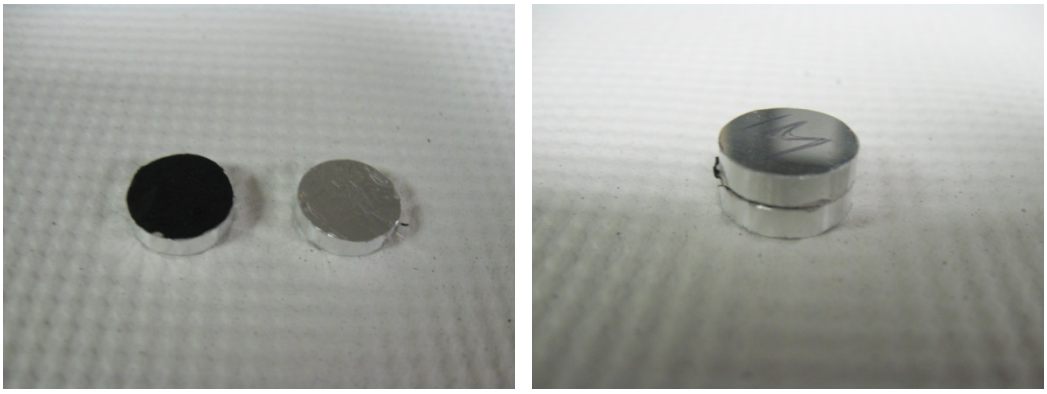

Figure 4.15 Sandwich assembly of MWCNT array infiltrated with 2.5 % nano silver

4.2.4 Arctic Silver 5 Infiltration

The Arctic Silver 5 Thermal Compound was infiltrated by a different technique. Because Arctic Silver 5 is thermal grease, not a thermoset material like the nano-sized particles dispersed in resin and TLPS materials, the grease was just applied to the array on the top side inside the cap-screw sandwich assembly (Figure 3.3) and thermally tested at varying pressures. The infiltration technique for the Arctic Silver 5 Thermal Compound is illustrated in Figures 4.16-4.17. The "top" aluminum substrate was evenly covered with the Arctic Silver 5, shown in Figure 4.17. When the grease-covered aluminum was placed onto the "dry" MWCNT array-covered "bottom" aluminum substrate and given a pressure of 75 psi, the array was successfully infiltrated with the viscous grease. A top view of the MWCNT infiltrated by the grease is shown in Figure 4.18. An effort was made to provide a homogenous infiltration for reliable LFA results.

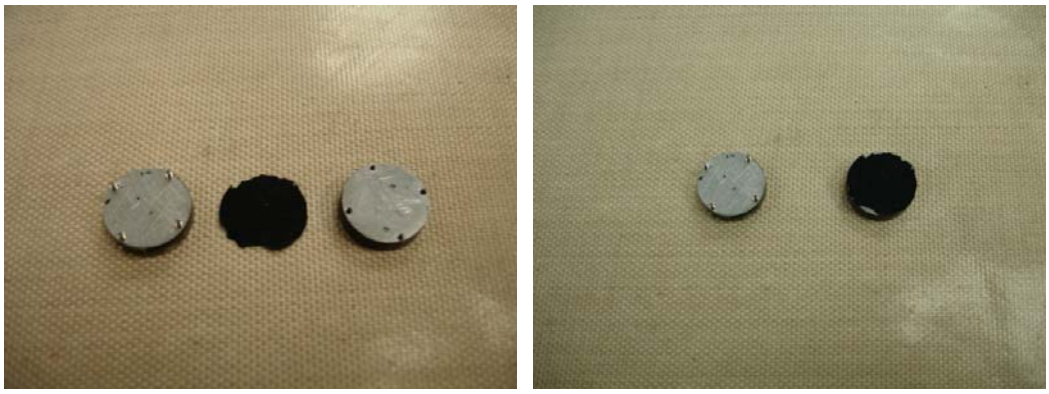

Figure 4.16 Placement of MWCNT array onto aluminum cap-screw assembly

Figure 4.17 Even, homogenous coverage of Arctic Silver 5 Thermal Compound on the top aluminum substrate

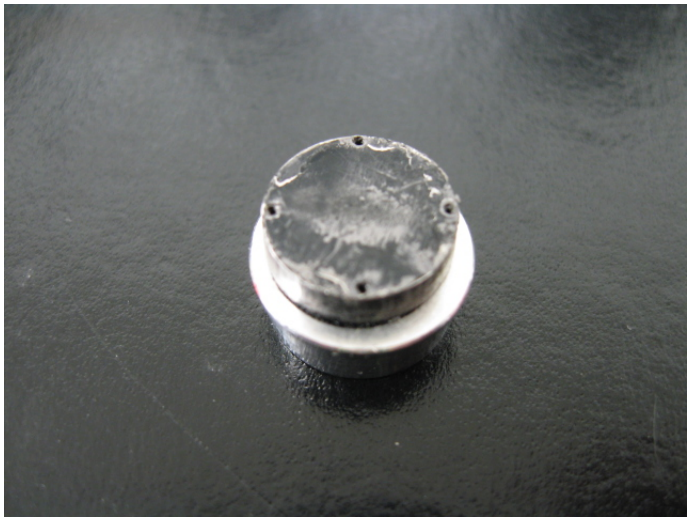

Figure 4.18 “Dry” MWCNT infiltrated with Arctic Silver 5 Thermal Compound

4.2.5 Nano Resin Infiltration SEM Imaging

The 2.5 % nano silver and 2.5 % nano copper had silver and copper particles, respectively, at <30 nm in diameter. These particle sizes allowed infiltration into the MWCNT array with ~80 nm spacing between each nanotube. The SEM image in 4.19 was of the interface composed of MWCNT array infiltrated with 2.5 % nano copper resin. The SEM images suggest that the resin successfully infiltrated through the array to create a homogenous interface that is advantageous for thermal transport between the aluminum substrates. Figure 4.20 of the interface composed of MWCNT infiltrated with 2.5 % nano silver tells a different story. The nano silver does not homogeneously infiltrate through the array and the result is an interface containing voids. The SEM showed us that it was not a continuous, solid interface like what was seen in Figure 4.19 for the nano copper infiltration. Heat transfers most effectively trough a solid, where phonon transport is not interrupted by air pockets. It is intuitive that the solid interface, free of voids, will give lower thermal contact resistances and diffusive more heat. This was the case, as seen in the thermal results to follow.

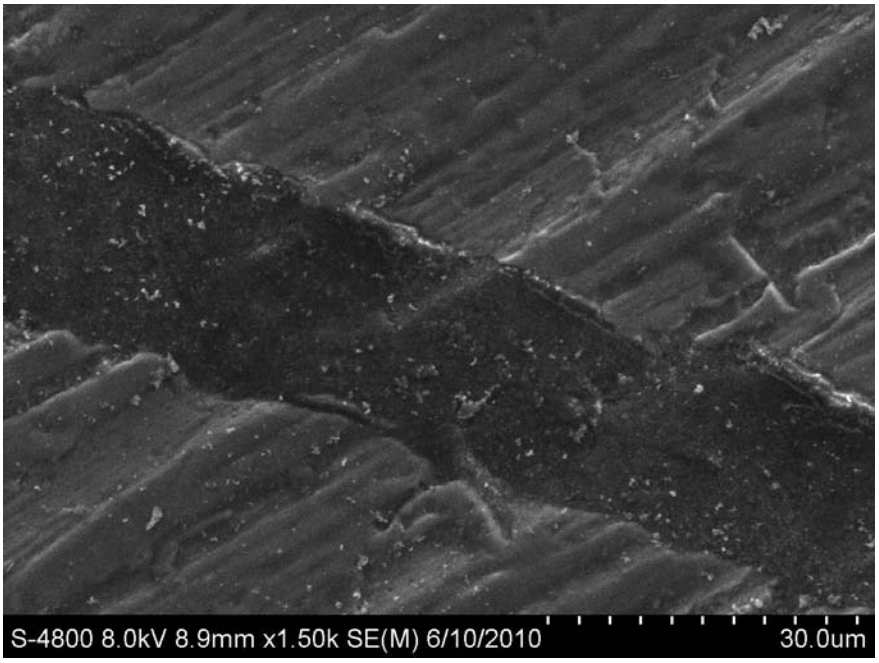

Figure 4.19 Interface composed of a MWCNT array infiltrated with 2.5 % nano copper resin bonding two aluminum substrates

Figure 4.20 Interface composed of a MWCNT array infiltrated with 2.5 % nano silver resin bonding two aluminum substrates

4.2.6 TLPS Infiltration SEM Imaging

The transient liquid phase (TLPS) formulations CELF 108 and CELV 310 were sintering conductive adhesives designed by Creative Electron to attach heat generating devices, like microprocessors and circuits, to heat sinks. The TLPS materials were composed of particles that are larger than the 80 nm spacing but, when the reflow temperature (175 °C) is reached during cure, it was postulated that the molten solder components could penetrate the cavities between the MWCNTs, particularly if the sidewalls of the MWCNTs are metalized. The SEM images suggest, however, that the TLPS was unable to infiltrate and, instead, formed a metallurgical bond between the MWCNT and the aluminum substrate. Figure 4.21 and Figure 4.22 pictured the interface composed of MWCNT infiltrated with TLPS CELF 108 and TLPS CELV 310, respectively. The images revealed a “sandwich effect”, where TLPS sandwiched the MWCNT.

Creative Electron designed TLPS to replace solder and, like solder, it forms metallurgical bonds to solderable surfaces. The particle sizes of the solder components were too large, even when molten, and the TLPS material sat at the top and bottom of the array, hence sandwiching the MWCNTs, not infiltrating. The TLPS and MWCNT array did, however, create a very homogeneous interface and there appears to be no air gaps or voids through the interface. The difference in material compositions and thermal properties, along with the “sandwich effect”,

essentially created four interfaces for potential phonon scattering. Energy is carried via phonons through materials, but an impedance mismatch between materials can cause phonons to scatter and reduce conductivity through the interface [18]. The goal is to create a solid interface, where heat can more easily transport via phonons, but traveling through different materials, in this case, aluminum, TLPS, MWCNTs, TLPS and back to aluminum, does not promote effective heat transfer.

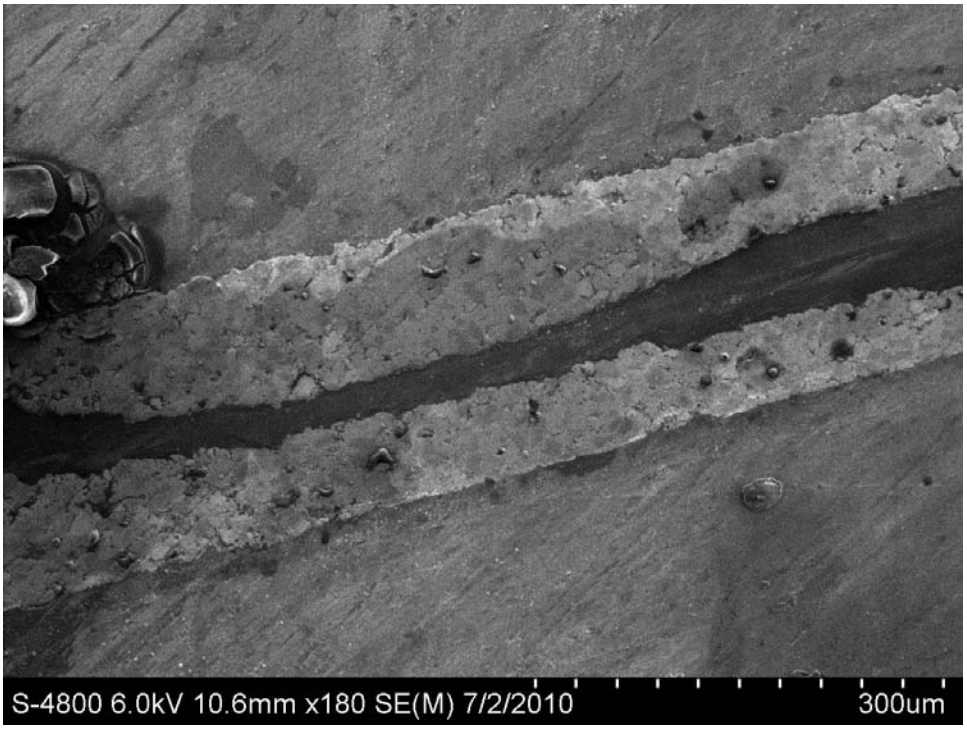

Figure 4.21 Interface composed of a MWCNT array infiltrated with TLPS formulation CELF 108 bonding two aluminum substrates

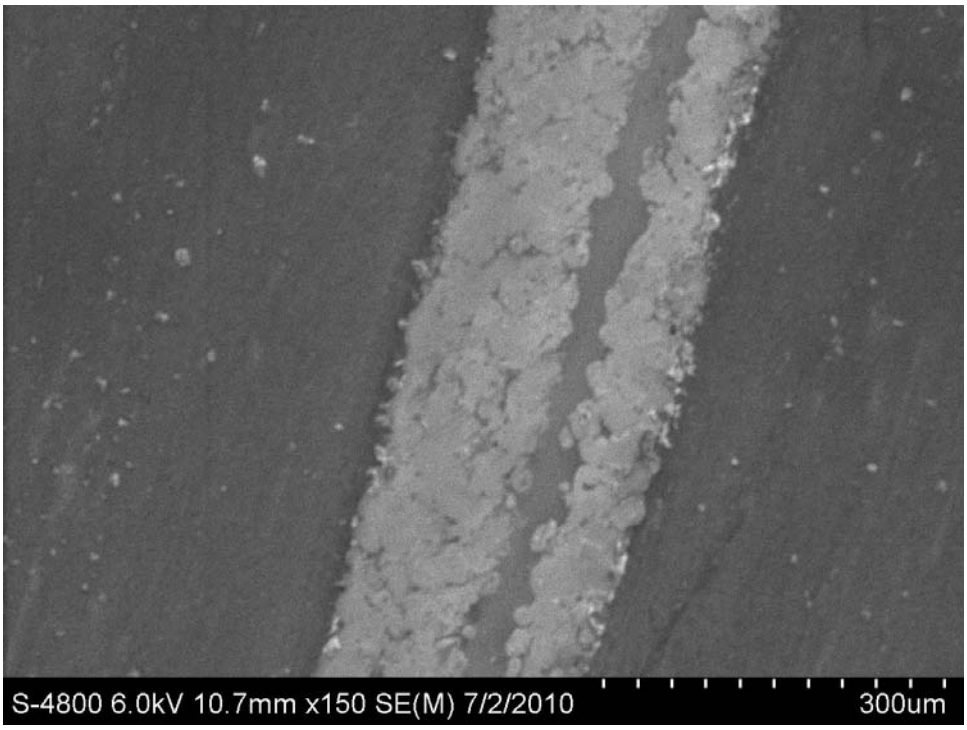

Figure 4.22 Interface composed of a MWCNT array infiltrated with TLPS formulation CELV 310 bonding two aluminum substrates

In order to further prove the infiltration of the nano copper-filled resins effective infiltration into the MWCNTs, we took a look at the interface at a lower magnification than Figure 4.19 at a magnification of 1.5k. The SEM image of the interface at a magnification of 180 shown in Figure 4.23 still does not illustrate the "sandwich effect" as seen with the TLPS interfaces. It appears that even at low magnifications, to more clearly see a larger area of the interface, the nano copper-filled resin infiltrated into the MWCNT array and gives a continuous, homogenous interface bonding the two aluminum substrates.

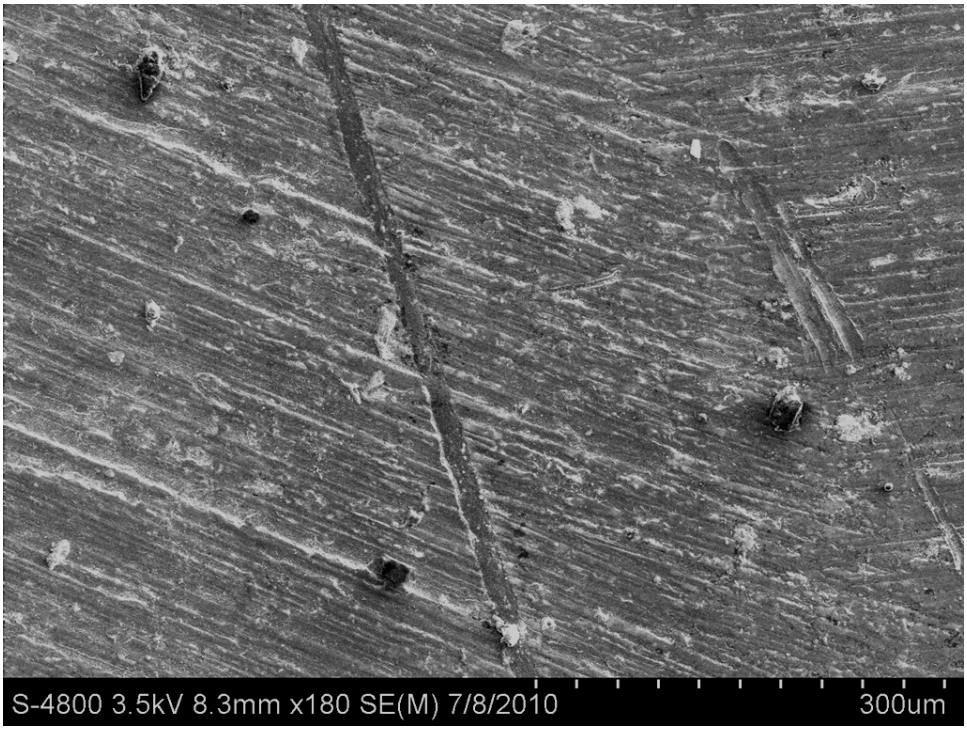

Figure 4.23 Low magnification image of interface composed of a MWCNT array infiltrated with 2.5 % nano copper resin bonding two aluminum substrates

4.3 Results

4.3.1 Vacuum Cleaning Results

Each of the interface materials were tested for thermal diffusivity of the stack "sandwich" (α), thermal interface contact resistance (R_c), and effective thermal conductivity (k_{eff}). A plot of the thermal diffusivity across the entire sandwich and the corresponding contact resistance through the interface, both on a log scale, of "dry" as-produced arrays and "dry" vacuumed arrays, is seen in Figure 4.24. The list of samples was recorded in order of decreasing thermal performance.

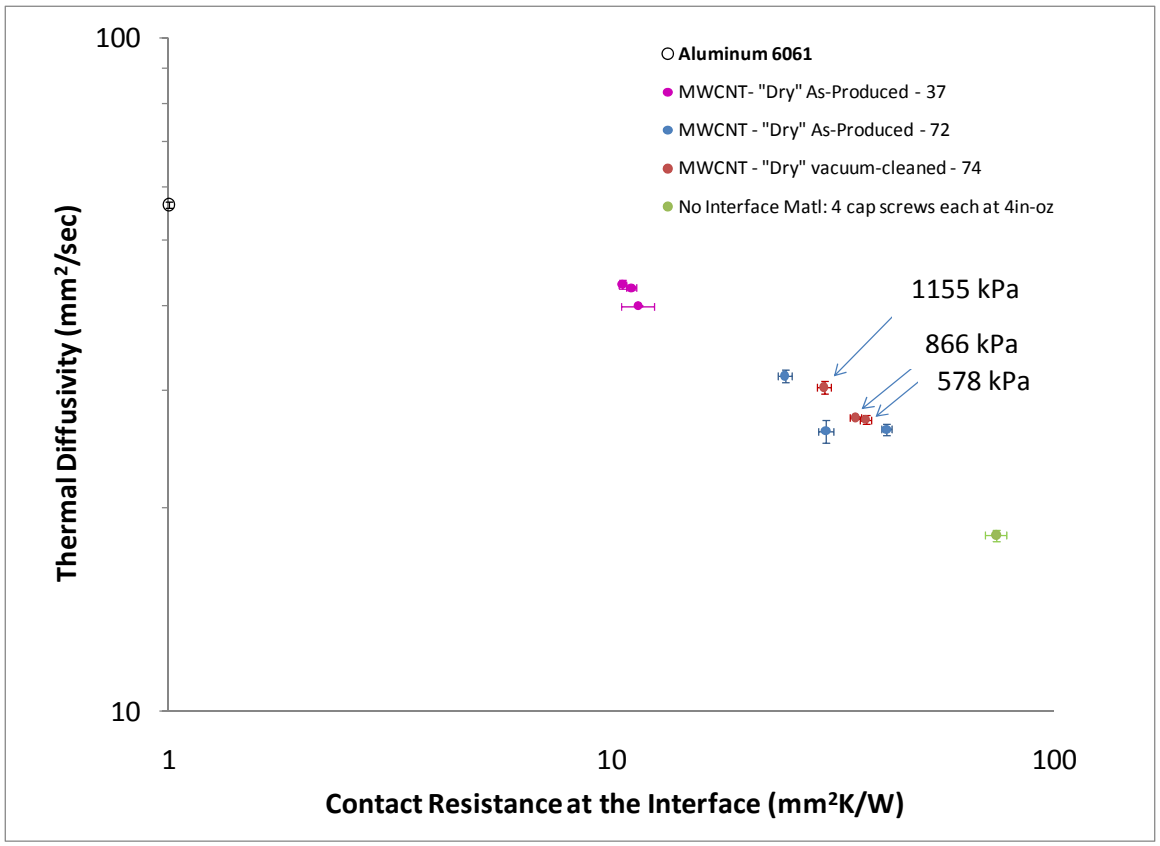

Figure 4.24 Thermal diffusivity of the sandwich plotted against contact resistance at the interface of MWCNT arrays cap-screw-bonded mill-finish Al substrates

As expected, the solid aluminum has the highest diffusivity and no contact resistance and the sandwich containing no interface material has poor thermal properties. The vacuum cleaned MWCNT – 74 array possessed contact resistances down to 30.2 mm^2K/W at 1155 kPa, which was comparable to the MWCNT – 72 as-produced array with interfacial contact resistance of 24.63 mm^2K/W at 1155 kPa. The vacuum cleaning attempt did not improve the thermal properties of the MWCNT – 72 array as anticipated. The as-produced array 37 outperformed both the MWCNT-72 array and MWCNT-74 array. The MWCNT-74, which appears to be cleaned by the SEM imaging in Figures 4.6 and 4.8, did not reach the excellent thermal properties of the MWCNT – 37 array. Even if the 74 array was entirely rid of amorphous carbon, it is intuitive that the 37 array would still be exceptional due to the shorter bond-line thickness. This result proves that when comparing thickness, reduction in amorphous carbon, and metallic coatings, the property that most improves the thermal performance of arrays in TIMs applications is a reduction in thickness.

4.3.2 Conductive Material Infiltration Results

Diffusivity across the assembly and the interfacial contact resistance across the interface is plotted in Figure 4.25 for the MWCNT arrays infiltrated with conductive adhesives 2.5 % nano copper, 2.5 % nano silver, Transient Liquid Phase Sinter (TLPS) CELV310, TLPS CELF108 and thermal grease Arctic Silver 5 Thermal Compound. The MWCNT – 74 vacuum-cleaned array was Au sputter coated and infiltrated with all four conductive adhesives and Arctic Silver 5. After discovering the excellent thermal properties of MWCNT -37, it was sputter coated and infiltrated with just Arctic Silver 5, because of the limited supply of creative electron materials.

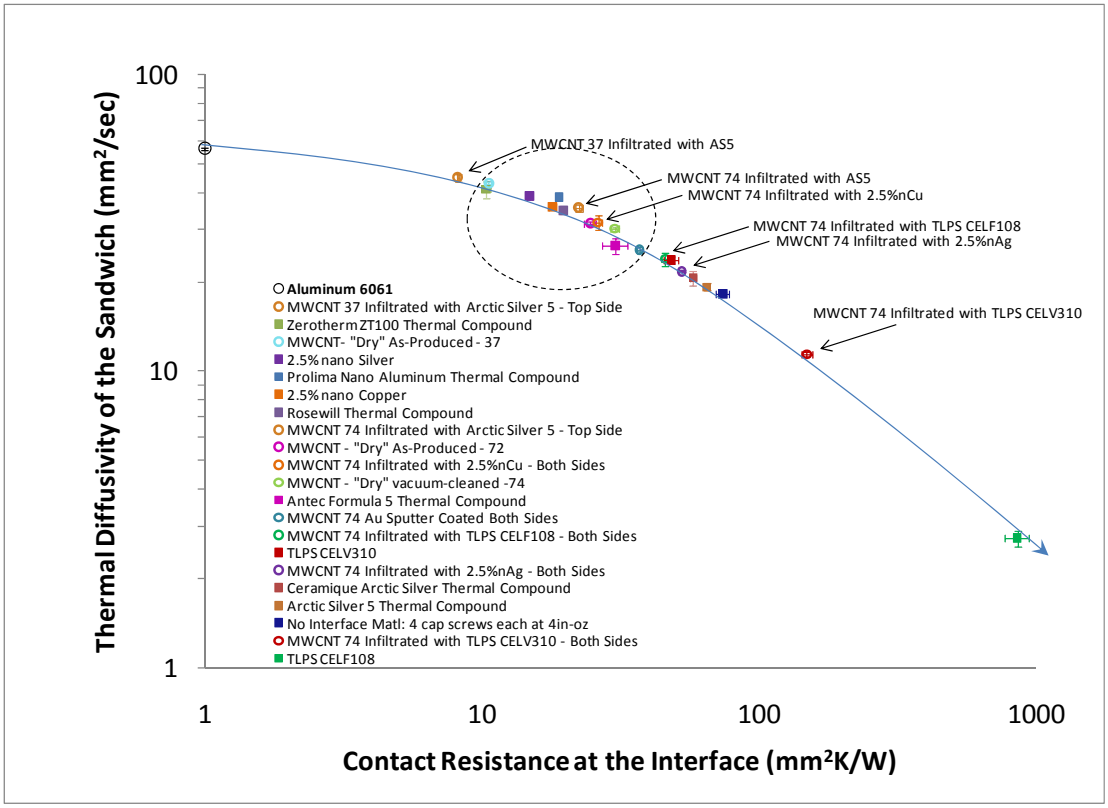

Figure 4.25 Thermal diffusivity of the sandwich plotted against contact resistance at the interface

The diffusivity across the sandwich and the contact resistance across the interface of all sandwich assemblies were shown in Figure 4.25. The list of samples was recorded in order of decreasing thermal performance. The MWCNT arrays cap-screw-bonded mill-finish Al

substrates were compared to thermal greases in hand-pressed mill-finish Al substrates , MWCNT arrays infiltrated with conductive adhesives bonding mill-finish Al substrates, and MWCNT arrays infiltrated with thermal grease in cap-screw-bonded mill-finish Al substrates. Although this plot is important to see all thermal tests relating to conductive resin infiltration, this all-encompassing plot was broken down in easier to understand sections and explained in detail in this chapter. It was appropriate to include Arctic Silver 5 infiltration, nano particle adhesives 2.5 % nano copper and 2.5 % nano silver, and Transient Liquid Phase Sinter (TLPS) CELV310 and TLPS CELF108 all in separate results sections. These three types of infiltrants are very different, which could be concluded from the comprehensive Figure 4.25. The key indicates each of the samples in decreasing thermal performance; however, there are many factors that change the infiltration and even the sandwich assembly including viscosity, conductive particle size, and conductivity.

The MWCNT arrays are all included in the circle and each infiltrated array was labeled appropriately. The infiltrated arrays, with the exception of MWCNT-37 infiltrated with Arctic Silver 5 grease, did not outperform MWCNT arrays alone. Similar diffusivity and contact resistance values are found for MWCNT – 74 infiltrated with Arctic Silver 5 Thermal Compound and 2.5 % nano copper compared to the “dry” MWCNT arrays and commercial conductive materials. The MWCNT – 74 infiltrated with 2.5 % nano Silver and the two TLPS materials had the lowest diffusivity values and the highest thermal contact resistance values most likely due to the poor infiltration shown in the SEM imaging in Figures 4.20-4.22. To determine the thermal performance of the MWCNT arrays infiltrated with conductive resin, the three very different infiltrants will be compared separately.

4.3.3 Arctic Silver 5 Infiltration Results

Diffusivity across the assembly and the interfacial contact resistance across the interface are plotted in Figure 4.26 for the MWCNT arrays infiltrated with Arctic Silver 5 Thermal Compound. The key indicates each of the samples in decreasing thermal performance. The MWCNT – 74 was the vacuum-cleaned array that was Au sputter coated prior to the small scale infiltration with Arctic Silver 5 on the top side. The MWCNT – 37 was also Au sputter coated prior to the small scale infiltration with Arctic Silver 5 on the top side.

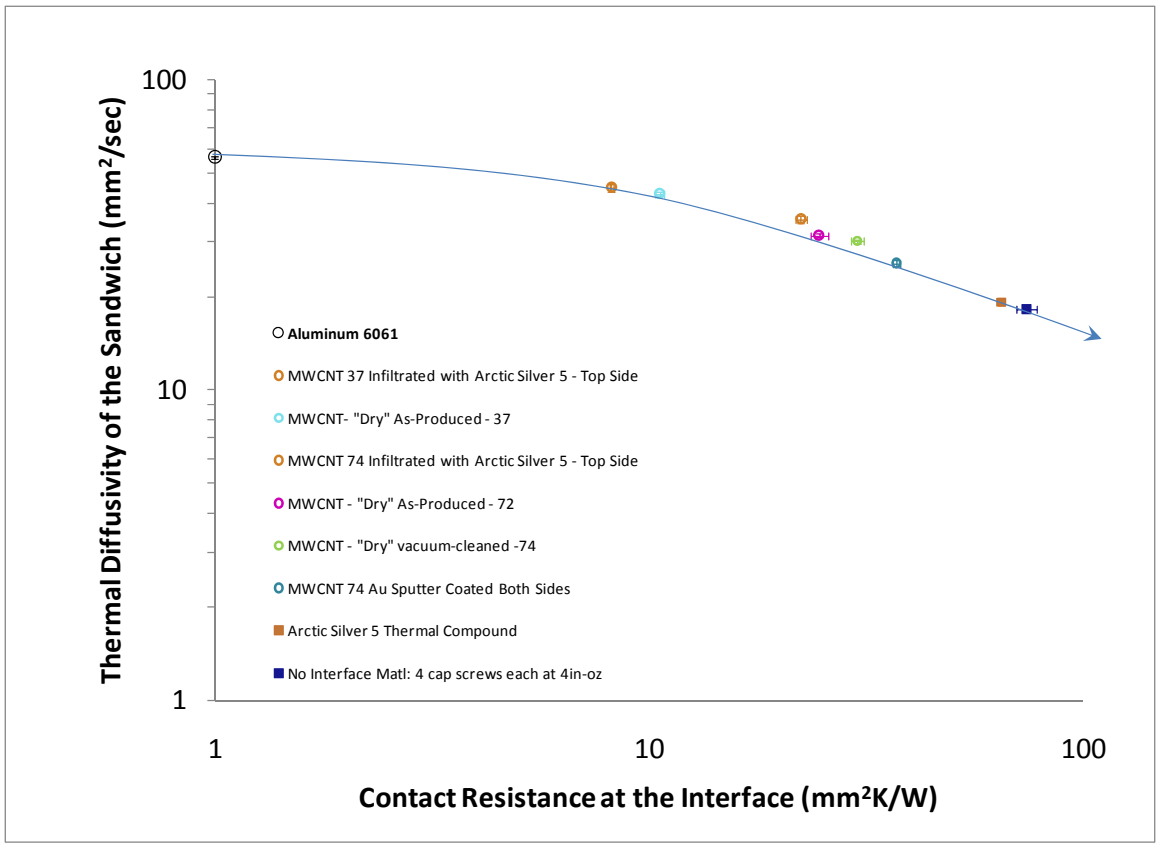

Figure 4.26 Thermal diffusivity of the sandwich plotted against contact resistance at the interface of MWCNT arrays and MWCNT arrays infiltrated with Arctic Silver 5 Thermal Compound cap-screw-bonding mill-finish Al substrates

The MWCNT arrays cap-screw-bonded mill-finish Al substrates (at 1155 kPa) were compared to Arctic Silver 5 (AS5) Thermal Compound in hand-pressed mill-finish Al substrates, and MWCNT arrays infiltrated with Arctic Silver 5 Thermal Compound in cap-screw-bonded mill-finish Al substrates (at 1155 kPa). This plot is Figure 4.26 included only the thermal tests relating to AS5. The exceptional "dry" as-produced MWCNT array was MWCNT – 37, so it is intuitive that this array infiltrated with Arctic Silver 5 outperforms all others, following solid aluminum. MWCNT 37 Au sputter coated and infiltrated with Arctic Silver 5 on the top side reached an interfacial contact resistance down to 8.19 mm^2K/W and thermal diffusivity of 45.07 mm^2/s at moderate pressure loads. These thermal property values are excellent for TIM applications. Not only can this TIM 1) conduct heat through an interface, it is also 2) re-workable. This was a significant discovery for improving MWCNT arrays for TIM applications. Also significant is the improvement over Arctic Silver 5 Thermal Compound alone with thermal contact resistance of 64.84 mm^2K/W and thermal diffusivity of 19.213 mm^2/s. Infiltrating the grease into MWCNT –

37 array was a 87 % improvement and infiltrating the grease into MWCNT – 74 array was a 65 % improvement over AS5 alone in terms of interfacial thermal contact resistance. This is noteworthy when considering the wide use of AS5 in TIM applications in the microelectronics industry. The addition of MWCNT arrays drastically improves the thermal performance without having to sacrifice a re-workable, non permanent material.

A more intrinsic property of a TIM, less dependent on interface parameters, is the effective thermal conductivity (k_{eff}) [25]. It essentially normalizes the thermal performance of the interface per bond-line thickness as t_i/R_c. The thermal diffusivity and the interfacial contact resistance are both functions of the thickness of the interface, which makes the properties dependent on the fabrication of the assembly. While each sample was given a constant pressure and measures were taken to keep a standard bond-line thickness for each assembly, regardless of infiltration, experimental error affects the nature of the assembly. To compare the CNT arrays, CNT arrays infiltrated with Arctic Silver 5, and AS5 alone, effective thermal conductivity is a crucial thermal property, which is seen in Figure 4.27.

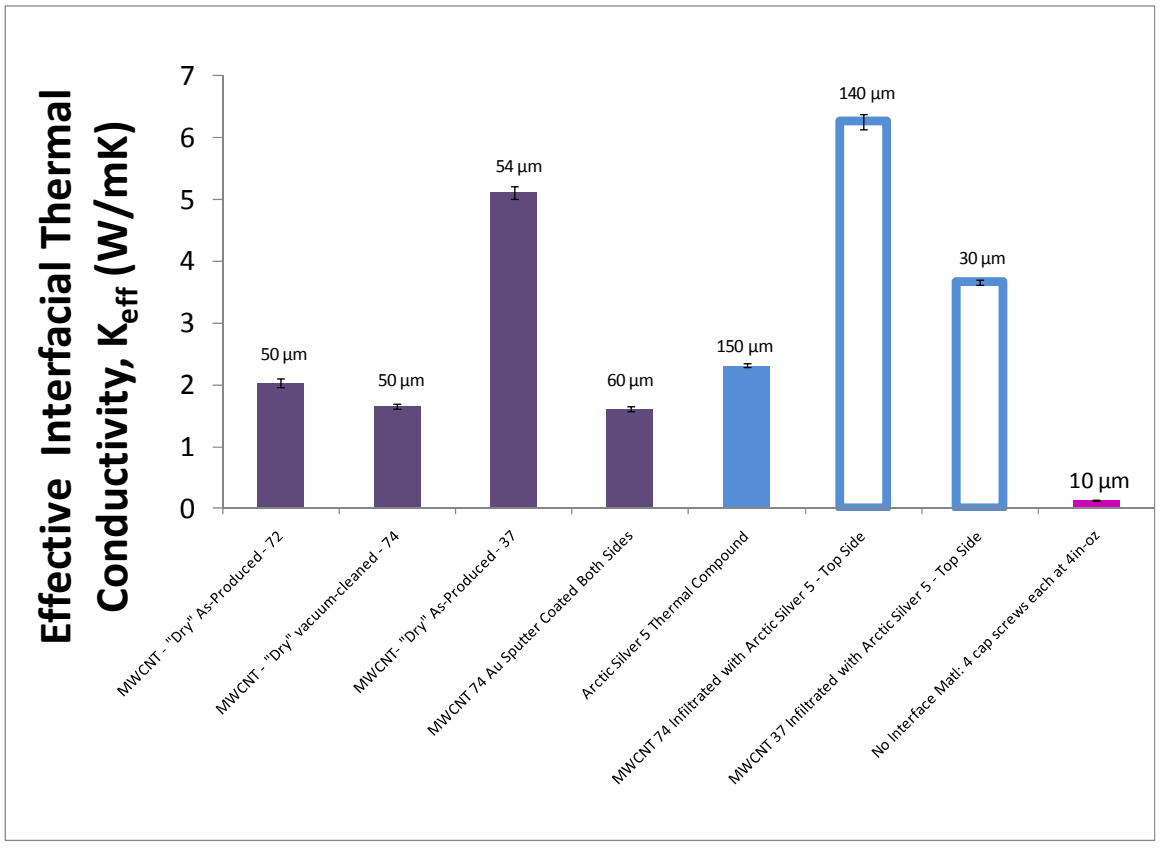

Figure 4.27 Effective interfacial conductivity of Arctic Silver 5 Thermal Compound Infiltration

Similar results are seen in Figure 4.27 as shown in Figure 4.26 for diffusivity and thermal contact resistance. The values of effective thermal conductivity of the MWCNT arrays infiltrated with Arctic Silver 5 are higher than Arctic Silver 5 with a K_{eff} of 2.31 W/mK. In the case of MWCNT- 74 and MWCNT -37 infiltrated with Arctic Silver 5, there were more than 2.5x and 1.5x improvement over AS5 alone, respectively.

4.3.4 Nano Resin Infiltration Results

Diffusivity across the assembly and the interfacial contact resistance across the interface are plotted in Figure 4.28 for the MWCNT arrays infiltrated with 2.5 % nano copper and 2.5 % nano silver adhesives. The key indicates each of the samples in decreasing thermal performance. The MWCNT – 74 was the vacuum-cleaned array that was also Au sputter coated prior to the small scale infiltration with nano materials on both sides.

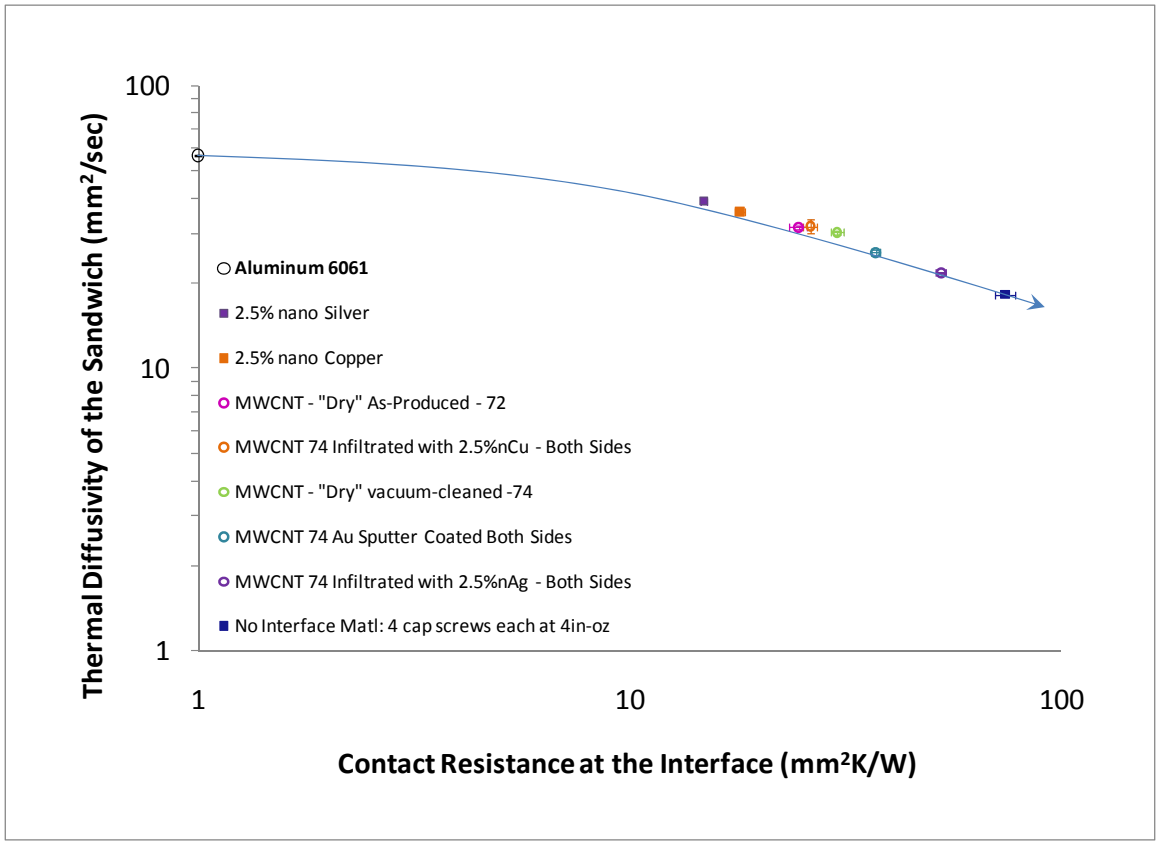

Figure 4.28 Thermal diffusivity of the sandwich plotted against contact resistance at the interface of MWCNT arrays and MWCNT arrays infiltrated with 2.5 % nano copper and 2.5 % nano silver adhesives bonding mill-finish Al substrates

The MWCNT arrays cap-screw-bonded mill-finish Al substrates (at 1155 kPa) were compared to 2.5 % nano copper and 2.5 % nano silver adhesives bonding mill-finish Al substrates (75psi, 200 °C, 45 minutes), and MWCNT arrays infiltrated with 2.5 % nano copper and 2.5 % nano silver adhesives bonding mill-finish Al substrates (75 psi, 200 °C, 45 minutes). This plot in Figure 4.28 included only the thermal tests relating to the nano materials. The 2.5 % nano silver-filled and 2.5 % nano copper-filled resins achieved thermal contact resistances down to 14.847 mm^2K/W and 17.99 mm^2K/W, respectively where "dry" MWCNT arrays only reached ~25 mm^2K/W. The lower contact resistance and higher diffusivity of the 2.5 %n Cu-filled resin infiltration compared to 2.5 % nano Ag-filled infiltration is due to the excellent infiltration of the copper-filled resin shown in the SEM imaging in Figures 4.19-4.20. The 2.5 % nano Ag-filled and 2.5 % nano Cu-filled resins outperformed both "dry" MWCNT arrays and "dry" MWCNT arrays infiltrated with nano-filled resins. However, unlike nano-filled resins and TLPS formulations, "dry" MWCNT arrays are re-workable and non-corrosive. Another advantage of "dry" MWCNT arrays are the extremely low bulk densities of 0.25 g/cc compared to 1.5 g/cc for nano-filled resins.

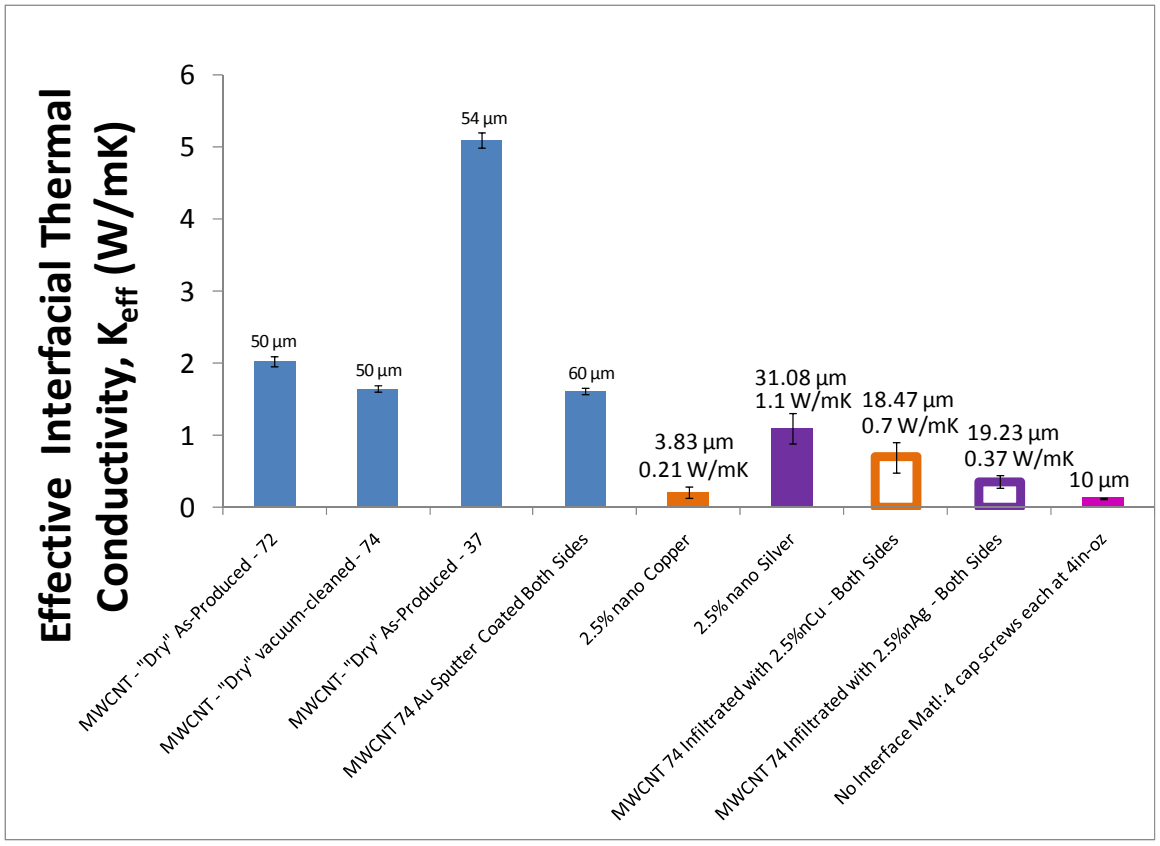

Figure 4.29 Effective interfacial conductivity of nano-filled resin Infiltration

Similar results are seen in Figure 4.29 as shown in Figure 4.28 for diffusivity and thermal contact resistance. The values of effective thermal conductivity of the MWCNT arrays infiltrated with the nano copper-filled resin are significantly higher than nano copper-filled resin alone. The opposite is true for the silver-filled resin, due to the poor infiltration shown in Figure 4.20. The SEM imaging of the side view of the sandwich assembly bonded by the infiltration of nano silver-filled resin within MWCNT array revealed poor infiltration and an uneven interface with gaps of air. The gap-filling nature of a TIM is an important property for reliable heat transfer through the interface.

4.3.5 TLPS Infiltration Results

Diffusivity across the assembly and the interfacial contact resistance across the interface are plotted in Figure 4.30 for the MWCNT arrays infiltrated with TLPS CELF 108 and CELV 310. The key indicates each of the samples in decreasing thermal performance. The MWCNT – 74 was the vacuum-cleaned array that was also Au sputter coated prior to the small scale infiltration with TLPS materials on both sides.

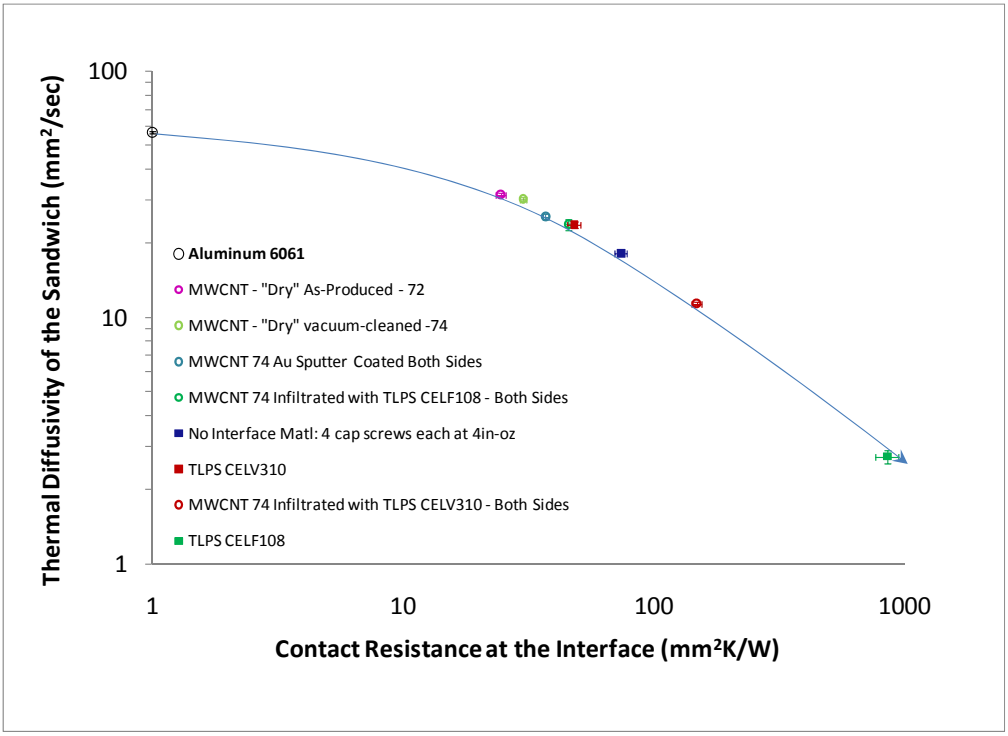

Figure 4.30 Thermal diffusivity of the sandwich plotted against contact resistance at the interface of MWCNT arrays and MWCNT arrays infiltrated TLPS CELF 108 and CELV 310 bonding mill-finish Al substrates

The MWCNT arrays cap-screw-bonded mill-finish Al substrates (at 1155 kPa) were compared to TLPS CELF 108 and CELV 310 bonding mill-finish Al substrates (75psi, 200 °C, 45 minutes), and MWCNT arrays infiltrated with TLPS CELF 108 and CELV 310 bonding mill-finish Al substrates (75psi, 200 °C, 45 minutes). This plot in Figure 4.30 included only the thermal tests relating to the TLPS materials. The TLPS materials were very viscous, with a bulk density of ~5.5 g/cc. This property of the material makes it difficult to create a TIM with a small bond-line. The high density material also does not make it an ideal candidate for infiltrating into a MWCNT array, as seen in Figure 4.21 and Figure 4.22. TLPS materials simply created a "sandwich-effect" and sintered to the aluminum instead of infiltrating through the nanotubes. For these reasons, interfacial thermal properties were poor. The infiltration of CLEF 108 within MWCNT -74 vacuum-cleaned and Au sputter coated array possessed an R_c value of 45.97 mm^2K/W; this was a dramatic improvement over CELF 108 with an R_c of 857.67 mm^2K/W. However these contact resistance values are relatively high when considering that "dry" MWCNT arrays reach R_c values of ~ 25 mm^2K/W. Infiltrating MWCNT -74 vacuum-cleaned and Au sputter coated array with CELV 310 resulted in an R_c value of 148.87 mm^2K/W—a decrease in thermal performance compared to CELV 310 alone with an R_c value of 48.38 mm^2K/W .

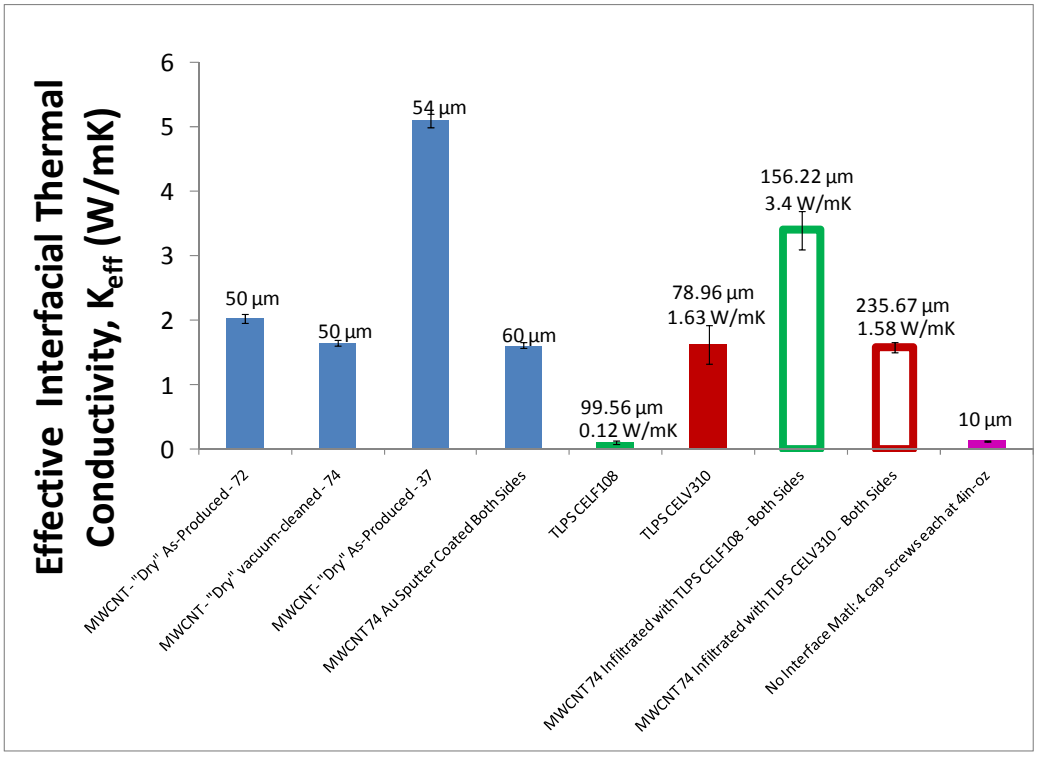

Figure 4.31 Effective interfacial conductivity of TLPS Infiltration

Similar results are seen in Figure 4.31 as shown in Figure 4.30 for diffusivity and thermal contact resistance. The values of effective thermal conductivity of the MWCNT arrays infiltrated with the CELF 108 adhesive are significantly higher than CELF 108 resin alone. The opposite is true for the CELV 310 material.

4.4 Concluding Remarks

The present chapter contains a characterization of "dry", un-infiltrated, 100 % carbon nanotube arrays that were "cleaned" in order to reduce amorphous carbon by water cleaning, vacuuming, and tape cleaning. Also presented here are techniques for improving the thermal conductivity of the MWCNT arrays by replacing the volume of air within the array with conductive greases and polymers.

When viewing our "dry" MWCNT arrays in the SEM, a layer of amorphous carbon evenly covered the top of the array. In our case, synthesizing arrays with the CVD method involves continuously depositing catalyst and carbon onto a quartz substrate, and different parameters, such as feed rate and temperature, contribute to an excess of catalyst deposited. The ideal MWCNT array for TIM applications for adhesion, phonon transport, conformability, and conductivity is an array with an average thickness of about 20 μm [56] and a composition of highly aligned [48], heavily packed [9] nanotubes with no amorphous carbon [68]. One focus of this chapter addressed improving the arrays with respect to the latter property. The MWCNT tips must reach the metal substrate for more effective phonon transport abilities [48].

The water cleaning technique attempted not only released the amorphous carbon from the MWCNT tips, but also distorted the adhesion forces between the nanotubes. The remaining array after the implementation of this method was cracked and unable to be harvested from the substrate and tested. The water cleaning technique was damaging to the entire array and was rejected as a viable option for ridding the array of amorphous carbon.

The tape cleaning technique explored involved cleaning the NT array on the small scale by a strip of pressure sensitive adhesive. In work by Liangti Qu *et al*. [70], they altered NT array surfaces using adhesive tape. Not only did they "clean" the array, they modified the surface to create highly aligned nanotubes of continuous length. Our preliminary test on a very small-scale is mentioned in this paper; however this is just an initial test to alter MWCNT surfaces. The scope of this work was simply to remove the insulating carbon layer. The pressure sensitive

adhesive was lightly placed on the "top" side of the array and successfully removed excess amorphous carbon, but unintentionally appeared to have removed small sections of the aligned array.

The most successful technique for modifying the surface of our "dry" 100 % MWCNT array was the vacuum-cleaning method presented in this chapter. The top of the array still attached to the quartz slide was simply passed over twice by a bagless canister vacuum's nozzle. The method removed approximately 0.1 g (5 wt. %) of weight from the slide, assumed to be the amorphous carbon. SEM imaging of the top side, before and after the vacuum technique was implemented, suggested that vacuum-cleaning achieved the goal of removing amorphous carbon from the "top side" of the array. When LFA tested in cap-screw bonded assemblies, thermal analysis reveals a similar interfacial thermal contact resistance and thermal diffusivity compared to the as-produced array. The reduction in amorphous carbon did not improve thermal transport capabilities of the arrays. Although the top appears to be free from the amorphous carbon, further surface modifications to improve the tangled, un-aligned nature of the "top side" to reveal aligned nanotube tips would significantly improve the thermal properties of the NT array TIM.

The "dry" arrays composed of vertically aligned MWCNT, with 85 % free volume, were also modified by infiltrating with conductive fillers and greases. Three different types of infiltrants were used—Arctic Silver 5 Thermal Compound (a commercial grease commonly used in TIM applications), nano-filled resins of 2.5 % nano copper and 2.5 % nano silver (developed by Creative Electron), and Transient Liquid Phase Sintering (TLPS) materials CELF 108 and CELV 310 (developed by Creative Electron for a solder replacement).

The Arctic Silver 5 (AS5) grease infiltrated within the MWCNT array revealed very significant, synergistic thermal interface improvements over MWCNT arrays and also AS5. Testing the AS5 infiltration within the top side of MWCNT arrays in cap-screw bonded assembly, resulted in interfacial contact resistance down to 8.19 mm^2K/W and a thermal diffusivity of 45.07 mm^2/s at moderate pressure loads. This was about an 87 % improvement over AS5 alone. The AS5 successfully filled the void between nanotubes and increased thermal performance through an interface—this was a great candidate for an exceptional MWCNT TIM.

The nano-filled resins and TLPS materials, developed by Creative Electron, were also infiltrated into the "dry" MWCNT arrays. These conductive adhesives permanently and strongly bonded

the aluminum substrates. The nano-sized (30 nm in diameter) copper successfully filled the spaces between the nanotubes, as seen in the SEM images in this chapter. The resin with nano-sized silver particles did not create a fully infiltrated TIM, indicated by the SEM images of the inhomogeneous interface. The thermal results indicate the importance of infiltration and an evenly filled, homogenous interface. The MWCNT array infiltrated with nano-sized copper-filled resins achieved a very low contact resistance of 26.23 mm^2K/W; this is almost half of the 52.63 mm^2K/W contact resistance found for the MWCNT array infiltrated with nano-sized silver-filled resin. Table 4.2 provides an overview and, from the results in the table, the lower contact resistance can be attributed to the better infiltration and the nature of the interface.

Table 4.2 Overview of MWCNT array infiltration with Creative Electron materials

Interface	Infiltration	R_c (mm^2K/W)	Bondline (μm)	K_{eff} (W/mK)
MWCNT Infiltrated with nano Ag-filled Resin	Poor	52.63	19.24	3x less than Ag-filled
MWCNT Infiltrated with nano Cu-filled Resin	Excellent	26.23	18.47	3.5x greater than Cu-filled
MWCNT Infiltrated with CELV310	Sandwich Effect	148.87	235.67	equal to CELV310
MWCNT Infiltrated with CELF108	Sandwich Effect	45.97	156.22	28x greater than CELF108

The table also includes the two TLPS materials, with particle sizes exceeding the 80 nm spacing between nanotubes, resulting in a "sandwich effect" and an inability to infiltrate through the MWCNT arrays. The TLPS material sat on the top and bottom of the array but a homogenous interface was created with no air gaps and an evenly filled interface. The thermal results are not impressive, mostly due to the very large bond-line caused by the viscous nature of the material.

This chapter does not exhaust all options for infiltrating arrays with high conductivity greases or adhesives. There are many thermal greases commercially available and many metallic materials that can be dispersed within an epoxy matrix. This chapter does prove that infiltrating the arrays with conductive materials with particle sizes small enough to fill the voids between nanotubes, is a promising way to improve MWCNT array TIMs or conventional TIMs.

Chapter 5 Discussion of Results and Conclusion

5.1 Introduction

In this thesis, the use of vertically-aligned MWCNT arrays as thermal interface materials (TIMs) was presented and discussed. Epoxy infiltrated MWCNT arrays, "dry" 100 % MWCNT arrays, and refined techniques of modifying "dry" MWCNT arrays are each thoroughly characterized by SEM imaging and LFA thermal testing for thermal diffusivity and thermal interfacial contact resistance. The results and subsequent discussion addresses suitability of each array as a heat conducting material between two solid substrates—characteristic of an excellent TIM.

5.2 Infiltrated MWCNT Arrays

5.2.1 Relationship Between MWCNT Array Composition and Thermal Performance

Chapter 2 and 4 characterize MWCNT arrays infiltrated with either an epoxy resin or a conductive grease or adhesive. They were thoroughly characterized for thermal properties as well as material composition of the array; an overview is given in Table 5.2. Theoretically there exists an ideal structure for a MWCNT array for TIM applications given in Table 5.1.

Table 5.1 Theoretical Structure of MWCNT Arrays for Most Effective TIM

Characteristic	Motivation	Background
MWCNT length < 150 µm	Even infiltration	T. Borca-Tasciuc *et al*. [60] Rensselaer Polytechnic Institute
MWCNT length 5-10 µm	Adhesion	Y. Zhao *et. al* [26]
15 % Nanotube Packing Factor	Compressibility	B. Cola, X. Xu, T. Fisher [9] Purdue University
High Aspect Ratio CNTs > 10^2	Compressibility	B. Cola, X. Xu, T. Fisher [9] Purdue University
NT Young's Modulus ~1 TPa	Conformability	P. Kim, C.M. Leiber [29] M. Gruigicic *et al.* [65] Clemson University
High Conductivity MWCNT arrays (3000 W/mK)	Conduct Heat	H. Huang et. al [13] Tsinghua University, Beijing

It can be assumed that the nanotube arrays presented in this thesis possess the latter three properties listed in Table 5.1. The measurement of the CNTs modulus and conductivity are out of the scope of this paper. The packing factor of the arrays infiltrated with epoxy resins are listed in Table 5.2 and each MWCNT length and subsequent bond-line thickness within sandwich assembly is also listed here. These properties, according to the background and Table 5.2, do affect thermal properties of the arrays when filling the interface between two solid substrates. Further explanation is found following the table.

Table 5.2 Overview of the infiltrated MWCNT arrays' composition and thermal properties presented

Interface	Infiltrant	Infiltration	Packing Factor (% Max NT/cm^2)	MWCNT length (μm)	Bondline Thickness (μm)	R_c (mm^{2}K/W)	α (mm^2/s)	K_{eff} (W/mK)
MWCNT - 37	AS5	Excellent	11	50	30	8.19	45.069	3.66
MWCNT - 71	Cyanate Ester	38.02%	14	100	33.79	18.10	36.69	1.87
MWCNT - 43	SR-4-3	44.04%	18	100	52.40	20.01	23.47	2.62
MWCNT - 74	AS5	Excellent	13	100	140	22.39	35.575	6.25
MWCNT - 44	SR-4-3	30.31%	16	100	61.66	24.72	29.73	2.49
MWCNT - 74	2.5%nCu	Excellent	13	100	18.47	26.23	31.742	0.70
MWCNT - 69	RMC 0138	43.83%	13	100	39.42	26.68	24.78	1.48
MWCNT - 45	SR-4-3	35.06%	17	100	70.07	29.33	32.64	2.39
MWCNT - 74	2.5%nAg	Poor	13	100	19.24	52.63	21.751	0.37
MWCNT - 74	CELF 108	Sandwich Effect	13	100	156.22	45.97	2.729	3.40
MWCNT - 74	CELV 310	Sandwich Effect	13	100	235.67	148.87	11.393	1.58

Our MWCNT arrays had either a 50 µm NT length (MWCNT – 37) or a 100 µm NT length seen amongst all other arrays. According to Table 5.1, MWCNT length < 150 microns encourages a more evenly infiltrated array and arrays with MWCNT lengths between 5-10 µm possess significant adhesion forces between MWCNTs. A shorter NT length also, not mentioned in this table, but mentioned in Chapter 2 with Equation 2.14, has a smaller interface thickness (bond-line, L), directly impacting the interfacial thermal contact resistance ($R_c = \frac{L}{k}$). According to Equation 2.14, a smaller bond-line thickness will result in an interface with less resistance to heat. This background, along with the clear result that MWCNT -37 outperformed all arrays, is evidence for the importance of a shorter NT length when determining the relationship between MWCNT array structure and a reliable TIM.

The packing factors of nanotubes for all arrays are between 11-18 % max NT/cm^2. According to Table 5.1 an average packing factor for compressibility and space for infiltration, was 15 % max NT/cm^2. The range of packing factors found for our arrays lie very close to this value. There are not specific trends from this thesis that suggest the best packing factor. The superior array, MWCNT-37 possess the smallest packing factor, however the excellent thermal properties are postulated to be dominated by the shorter NT length. The packing factors are all very close to one another and this array structure property does not seem to dramatically affect the thermal properties.

5.2.2 Applications

Addressed in Chapter 1 was the motivation for TIM research in general. Advances in electronics have led to higher power outputs in microelectronics that continue to diminish in size. Many times microelectronics are composed of multilayer components and integrated circuits. The ever increasing power outputs in a smaller package create thermal management issues. Heat spreaders are often incorporated into the circuits to leverage available area and dilute thermal loads. Conducting heat through spreaders and through the thickness of multilayer components, involves a path through an interface with serious resistance to heat flow. To mitigate this issue, a TIM is placed in any available volume for increased heat conduction and adhesion.

A MWCNT array composed of NTs with a high conductivity of 3000 W/mK [13] that, when infiltrated with a polymer that possesses adhesive properties, creates a great composite TIM

candidate. The MWCNT arrays infiltrated with either epoxy resin or conductive adhesives possess thermal properties that show improvements over commercial thermal adhesives currently used between component layers and between a heat source and a heat spreader. The results suggest that the highly aligned MWCNT arrays offer a breakthrough material solution for aircraft, spacecraft and missile system thermal management applications. Each of the infiltrated arrays, with the exception of the MWCNT – 74 infiltrated with CELV 310 or CELF 108 (highly viscous TLPS materials with sintering particles that are too large to wick into the NT array) offer replacements for Ther-o-bond, silver-filled epoxy, and arctic silver adhesives, due to exceptional thermal properties, lower bulk densities, and non-corrosive nature.

5.3 Dry, Un-infiltrated MWCNT Arrays

5.3.1 Relationship Between MWCNT Array Composition and Thermal Performance

Chapter 4 characterized "dry" MWCNT arrays for thermal properties as well as material composition of the array; an overview is given in Table 5.3. The ideal structure presented in Table 5.1 also applies for un-infiltrated arrays in TIM applications. The packing factor of the arrays, each MWCNT length and subsequent bond-line thickness for the cap-screw bonded sandwich assemblies are listed in Table 5.3. The relationship between the actual/ideal properties and thermal performance are explained following the table.

Table 5.3 Overview of the Dry MWCNT arrays' composition and thermal properties presented in this thesis

Interface	Packing Factor (% Max NT/cm^2)	MWCNT length (µm)	Bondline Thickness (µm)	R_c (mm^{2}K/W)	α (mm^2/s)	K_{eff} (W/mK)
MWCNT- "Dry" As-Produced - 37	11	50	54	10.58	43.038	5.10
MWCNT - "Dry" As-Produced - 72	14	100	50	24.63	31.511	2.03
MWCNT - "Dry" vacuum-cleaned - 74	13	100	50	30.25	30.254	1.65

Our un-infiltrated MWCNT arrays had either a 50 µm NT length (MWCNT – 37) or a 100 µm NT length (MWCNT-72, MWCNT-74). Although the "dry" arrays do not possess the permanent bonding and the large adhesion forces as compared to the arrays infiltrated with thermoset materials, there are adhesion forces between the dry NTs.

Wei Lin *et al.* [49] improved conductivity by 2 orders of magnitude and improved adhesion with the addition of a molecular phonon coupler. A van der waals force dominated adhesion has interfacial strengths at <0.05 MPa. Lin found, through die shear tests, the interfacial strengths of the assembly were 0.23-0.36 MPa. The large improvement in conductivity was related to this improved adhesion. According to Table 5.1 and work by Yang Zhao *et al*. [26], NTs can possess adhesion forces between one another at about 0.117 MPa, exceeding typical interactions dominated by van der Waals forces at <0.05 MPa [49]. An optimal height of MWCNT array for improved adhesion is 5-10 µm [26]. The MWNCT- "dry" As-produced – 37 is composed of nantotubes with lengths of about 50 µm, closer to the optimal height. The significantly lower resistance to heat (10.58 mm^2K/W) compared to the other two arrays is associated with the shower NT length dominating greater adhesion forces; and, according to the definition of thermal contact resistance ($R_c = \frac{L}{k}$), a smaller bond-line thickness will result in an interface with less resistance to heat.

5.3.2 Applications

The thermal grease with the lowest contact resistance found was Zerotherm Thermal Grease with an interfacial contact resistance value of 10.36 mm^2K/W. The NT arrays performed very similarly to the thermal greases; for example, the MWCNT – 37 array reached a resistance of 10.58 mm^2K/W, according to Table 5.3. The "dry" arrays could quite possibly replace thermal greases commonly used in integrated circuits for thermal management of CPUs. Aside from having similar thermal properties, MWCNT arrays are easier to handle and can withstand higher temperatures and high vacuum environments, as explained in Chapter 3. Therefore, possible applications where "dry" arrays are superior to thermal greases are within interfaces created by gallium arsenide (GaAs) components, which is a compound used in higher power applications. GaAs components, allowing operation temperatures to reach 125 °C [5], often make-up satellites and other spacecraft because of higher power output requirements over a long period of flight time.

There is much area for improvement in developing MWCNT arrays for thermal interface applications. The thermal performance can be drastically increased by reducing the length of NTs and reducing the amount of amorphous carbon, while still maintaining a high concentration of NTs within the array. Further research will focus on the delicate balance of these parameters and how this influences infiltration and thermal performance, while obtaining continuous arrays for large, commercial applications.

REFERENCES

1. Ngo, Q., Brett A. Cruden, Alan M. Cassell, Gerard Sims, M. Meyyappan, Jun Li, and Cary Y. Yang, *Thermal Interface Properties of Cu-filled Vertically Aligned Carbon Nanofiber Arrays.* Nano Letters, 2004. **4**(12): p. 2403-2407.
2. Arden, W., et al., *International Technology Roadmap for Semiconductors*, in *Emerging Research Devices*. 2009.
3. Singhal, V., T. Siegmund, and S.V. Garimella, *Optimization of thermal interface materials for electronics cooling applications.* Ieee Transactions on Components and Packaging Technologies, 2004. **27**(2): p. 244-252.
4. Veedu, V.P., et al., *Multifunctional composites using reinforced laminae with carbon-nanotube forests.* Nature Materials, 2006. **5**(6): p. 457-462.
5. Silverman, E.M., *Product Development of Engineered Thermal Composites for Cooling Spacecraft Electronics.* Technology Review Journal, 2005: p. 19.
6. Cola, B., X. Xu, T.S. Fisher, *Increased real contact in thermal interfaces: A carbon nanotube/foil material.* Applied Physics Letters, 2007. **90**: p. 0935131-0935133.
7. Prasher, R., *Thermal Interface Materials: Historical Perspective, Status, and Future Directions.* Proceedings of the IEEE, 2006. **94**(8): p. 1571-1586.
8. De Mey, G., et al., *Influence of interface materials on the thermal impedance of electronic packages.* International Communications in Heat and Mass Transfer, 2009. **36**(3): p. 210-212.
9. Cola, B., J. Xu, T. S. Fisher, *Contact mechanics and thermal conductance of carbon nanotube array interfaces.* International Journal of Heat and Mass Transfer, 2009. **52**: p. 3490-3503.
10. Sartre, V., M. Lalleman *Enhancement of thermal contact conductance for electronic systems.* Applied Thermal Engineering, 2001. **21**: p. 221-235.
11. Sheri, L., M. Early, M. Pellilo, *Thermal Interface Material Performance in Microelectronics Packaging Applications.* Microelectronics Journal, 1997. **28**: p. 534-544.
12. Shaikh, S., Khalid Lafdi, Edward Silverman, *The effect of a CNT interface on the thermal resistance of contacting surfaces.* Carbon, 1997. **28**(695-703).
13. Huang, H., C. Liu, Y. Wu, *Aligned Carbon Nanotube Composite Films for Thermal Management.* Advanced Materials, 2005. **17**(13): p. 1652-1656.
14. Xu, J., Timothy S. Fisher, *Enhancement of thermal interface materials with carbon nanotube arrays.* International Journal of Heat and Mass Transfer, 2009. **49**: p. 1658-1666.
15. Shaikh, S., L. Li, K. Lafdi, J. Huie, *Thermal conductivity of an aligned carbon nanotube array.* Carbon, 2007. **45**(13): p. 2608-2613.
16. Incropera, F.P., David P. Dewitt, Theodore L. Bergman, Adrienne S. Lavine, *Introduction to Heat Transfer.* 2007.
17. M.S. Dresselhaus, P.C.E., *Phonons in Carbon Nanotubes.* Advances in Physics, 2000. **49**(705-814).
18. Sihn, S., Sabyasachi Ganguli, Ajit K. Roy, Liangti Qu, Liming Dai, *Enhancement of Through-Thickness Thermal Conductivity in Adhesively Bonded Joints Using Aligned Carbon Nanotubes.* Composites Science and Technology, 2007. **68**(3-4): p. 658-665.
19. Cahill, D.G., et al., *Nanoscale thermal transport.* Journal of Applied Physics, 2003. **93**(2): p. 793-818.

20. Berber, S., Y.-K. Kwon, and D. Tománek, *Unusually High Thermal Conductivity of Carbon Nanotubes.* Physical Review Letters, 2000. **84**(20): p. 4613-4616.
21. Cola, B.A., *Carbon nanotubes as high performance thermal interface materials*, in *Electronics Cooling*. 2010. p. 10-15.
22. Jaques, D.N., Andrews, R.J., *Process for the Continuous Production of Aligned Carbon Nanotubes*. 2007: U.S. .
23. Andrews, R., D. Jacques, A.M. Rao, F. Derbyshire, D. Qian, X. Fan, E.C Dickery, J. Chen, *Continous production of aligned carbon nanotubes: a step closer to commercial realization.* Chemical Physics Letters, 1999. **303**: p. 467-474.
24. Lee, H.J., *Thermal Diffusivity in Layered and Dispersed Composites*. 1975, Purdue University.
25. Milosevic, N.D., *Determination of Transient Thermal Interface Resistance Between Two Bonded Metal Bodies using the Laser-Flash Method.* International Journal of Thermophysics, 2008. **29**: p. 2072-2087.
26. Zhao, Y., Tao Tong,Lance Delzeit, Ali Kashani, M. Meyyappan, Arun Majumdar,, *Interfacial energy and strength of multiwalled-carbon-nanotube-based dry adhesive.* Journal of Vacuum Science and Technology, 2005. **24**(1): p. 331-335.
27. Amama, P., Baratunde A Cola, Timothy D Sands, Xianfan Xu, and Timothy S Fisher, *Dendrimer-assisted controlled growth of carbon nanotubes for enhanced thermal interface conductance.* Nanotechnology, 2007. **18**.
28. Cola, B.A., Placidus B. Amama, Xianfan Xu, Timothy S. Fisher, *Effects of Growth Temperature on Carbon Nanotube Array Thermal Interfaces.* Journal of Heat Transfer, 2008. **130**: p. 1145031-1145034.
29. Kim, P.C.M.L., *Nanotube nanotweezers.* Science, 1999. **286**(5447): p. 2148-2150.
30. Frank, S., P. Poncharal, Z.L. Wang, W.A. De Heer, *Carbon nanotube quantum resistors.* Science, 1998. **280**(5370): p. 1744-1746.
31. W. Yi, L.L., Z. Dian-lin, Z.W. Pan, S.S. Xie, *Linear specific heat of carbon nanotubes.* Physical Review B, 1999. **59**(14).
32. Weisenberger, M., *Applications of Multiwall Carbon Nanotube Composites: Mechanical, Electrical, and Thermal Properties*. 2007, University of Kentucky.
33. Endo, M., Takuaya Hayashi, Yoong Ahm Kim, Mauricio Terrones, and Midlred S. Dresselhaus, *Applications of carbon nanotubes in the twenty-first centure.* The Royal Society, 2004: p. 2223-2239.
34. M. S. Dresselhaus, G.D., and P. C. Eklund, *Science of Fullerenes and Carbon Nanotubes*. 1996, San Diego: Academic Press.
35. Dresselhaus, M.S., G. Dresselhaus, and A. Jorio, *Unusual Properties and Structure of Nanotubes.* Annual Review of Materialls Research, 2004. **34**: p. 247-278.
36. Hu, X.J., Padilla, A. A., Xu, J., Fisher, T. S.,Goodson, K. E., *3-omega measurements of vertically oriented carbon nanotubes on silicon.* Journal of Heat Transfer-Transactions of the Asme, 2006. **128**(11): p. 1109-1113.
37. Coleman, J.N.K., U.; Blau, W. J.; Gun'ko, Y. K., *Small but strong: A review of the mechanical properties of carbon nanotube-polymer composites.* Carbon, 2006. **44**(9): p. 1624-1652.
38. Cahill, D.G., W.K. Ford, K.E. Goodson, G.D. Mahan, A. Majumdar, H.J. Maris, *Nanoscale Thermal Transport.* Applied Physics, 2003. **93**(2): p. 793-818.
39. Siochi, E.J., D. C. Working, C. Park, P.T. Lillehei, J.H. Rouse, C.T. Toping, A.R. Bhattacharyya, and S. Kumar, *Melt processing of SWCNT-polyimide nanocomposite fibers.* Composites Part B: Engineering, 2004. **35**(5): p. 439-446.

40. Biercuk, M.J., M.C. Llaguno, M. Radosavljevic, J.K. Hyun, A.T. Johnson, J.E. Fischer, *Carbon nanotube composites for thermal management.* Applied Physics Letters, 2002. **80**(15): p. 2767-2769.
41. Liu, C.H., H. Huang, Y. Wu, and S. S. Fan, *Thermal conductivity improvement of silicone elastomer with carbon nanotube loading.* Applied Physics Letters, 2004. **84**(21): p. 4248-4251.
42. Gong, Q.-m., Zhi Li, Xiao-dong Bai, Dan Li, Yun Zhao, Ji Liang, *Thermal properties of aligned carbon nanotube/carbon nanocomposites.* Materials Science and Engineering A, 2004. **384**: p. 209-214.
43. Roy, A.K., et al., *Thermal interface tailoring in composite materials.* Diamond and Related Materials, 2010. **19**(2-3): p. 268-272.
44. Q. Zhang, J.L., R. Sager, L. Dai, J. Baur, *Hierarchical composites of carbon nanotubes on carbon fiber: Influence of growth condition on fiber tensile properties.* Composites Science and Technology, 2009. **69**(5): p. 594-601.
45. Wei Lin, R.Z., Kyoung-Sik Moon Wong, C.P. , *Synthesis of High-Quality Vertically Aligned Carbon Nanotubes on Bulk Copper Substrate for Thermal Management* IEEE Transactions on Advanced Packaging, 2010. **33**(2): p. 370 - 376
46. Chen, W., Liangti Qu, Dongwook Chang, Liming Dai, Sabyasachi Ganguli and Ajit Roy, *Vertically-aligned carbon nanotubes infiltrated with temperature-responsive polymers: smart nanocomposite films for self-cleaning and controlled release.* The Royal Science of Chemistry, 2007: p. 163–165.
47. Xu, J. and T.S. Fisher, *Enhanced thermal contact conductance using carbon nanotube array interfaces.* Ieee Transactions on Components and Packaging Technologies, 2006. **29**(2): p. 261-267.
48. Ganguli, S., S. Sihn, A. K. Roy, L. Dai, L. Qu, *Metalized Nanotube Tips Improve Through Thickness Thermal Conductivity in Adhesive Joints.* Journal of Nanoscience and Nanotechnology, 2009. **9**(3): p. 1727-1733.
49. Lin, W., Rongwei Zhang, Kyoung-Sik Moon, C.P. Wong *Molecular phonon couplers at carbon nanotube/substrate interface to enhance interfacial thermal transport.* Carbon, 2009. **48**: p. 107-113.
50. Xu, Y., et al., *Thermal properties of carbon nanotube array used for integrated circuit cooling.* Journal of Applied Physics, 2006. **100**(7): p. 0743021-0743025.
51. Cola, B.A., Jun Xu, Changrui Cheng, Xianfan Xu, and Timothy S. Fisher, Hanping Hu, *Photoacoustic characterization of carbon nanotube array thermal interfaces.* Journal of Applied Physics, 2007. **101**(054313): p. 1-9.
52. Iijima, S., *Helical microtubules of graphitic carbon.* Nature Materials, 1991. **354**: p. 56-58.
53. Blazei, D., *Thermal Interface Materials.* Electronics Cooling, 2003. **9**(4): p. 14-20.
54. Cola B., X.X., T.S. Fisher, *Increased real contact in thermal interfaces: A carbon nanotube/foil material.* Applied Physics Letters. **90**(2007): p. 0935131-0935133.
55. Andrews R., D.J., A.M. Rao, F. Derbyshire, D. Qian, X. Fan, E.C Dickery, J. Chen, *Continous production of aligned carbon nanotubes: a step closer to commercial realization.* Chemical Physics Letters. **303**(1999): p. 467-474.
56. Garcia, E.J., Brian L. Wardle *, A. John Hart, *Joining prepreg composite interfaces with aligned carbon nanotubes.* Composites: Part A, 2008(39): p. 1065–1070.
57. Ivanov, I., Alexander Puretzky, Gyula Eres, Hsin Wang, Zhengwei Pan, Hongtao Cui, and J.H. Rongying Jin, and David B. Geohegan, *Fast and highly anisotropic thermal transport through vertically aligned carbon nanotube arrays.* Applied Physics Letters, 2006. **89**: p. 2231101-2231103.

58. Xu, J., *Carbon Nanotube Array Theral Interfaces*. 2006, Purdue University: 2006. p. 199.
59. Garcia, E.J., A. J. Hart, B. L. Wardle, and A. H. Slocum, *Fabrication of composite microstructures by capillarity-driven wetting of aligned carbon nanotubes with polymers.* Nanotechnology, 2007. **18**(16): p. 165602-165618.
60. Borca-Tasciuc, e.a., *Anisotropic Thermal Diffusivity Characterization of Aligned Carbon Nanotube-Polymer Composites.* Journal of Nanoscience and Nanotechnology, 2007. **7**: p. 1581–1588.
61. Rotkin, S.V., Vasili Perebeinos, Alexey G. Petrov, and Phaedon Avouris, *An Essential Mechanism of Heat Dissipation in Carbon Nanotube Electronics.* Nano Letters, 2009. **9**(5): p. 1850-1855.
62. Parker, W.J., R.J. Jenkins, C.P. Butler, F.L. Abbott, *Flash Method of Determining Thermal Diffusivity, Heat Capacity, and Thermal Conductivity.* Journal of Applied Physics, 1960. **32**(9): p. 1679-1684.
63. Parker W.J., R.J.J., C.P. Butler, F.L. Abbott, *Flash Method of Determining Thermal Diffusivity, Heat Capacity, and Thermal Conductivity.* Journal of Applied Physics. **32**(1960): p. 1679-1684.
64. *CRC Handbook of Chemistry and Physics*, ed. W.M. Haynes. 2011.
65. M. Grujicic, C.L.Z., E.C. Dusel, *The effect of thermal contact resistance on heat management in the electronic packaging.* Applied Surface Science, 2005. **246**: p. 290–302.
66. Irschick D.J, A.C.C., Petren K, Fisher R.N, Losos J.B, Ellers O., *A comparative analysis of clinging ability among pad-bearing lizards.* Biological Journal of the Linnean Society, 1996. **59**: p. 21-35.
67. Cao, A., P.L. Dickrell, W.G. Sawyer, M.N. Ghasemi-Nejhad, P.M. Ajayan, *Supercompressible foamlike carbon nanotube films.* Sceince, 2005. **310**: p. 1307-1310.
68. Maschmann, M.R., Placidus B. Amama, Amit Goyal, Zafar Iqbal, and T.S.F. Roy Gat, *Parametric study of synthesis conditions in plasma-enhanced CVD of high-quality single-walled carbon nanotubes.* Carbon, 2006. **44**: p. 10-18.
69. Zheng, B., Y. Li, J. Liu, *CVD Synthesis and purification of single-walled carbon nanotubes on aerogel-supported catalyst.* Applied Physics A, 2001. **74**: p. 345-348.
70. Qu, L., Yang Zhao, Yue Hu, Han Zhang, Yan Li, Wei Guo, Hongxia Luo and Liming Dai, *Controlled removal of individual carbon nanotubes from vertically aligned arrays for advanced nanoelectrodes.* Journal of Materials Chemistry, 2010. **20**: p. 3595 - 3599.

VITA

Carissa Don Russell

Born March 4, 1987, Louisville, Kentucky

Education

Bachelor of Science, Mechanical Engineering, University of Kentucky, Lexington, Kentucky, USA, August 2005-May 2009.

Graduate studies, University of Kentucky, Center for Applied Energy Research, Lexington, Kentucky, USA, May 2006-August 2010. Advisor: Dr. Rodney Andrews.

Professional positions

2010	Mechanical Engineer, The US Army Aviation and Missile Research, Development and Engineering Center, Huntsville, Alabama.
2009-2010	Graduate Research Assistant, Center for Applied Energy Research, University of Kentucky, Lexington, Kentucky.
2007	Intern, Cummins, Inc., Columbus, Indiana.
2006-2009	Undergraduate Research Assistant, Center for Applied Energy Research, University of Kentucky, Lexington, Kentucky.

Awards and scholarships

2010	Department of Defense, The Science, Mathematics and Research for Transformation (SMART) Scholarship for Service.
2009-2010	University of Kentucky, Center for Applied Energy Research, Research Assistantship.
2007	Cummins, Inc., Cummins Diversity Scholarship.
2006-2009	Society of Women Engineers and DiamlerChrysler, Scholarship.

2006 University of Kentucky, Department of Mechanical Engineering, Margaret Ingels Scholarship.

2005-2009 University of Kentucky, Provost Scholarship.

Conference proceedings

Carissa Dowden, Matthew C. Weisenberger, John Craddock, Karen Petty, Toni Shields, A.T. Owens, Rich Foedinger, Simon Chung. *Epoxy-filled Multiwall Carbon Nanotube Arrays for Thermal Interface Applications.* International Carbon Conference; 2010; Clemson, South Carolina, USA; 2010.

Carissa Dowden, Matthew C. Weisenberger, John Craddock, Karen Petty, Toni Shields, A.T. Owens, Rich Foedinger, Simon Chung. *Epoxy-Filled Multiwall Carbon Nanotube Arrays As Adhesive Thermal Interface Materials.* Society for the Advancement of Material and Process Engineering; 2010; Seattle, Washington, USA; 2010.

Carissa Dowden, Matthew C. Weisenberger, Ashley Whitlow, John Craddock, Rodney Andrews, and Keith Roberts. *Tensile Properties of PAN-based Carbon Fiber Containing Multiwall Carbon Nanotubes.* International Carbon Conference; 2009; Biarritz, France; 2009.